Science

RESEARCH ARTICLES

Cite as: T. Huang *et al*., *Science* 10.1126/science.adv5429 (2026).

A negative feedback loop between TERMINAL FLOWER1 and LEAFY protects inflorescence indeterminacy

Tian Huang[1], Charles Hodgens[2]†, Sandhan Prakash[1]†, Marco Marconi[3], Krzysztof Wabnik[3,4], Rosangela Sozzani[2]*, Doris Wagner[1]*

[1]Department of Biology, University of Pennsylvania, Philadelphia, PA, USA. [2]Plant and Microbial Biology Department and NC Plant Sciences Initiative, North Carolina State University, Raleigh, NC, USA. [3]Centro de Biotecnología y Genómica de Plantas (CBGP, UPM-INIA) Universidad Politécnica de Madrid (UPM) - Instituto Nacional de Investigación y Tecnología Agraria y Alimentaria (INIA, CSIC), Campus de Montegancedo, Pozuelo de Alarcón, Madrid, Spain. [4]Departamento de Biotecnología-Biología Vegetal, Escuela Técnica Superior de Ingeniería Agronómica, Alimentaria y de Biosistemas, Universidad Politécnica de Madrid (UPM), Madrid, Spain.

†These authors contributed equally to this work.

*Corresponding author. Email: ross_sozzani@ncsu.edu (R.S.); wagnerdo@sas.upenn.edu (D.W.)

Inflorescences of flowering plants adopt diverse genetically programmed and environmentally tuned architectures. By contrast, continued maintenance of the stem-cell pool within the apical meristem is unresponsive to environmental cues. Through a combination of modeling and experimentation in *Arabidopsis*, we reveal a negative feedback loop that buffers environmental signals. This loop comprises the determinacy-promoting pioneer transcription factor LEAFY (LFY) and the indeterminacy-promoting transcriptional co-repressor TERMINAL FLOWER1 (TFL1). At the transition to the flower-producing reproductive phase, LFY directly and quantitatively up-regulates expression of *TFL1*. TFL1 in turn negatively feeds back on *LFY* to prevent LFY overaccumulation. This blocks inflorescence termination even under strong florally inductive signals. Our work uncovers a mechanism for robust environmental buffering involving differential responses of two cell populations to the same environmental stimulus.

Inflorescences are flower-bearing shoots that develop upon perception of inductive seasonal and endogenous cues during the reproductive phase of development. Inflorescence architecture contributes to reproductive fitness of flowering plants by controlling time to flowering and seed set (*1*, *2*). Across different plant species, inflorescence architecture types are classified as determinate (e.g., the panicle in rice) or indeterminate (e.g., the raceme in *Arabidopsis thaliana*, hereafter shortened to *Arabidopsis*) (*3*, *4*). Inflorescence determinacy is an important agronomic trait and has been selected for multiple times in crop breeding as it allows for shorter growth cycles, higher planting densities and ease of harvest (*2*). Determinate inflorescences generally differentiate into a terminal flower at the shoot tip and stop producing new lateral organs, while indeterminate inflorescences maintain their stem cell pool in the apical inflorescence meristem and continue to produce lateral meristems at their flanks until senescence (Fig. 1A). In *Arabidopsis,* inflorescence development happens in two phases (*5*). In the first inflorescence phase (I1 phase), lateral meristems give rise to leaves and to axillary meristems that develop into indeterminate shoots (Fig. 1A). Subsequently in the I2 phase, lateral meristems produce determinate flowers (Fig. 1A). This lateral meristem identity switch is triggered by florally inductive seasonal cues such as long day photoperiod (*6*, *7*).

By contrast, inflorescence meristem indeterminacy is insensitive to environmental perturbation (*6*–*11*). How the inflorescence meristem is buffered from floral inductive cues is not understood. It is also unclear how two different meristems in close proximity at the shoot apex (the lateral meristem and the inflorescence meristem; Fig. 1, A and B, and fig. S1A) produce opposite responses to systemic signals that promote floral fate in inductive environmental conditions (*12*). Diverse qualitative models have been proposed (*13*), yet mechanistic insight is lacking. Using combined experimental data and computer modeling, we uncover a negative feedback loop in the center of the inflorescence meristem that acts in proportional response to the strength of the floral inductive signal. This feedback loop, involving the pioneer transcription factor LEAFY (LFY) and the transcriptional co-repressor TERMINAL FLOWER1 (TFL1) (*7*, *14*), enables the dynamic and precise control of LFY accumulation, thereby preventing inflorescence meristem termination. Our combined findings provide a mechanism for robust maintenance of inflorescence meristem indeterminacy. We further show that this negative feedback loop is blocked in lateral meristems, thereby allowing opposite responses to the same systemic signal in two meristem types that are in close proximity.

Shoot indeterminacy relies on a conserved *cis*-regulatory region of *TFL1*

TFL1 is the key evolutionary conserved, promoter of meristem indeterminacy in flowering plants (*2*, *15*) (Fig. 1A). In *tfl1* mutants, all indeterminate shoot meristems are converted to determinate flowers (Fig. 1A and fig. S1A). TFL1 mRNA and protein are present in all shoot meristems but expression increases specifically in the I2 phase inflorescence meristem when the inflorescence starts producing flowers (Fig. 1B) (*16*–*18*). We observed that *TFL1* is transcribed below the stem cell organizing center in a U-shaped

region (Fig. 1B and fig. S1B). The domain of TFL1 protein accumulation was broader, consistent with its ability to move between cells (fig. S1, C and D) (*17*, *19*).

We sought to identify *cis*-regulatory regions of *TFL1* that might be responsible for inflorescence meristem indeterminacy. The 3′ intergenic sequences of *TFL1* are key regions for controlling expression (*20*–*22*). We focused on three conserved 3′ regions of *TFL1*, regions V (456 bp), VI (700 bp), and VII (527 bp) that are occupied by many transcription factors, as shown by published chromatin immunoprecipitation sequencing (ChIP-seq) and DNA affinity purification sequencing (DAP-seq) datasets (*23*) (Fig. 1C). Further, these regions largely overlap with three regulatory blocks previously defined (*21*) through phylogenetic shadowing and 3′ *TFL1* locus truncations (Fig. S2A). To assess the functional contribution of each region to inflorescence architecture, we generated genomic *TFL1* constructs (gTFL1-mEGFP) with one regulatory region deleted (dV, dVI, or dVII gTFL1-mEGFP) (fig. S2B) and tested for their ability to rescue the inflorescence phenotypes of the *tfl1-1* null mutant. As expected, gTFL1-mEGFP rescued the terminal flower phenotype of *tfl1-1* in most primary transformants (85.7%, n=28; Fig. 1D and fig. S3, A and B). Transgenes lacking either region V or VI similarly achieved near-complete rescue (92.9%, n=28, and 83.9%, n=31, respectively). However, deletion of region VII (dVII gTFL1-mEGFP) failed to rescue the inflorescence meristem termination of *tfl1-1* (0%, n=27), although other aspects of the *tfl1-1* mutant phenotype were restored (Fig. 1, A and D; and figs. S3, A and B, and S4, A and B). To confirm the importance of region VII, we generated CRISPR deletions (*24*) at the endogenous *TFL1* locus (fig. S2C). Two independent criVII mutants lacking most of region VII also developed terminal flowers (0% indeterminacy, n≥10) (Fig. 1E and figs. S2C and S3, B and C) but did not display other *tfl1* mutant phenotypes (fig. S4, C and D).

ChIP-seq data (*14*) revealed that the LFY transcription factor directly binds *TFL1* regulatory region VII (Fig. 1C). LFY is known to be a pioneer transcription factor that promotes floral fate in meristems (*14*) and *LFY* gain-of-function inflorescences phenocopy *tfl1* mutants, and vice versa (*5*, *15*, *25*, *26*). To test whether LFY contributes to *TFL1* regulation through region VII, we next searched for putative LFY binding sites in region VII using published motif prediction tools (*27*, *28*) and mutated these sequences within the genomic rescue construct (mLFYBS, fig. S2, B and D). Similar to dVII gTFL1-mEGFP *tfl1-1*, most mLFYBS gTFL1-mEGFP *tfl1-1* plants formed determinate inflorescences (12.9% indeterminacy, n=31) (Fig. 1F and fig. S3, B and D) while rescuing all other shoot phenotypes of *tfl1-1* (fig. S4, E and F). These results indicate that LFY binding sites account for most of the effect of region VII deletion (Fig. 1, D and F). Supporting this, ChIP–quantitative polymerase chain reaction (qPCR) using an anti-LFY antibody (*29*) showed that LFY binding to mLFYBS gTFL1-mEGFP was abolished (fig. S2E), indicating that all LFY binding sites were successfully mutated. Together, these results identify region VII of *TFL1* and its LFY binding motifs as a critical regulatory elements for repressing terminal flower formation.

Region VII and its LFY binding sites promote TFL1 accumulation

To assess how region VII and its LFY binding sites influence *TFL1* expression during developmental transitions, we analyzed TFL1-mEGFP accumulation in the inflorescence meristem in fixed longitudinal tissue slices collected at different developmental time points (Fig. 1, G and H). To avoid experimental biases, we selected representative homozygous transgenic plants (Fig. S3, E and F, and Methods). Prior to flower formation (I1 phase, Fig. 1A), dVII gTFL1-mEGFP *tfl1-1* and mLFYBS gTFL1-mEGFP *tfl1-1* plants showed TFL1 accumulation levels comparable to those of the gTFL1-mEGFP *tfl1-1* control (Fig. 1G and fig. S5A). As expected, at the onset of flower formation (I1-to-I2 transition), gTFL1-mEGFP fluorescence increased in the inflorescence meristem (Fig. 1, G and H, and fig. S5, A and B). In contrast, both dVII gTFL1-mEGFP and mLFYBS gTFL1-mEGFP protein levels decreased during the I1-to-I2 transition, with low levels persisting thereafter (Fig. 1, G and H, and fig. S5, A and B). Using mRNA fluorescence in situ hybridization based on hybridization chain reaction (HCR FISH), we found that the *TFL1-mEGFP* transcripts from dVII gTFL1-mEGFP and mLFYBS gTFL1-mEGFP were comparably reduced (Fig. 1I and fig. S5C). This decrease in *TFL1* transcript abundance was also confirmed in criVII mutants carrying an endogenous deletion of region VII (fig. S5D).

To determine whether this transcriptional down-regulation is a consequence of premature inflorescence meristem determinacy, we analyzed dVII and mLFYBS gTFL1-mEGFP in a heterozygous *tfl1-1* background, where inflorescences remain indeterminate (fig. S6A) (*15*). Despite maintaining inflorescence meristem indeterminacy, after the I1-to-I2 transition, these plants still showed reduced accumulation of versions of gTFL1-mEGFP that lacked region VII or its LFY binding sites (fig. S6, B and C). This indicates that the observed loss of TFL1 expression is not a secondary effect of altered meristem fate. In summary, *TFL1* regulatory region VII, and the LFY binding sites therein, are required for *TFL1* up-regulation and expression from the I1-to-I2 transition onwards. This regulatory input is required to maintain inflorescence meristem indeterminacy as plants transition to reproductive development.

LFY protein and mRNA are present in the inflorescence meristem

Our findings suggest a direct role for LFY in upregulating *TFL1* expression. Although prior studies and the widely used translational reporter pLFY-GLFY reported no LFY in the inflorescence meristem center where *TFL1* is transcribed (*16*, *30*–*33*) (fig. S7A), we employed complementary methods with high sensitivity and specificity to test LFY protein and *TFL1* transcript overlap in the

inflorescence meristem during the I2 phase. CRISPR gene targeting/knock-in to tag endogenous *LFY* with mScarlet-I revealed low but reproducible LFY-mScarlet-I protein in the inflorescence meristem center (Fig. 2A and fig S7A). A similar pattern was observed in our genomic LFY reporter (gGLFY) (fig. S7, A and B) (*7*), further validating the result. Next, we directly compared LFY protein and *TFL1* transcript distribution by combined immunohistochemistry and RNA FISH in a single optical section. Nuclear-localized LFY protein was clearly detectable in the inflorescence meristem center, fully overlapping with the *TFL1* mRNA domain (Fig. 2B). No immunohistochemistry signal was present in the *lfy-1* null mutant, confirming the specificity of the LFY antibody (*29*) (fig. S7C). Given that LFY protein can move between cells (*31*, *32*), we next asked whether *LFY* is transcribed in the inflorescence meristem center. In individual optical sections of wholemount FISH samples, *LFY* mRNA was detected in the *TFL1* expression domain in the inflorescence meristem center (Fig. 2C). Similarly, *mScarlet-I* RNA was present in the center of the inflorescence meristem in gene targeted LFY-mScarlet-I plants, but not in the wild type (fig. S7D). Thus, in contrast to prior data, we found that *LFY* is transcribed at the I2 stage in the inflorescence meristem center domain where *TFL1* is expressed.

TFL1 mRNA and protein levels were decreased in *lfy* loss-of-function mutants, suggesting that the presence of LFY is necessary for TFL1 accumulation in the inflorescence meristem (Fig. 2D and fig. S7, E and F). This prompted us to take a closer look at the commonly used pLFY-GLFY reporter in the null *lfy-12* background (*30*, *31*). pLFY-GLFY plants displayed the expected LFY protein and mRNA accumulation in flower primordia (Fig. 2E and fig. S7B). However, neither GLFY RNA nor protein accumulated in the inflorescence meristem center (Fig. 2E and fig. S7B). pLFY-GLFY differs from gGLFY in that it does not contain the two *LFY* introns (*7*, *31*) (fig. S7A), suggesting that intronic regulatory regions are required for *LFY* transcription in the inflorescence meristem center. We found no evidence of pLFY-GLFY protein movement from meristems or young flower primordia into the inflorescence meristem (fig. S7, B and G). Loss of LFY protein specifically in inflorescence meristem center negatively impacted *TFL1* expression, which was only weakly detected at the border of the peripheral *LFY* expressing domain in pLFY-GLFY *lfy-12* (Fig. 2E and fig. S7H). We conclude that *LFY* transcription in the center of the inflorescence meristem is required for *TFL1* up-regulation and expression from the I1-to-I2 transition onwards.

To further clarify the temporal dynamics of *TFL1* and *LFY* mRNA accumulation during inflorescence development we conducted RNA FISH at different stages of inflorescence development in wild-type plants (Fig. 2F and figs. S8 and S9). During the I1 phase, *TFL1* was expressed at low levels in the subapical domain of the inflorescence meristem and in axillary meristems and *LFY* was absent from these regions (Fig. 2F and fig. S8, A to C), consistent with region VII-independent accumulation of *TFL1* at this stage (figs. S3, E and G; S5A; and S8, A and C). Only during and after the I1-to-I2 transition was *LFY* expression detected in the center of the inflorescence meristem where *TFL1* is up-regulated (Fig. 2F and fig. S9). Taken together, our data link spatiotemporal transcription of *LFY* to up-regulation of its direct target *TFL1*.

TFL1 and LFY form a negative feedback loop

Although our data show that LFY directly up-regulates *TFL1* in the center of the I2 phase inflorescence meristem, TFL1 and LFY are known to have opposite roles in inflorescence indeterminacy (*5*, *15*, *25*, *26*). Moreover, we previously showed that TFL1 represses *LFY* (*7*). To reconcile these findings, we hypothesized that, rather than operating in a simple antagonistic or mutually exclusive manner (*13*), LFY and TFL1 may instead participate in a negative feedback loop in the inflorescence meristem. In this loop, LFY activity would promote *TFL1* expression, while TFL1 would in turn repress *LFY* transcription. If such a regulatory loop exists, then transiently perturbing one component (LFY or TFL1) should lead to predictable changes in the other.

To test this model, we selectively perturbed each node. First we expressed a dexamethasone inducible artificial microRNA against *LFY* in the *TFL1* expression domain (amiRLFY) of gGLFY *lfy-1*. After 20 hours of treatment, gGLFY expression was reduced in the inflorescence meristem (Fig. 3, A and B, and fig. S10, A to C). This was accompanied by a dramatic reduction in *TFL1* mRNA levels, consistent with a promotive role for LFY (Fig. 3, A and B, and fig. S10, A to C). Supporting this, dexamethasone-induced elevated LFY accumulation in the nucleus (35S:LFY-GR) (*29*) broadly increased *TFL1* expression in the inflorescence meristem within 20 hours (fig. S11, A to D). This induction was abolished by mutating or deleting region VII of *TFL1* (fig. S11E), as expected (Fig. 1, D and F, and fig. S2E). To test the reciprocal interaction, we developed an estradiol inducible anti-GFP degron system and successfully depleted TFL1-GFP protein within 20 hours of inducing degradation (Fig. 3, C and D, and fig. S10D). This resulted in a significant increase in *LFY* transcript levels in the inflorescence meristem center, consistent with a repressive role for TFL1 (Fig. 3, C and D, and fig. S10, D and E). Similarly, in plants that ectopically express *TFL1* in the inflorescence, we observed reduced *LFY* expression in the inflorescence meristem (fig. S12, A to C). These complementary experiments support a model in which LFY and TFL1 regulate each other, forming a dynamic negative feedback loop.

To further investigate the regulatory logic of this loop, we developed a unitless (non-dimensionalized) computational model using delay differential equations to describe the mutual regulation of LFY and TFL1 in both wild-type and mutant backgrounds (Fig. 3, E to H, and supplementary text). Model parameters were tuned to fit experimental observations, resulting in N=20,000 accepted parameter sets (figs. S13A and S14A). We then simulated the effect of perturbing TFL1 or LFY production and degradation

(Fig. 3I and figs. S11G and S12D). The model accurately recapitulated the positive correlation between a change in LFY accumulation and that of *TFL1* (simulated amiRLFY, pLFY-GLFY, and inducible LFY overexpression) (Fig. 3I and fig. S11G) and the negative correlation between changes in TFL1 and *LFY* levels (simulated TFL1 degron, and TFL1 overexpression) (Fig. 3I and fig. S12D), in agreement with our experimental data (Figs. 2 and 3 and figs. S11 and S12).

Although negative feedback loops can produce oscillatory behavior (*34*), strong oscillations (defined as >10% deviation from the midpoint value in the final portion of the simulation) were rare across the accepted parameter sets (figs. S13B and S14B). Global sensitivity analyses revealed that in addition to their individual degradation rates, LFY levels are primarily governed by its own basal production rate, while TFL1 accumulation was most sensitive to both LFY-independent and LFY-dependent production rates (fig. S14C).

We next used the model to make testable predictions beyond the scope of the criteria used to evaluate parameter sets. Simulations suggested that loss of LFY regulation of *TFL1* should lead to increased *LFY* accumulation, in addition to decreased *TFL1* levels (Fig. 3I, *lfy* mutant and dVII *tfl1*). In other words, specific manipulation of a given node in the feedback loop should uncover transcriptional feedback to that node. We validated this prediction in plants whose genotype allows us to monitor transcriptional response when protein activity is reduced or lost. Using dVII gTFL1-mEGFP *tfl1-1* and mLFYBS gTFL1-mEGFP *tfl1-1* plants, we indeed observed elevated *LFY* transcript levels in the center of the inflorescence meristem relative to the control, as well as reduced *TFL1* accumulation (Fig. 3, J to M). Similarly, weak *lfy-2* missense mutants displayed increased accumulation of non-functional *LFY* transcripts in addition to reduced accumulation of *TFL1* transcripts (fig. S15, A to D). The model also predicted that *tfl1* mutants should show increased *TFL1* levels in addition to increased *LFY* transcript accumulation (Fig. 3I). Indeed, the inflorescence meristem of the strong *tfl1-1* missense mutants had elevated accumulation of nonfunctional *TFL1* (*17*) and of functional *LFY* transcripts (*16*) prior to terminating. Likewise, inducible depletion of TFL1-GFP protein in the inflorescence meristem triggered increased transcription of both *TFL1* and *LFY* (fig. S15, E to H). Together, the experimental results and simulations consistently showed that perturbing the function of one component feeds back to influence its own expression via the other node, strongly supporting the existence of a LFY-TFL1 negative feedback loop mechanism in the inflorescence meristem from the I1-to-I2 transition onwards.

Finally, we examined the effect of the LFY-TFL1 negative feedback loop on inflorescence (in)determinacy phenotypes. It is known that constitutive LFY overexpression causes inflorescence meristem determinacy (*25*). Accordingly, genetic perturbations that trigger *LFY* over-accumulation in the inflorescence meristem center (TFL1 degron, dVII, and mLFYBS) (Fig. 3, C, D, and J to M) resulted in terminal flower formation (Fig. 1, D to F, and fig. S10G). In contrast, mutants that lose LFY function or accumulation in the shoot center (*lfy-1*, amiRLFY or pLFY-GLFY *lfy-12*) do not terminate, despite failure to up-regulate *TFL1* (fig. S7I and fig. S10F) (*35*). These findings indicate that LFY accumulation in the inflorescence meristem is a key output of the LFY-TFL1 negative feedback loop and that it governs the choice between determinate or indeterminate fate in the inflorescence meristem (Fig. 3, E to H).

Floral induction directs *TFL1* up-regulation via LFY

To connect the negative feedback loop to environmental cue-mediated TFL1 up-regulation in the inflorescence meristem center, we examined the response of I2 stage inflorescences to a strong floral inductive signal – far-red-enriched long-day photoperiod (FRP) (*7*, *8*) (fig. S16A). After a 24-hour treatment, both *TFL1* and *LFY* expression increased in the inflorescence meristem of wild-type plants (Fig. 4, A and B, and fig. S16, B and C). FRP promotes transcription of *FLOWERING LOCUS T* (*FT*) (*36*, *37*), a mobile transcriptional co-activator also known as florigen (*12*). FT is a TFL1 paralog and acts as a systemic signal that moves from its site of production in the leaves to the shoot apex, where it promotes floral fate (*7*, *12*). FT is necessary for *LFY* induction by FRP and competes with TFL1 for access to the *LFY* locus (*7*). Consistent with a model where FT mediates the FRP photoperiod induced up-regulation of *TFL1* and *LFY*, inducible expression of FT also triggered up-regulation of both *TFL1* and *LFY* in I2 phase inflorescence meristem (Fig. 4, C and D, fig. S17, A to D).

To determine whether the increase in *TFL1* expression is a consequence of LFY up-regulation, we analyzed the effect of FRP induction or inducible FT overexpression in wild-type morphology plants containing *TFL1* transgenes with or without LFY binding sites. As expected, gTFL1-mEGFP was strongly induced by FRP (Fig. 4E). In contrast, *TFL1-mEGFP* levels remained low in FRP-treated dVII and mLFYBS gTFL1-mEGFP lines (Fig. 4E and fig. S16, D and E), indicating that region VII and the LFY binding sites it contains are required for *TFL1* activation by FRP. These same elements were also necessary for elevated *TFL1* expression in response to inducible FT overexpression (Fig. 4F and fig. S17, E and F). Together, these findings demonstrate that inductive photoperiod cues and FT promote *TFL1* transcription through LFY.

To capture these interactions computationally, we updated our model to include FT as input to the negative feedback loop and incorporated competition between FT and TFL1 for *LFY* locus binding (*7*) (Fig. 4G and supplementary text). We then parameterized a 3-node model consisting of FT, LFY, and TFL1 (fig. S18A). Simulations using N=20,000 accepted parameter sets successfully recapitulated the observed increase in *TFL1* and *LFY* expression levels upon elevating FT abundance (Fig. 4H). While the 3-node model behaved similarly to the previously described 2-node model (fig. S18, B to D), a global sensitivity analysis showed LFY

levels were more sensitive to FT-related parameters than to LFY's basal production rate (fig. S18E). Taken together, our data and modeling suggest that *TFL1* integrates floral cue intensity and FT levels via LFY.

TFL1 up-regulation buffers *LFY* accumulation under strong floral inductive cues

Shoot indeterminacy is insensitive to environmental perturbation (*6–11*). We propose that the function of the LFY-TFL1 negative feedback loop is to dynamically buffer *LFY* transcript accumulation, thereby ensuring robust maintenance of indeterminacy when florally-inductive signals and FT levels fluctuate, such as at the onset of flower formation. To rigorously test this hypothesis, we induced the I1-to-I2 transition in short-day-grown plants using a strong FRP photoperiod stimulus and assessed daily changes in *LFY* and *TFL1* levels in the center of the inflorescence meristem via time-course whole-mount FISH. After a single 24-hour treatment (+FRP), plants were transferred to long-day photoperiod (LD) to allow continued inflorescence development (fig. S19A).

As expected, immediately after induction by FRP, both *LFY* and *TFL1* levels increased in the inflorescence meristem (Fig. 5, A and B, and fig. S19B). One day later (+FRP+1LD), *TFL1* levels increased further to reach their maximum, while *LFY* expression declined, consistent with a functional negative feedback loop (Fig. 5, A and B). By +FRP+2LD, the *TFL1* level decreased, likely due to reduced *LFY* levels (Fig. 5, A and B). From +FRP+3LD onwards, the levels of *TFL1* and *LFY* moved toward a steady state, and stabilized at levels approximately two-fold higher than their starting points (Fig. 5, A and B). Similar dynamics were also observed in transgenic rescue plants (gTFL1-mEGFP *tfl1-1*; fig. S20, A to C) and in wild-type plants exposed to strong floral cues later in development (fig. S21). Consistent with the presence of an intact feedback loop, all plants maintained inflorescence indeterminacy (figs. S19E and S20D).

We next incorporated this experimental timeline into our 3-node FT, LFY, and TFL1 computational model, using estimated FT inputs based on experimental treatments (Fig. 5, A and B, and fig. S19A) and known kinetics for FT protein levels under changing inductive conditions (*38*) (supplementary text). Using the pulsed FT input, we re-parameterized the model, identifying N=1,617 sets of parameters that faithfully recapitulated the observed temporal dynamics of *LFY* and *TFL1* accumulation in the wild type and did not alter other outcomes of the 3-node model (fig. S22). Incorporating the time-course data helped constrain the acceptable parameter space, particularly for LFY and TFL1 degradation rates (fig. S22A as compared to fig. S18A).

Using the updated model, we simulated scenarios in which LFY activity was compromised, such as in deletion of region VII, *lfy* mutant or mutation of LFY binding sites. In all cases, the model predicted disruption of feedback loop dynamics, including a failure to re-establish steady-state expression due to insufficient *TFL1* up-regulation, followed by *LFY* overaccumulation (Fig. 5F and fig. S22E). These predictions were then validated experimentally. For instance, when LFY binding to the *TFL1* locus is reduced by deletion of most of region VII via CRISPR editing (criVII, fig. S2C), *TFL1* failed to accumulate at timepoint +FRP+1LD and, as a consequence, *LFY* over accumulated (Fig. 5C and fig. S19, B and C). Even stronger effects were seen in plants that lack the entire region VII (dVII gTFL1-mEGFP *tfl1-1*; fig. S20, A to C). Reduced *TFL1* accumulation and *LFY* overaccumulation were also observed in mLFYBS gTFL1-mEGFP *tfl1-1* transgenic plants (fig. S20, A to C) and in *lfy-1* mutants (fig. S19, B and D). Lastly, as expected, FRP triggered inflorescence meristem determinacy in all plant lines where the negative feedback loop is defective and that have a functional copy of LFY (i.e., criVII, dVII *tfl1*, and mLFYBS *tfl1*; fig. S19E and fig. S20D). These findings confirm that proper feedback loop dynamics are essential for the rapid return of LFY to a steady state, this buffers environmental cues that result in elevated FT levels and threaten shoot indeterminacy.

To further probe the buffering capacity of the negative feedback loop, we tested its response to a two-fold change in *TFL1* gene dosage, as observed in phenotypically wild-type *tfl1-1* heterozygotes (*15*). Gene dosage changes provide a physiologically relevant test for robustness in biological systems (*39*). The model predicted that this would affect the amplitude, but not the timing, of the negative feedback loop dynamics (Fig. 5G and fig. S22, E and F). Experimental data supported this prediction (Fig. 5D). Compared to wild type, *tfl1-1* heterozygotes exhibited slightly elevated *LFY* and substantially increased *TFL1* expression immediately following the stimulus. Near wild-type *LFY* levels are reached one day later, at the same time-point when the wild type displays reduced *LFY* accumulation (+FRP+1LD). One day later, *TFL1* levels reach low steady-state levels in both genotypes. This suggests that the negative feedback loop dynamically increases *TFL1* to compensate for reduced gene dosage, effectively curbing LFY overaccumulation in *tfl1-1* heterozygote plants.

At first glance, it may seem counterintuitive to couple the up-regulation of the indeterminacy-promoting factor *TFL1* to LFY, a key promoter of floral fate whose overaccumulation can trigger inflorescence meristem determinacy (*25*). To explore the biological rationale for this configuration, we rewired the computer model (Fig. 5H) by eliminating LFY-mediated *TFL1* regulation and instead constitutively elevated TFL1 levels. The rewired model failed to attenuate the LFY accumulation during the strong pulse of FT (Time 3; Fig. 5, H and I, and fig. S22E). This suggests that the buffering capacity of the system relies on dynamic TFL1 up-regulation that occurs in parallel with rising LFY levels, thereby limiting LFY accumulation, especially under fluctuating environmental conditions (Fig. 5, H and I, and fig. S22E). In other words, the feedback loop enables *TFL1* to be induced in proportion to the strength of floral signals, ensuring that peak LFY expression is suppressed, LFY decays rapidly, and inflorescence meristem indeterminacy is preserved even in the face of strong inductive cues (Fig.

5I and fig. S22E).

Exit from the negative feedback loop

We next investigated how the LFY-TFL1 negative feedback loop behaves when LFY is strongly overexpressed, a condition known to trigger inflorescence determinacy (*25*). To do so, we analyzed an allelic series of gLFY transformants displaying a gradient of expression levels (fig. S23, A to C) (*40*). In this series, 47.8% of the gLFY plants (n=46) formed terminal flowers very early (<1 cm bolt inflorescence). Whole-mount FISH in the remaining plants (n=22, at 1 cm bolt) revealed that when *LFY* levels were slightly elevated, *LFY* and *TFL1* levels remained positively correlated and inflorescence meristems were indeterminate (fig. S23, A to C), consistent with an active LFY-TFL1 negative feedback loop. Transformants showing higher *LFY* levels, however, displayed a decrease in *TFL1* accumulation and failed to maintain inflorescence indeterminacy (fig. S23, A to C). To probe the limits of feedback regulation, we turned to computational modeling. Simulations indicated that *TFL1* up-regulation by LFY and *LFY* repression by TFL1 saturate at high LFY levels (fig. S23, D and E). This saturation could limit the buffering capacity of the negative feedback loop. However, the model failed to reproduce the observed anti-correlation between *LFY* and *TFL1* levels in the inflorescence meristem of gLFY T1 plants that converted to a terminal flower (fig. S23D). Indeed, a reduction in *TFL1* is also observed in terminating inflorescence meristems of the *tfl1-1* mutants (fig. S23F). Thus, loss of *TFL1* expression likely requires additional factor(s), here termed X, that are directly or indirectly up-regulated by strongly elevated LFY and that repress *TFL1* expression during inflorescence meristem commitment to terminal flower fate (fig. S23G). To test this hypothesis, we extended our model to include the hypothetical factor(s) X, forming a 4-node regulatory circuit (fig. S24, A to E). Adding factor(s) X did not alter previous model outcomes but allowed the model to predict exit from the negative feedback loop and the loss of *TFL1* levels observed when LFY levels are strongly elevated (fig. S24, B to E). The expanded model provides a plausible mechanism for how LFY overaccumulation can overcome the buffering capacity of the negative feedback loop mechanism, repress *TFL1*, and initiate commitment to terminal flower fate.

Context specific response of two meristems in close proximity

Lateral meristems of the inflorescence rapidly adapt floral fate and determinacy in response to floral inductive cues and elevated FT, while the inflorescence meristem remains indeterminate. This raises a key question: how can two closely positioned meristems (the inflorescence meristem and lateral meristems at the shoot apex; fig. S1A) respond differentially to the same systemic signal? Both FRP and FT increased *LFY* expression in the inflorescence meristem and in the lateral meristems of I2 inflorescences (Fig. 4, A and C). However, we observed that while LFY strongly up-regulated *TFL1* in the inflorescence meristem in response to FRP or FT, it did not trigger activation of *TFL1* expression in lateral meristems (Fig. 4, A, C, E, and F). Similarly, inducible LFY overexpression (35S:LFY-GR) up-regulated *TFL1* in the inflorescence meristem but not in lateral meristems or flowers (fig. S11, C and F). These findings support the idea that up-regulation of *TFL1* by LFY is context-dependent. In this scenario, lateral meristems are unable to support *TFL1* up-regulation by LFY because they lack an activator or express a repressor of this program.

In our 4-node model above, we introduced hypothetical factor(s) X that repress *TFL1* expression in response to strongly elevated LFY levels during inflorescence meristem termination (figs. S23G and S24). This switch from direct activation to indirect repression of *TFL1* by LFY provides a mechanism for exiting the feedback loop. It is conceivable that factor(s) X could also prevent *TFL1* up-regulation in lateral meristems after the floral transition. To achieve this, we predict increased levels of factor(s) X in the lateral meristem relative to the inflorescence meristem. One mechanism for this is a higher basal X expression rate in lateral meristems. Indeed, simulations with elevated X production in lateral meristems predict markedly reduced TFL1 levels compared to the inflorescence meristem (fig. S24F), supporting a role for factor(s) X in repressing *TFL1* in this context. Alternatively, co-factors that promote the activation of *X* by LFY might be present specifically in lateral meristems and boost X accumulation (fig. S24G). Through these mechanisms, our model provides a testable framework for how two meristems located in close proximity at the shoot apex can exhibit differential response to the same systemic signal (FT) such that lateral meristems, but not the inflorescence meristem, commit to floral fate.

Discussion

We set out to understand how two cell populations in close proximity can manifest opposite responses to an environmentally triggered systemic signal (*12*) and to elucidate the mechanism that programs developmental robustness to environmental cues. We identify a negative feedback loop where LFY can promote indeterminacy in inflorescence meristems by upregulating *TFL1* expression, in addition to its known role in promoting flower fate and determinacy in the lateral meristems (*25*, *26*). We show that up-regulation of *TFL1* by LFY is blocked in lateral meristems that adopt a floral fate.

The role for LFY in promoting indeterminacy may be ancestral while its role in floral fate and determinacy may be derived (*41*, *42*). Promoting indeterminacy is the main role of LFY orthologs in monocots like rice (*43*, *44*). Furthermore, based on published data (*45*, *46*), we find evidence that the negative feedback loop we identified is likely conserved in other indeterminate eudicots such as Antirrhinum, even though the expression of the *LFY* ortholog *FLO* was not detected in the shoot center, likely due to use of lower sensitivity ISH methods. Our computational simulations, together with experimental data in *Arabidopsis* indicate that the robust maintenance of inflorescence meristem indeterminacy under fluctuating environmental signals depends on the negative

feedback loop. The feedback loop uniquely supports transcriptional up-regulation of *TFL1* by LFY in a manner that is proportional to cue/input intensity (FT levels), which dynamically keeps LFY from over accumulating. The LFY-TFL1 negative feedback loop also buffers genetic perturbation such as reduction in *TFL1* dose in heterozygous mutants. We propose the negative feedback loop as an ideal mechanism for local phenotypic robustness to strong incoming (environmental) signals important for development.

How do lateral meristems escape the indeterminacy program, given that LFY is also activated in these meristems? We find that even under very strong inductive cues and when expressed at high levels LFY triggers *TFL1* transcription only in the inflorescence meristem not in lateral meristems. This is not due to differential chromatin accessibility of its target loci, because the pioneer factor LFY binds both floral targets and *TFL1* in the context of nucleosomes (*14*) (fig. S2F). Instead, absence of activators that promote *TFL1* up-regulation together with LFY in the inflorescence meristem or presence of repressors that repress *TFL1* expression in the lateral meristems likely prevent LFY from actuating the indeterminacy program. In support of this idea, unlike LFY alone, LFY fused to a strong activation domain (VP16) can stimulate *TFL1* expression outside of the inflorescence meristem (*22*, *47*, *48*). When LFY is overexpressed in the inflorescence meristem, additional factor(s) we named X are required to exit the feedback loop, leading to loss of *TFL1* expression and commitment to floral fate. Simulations further show that if X levels are higher in the lateral meristems than in the inflorescence meristem, lateral meristems can escape the indeterminacy program triggered by LFY and instead adopt floral fate in response to florally inductive cues. Our data thus predict that factor(s) X may generate the context specific response to a shared systemic signal in two adjacent meristem types. In this manner, *Arabidopsis* inflorescences exhibit environmentally responsive plasticity in the lateral meristems and phenotypic robustness in the inflorescence meristem. This enables both early and continued production of flowers, a likely adaptation to fluctuating environments.

Materials and methods

Plant materials and growth conditions

tfl1-1 (*15*), *lfy-1* (*26*), *lfy-2* (*26*), gTFL1-GFP *tfl1-1* (*7*), gGLFY *lfy-1* (*7*), pLFY-GLFY *lfy-12* (*31*), 35S:TFL1 (*5*) are in the Col-0 ecotype. All mutants (*tfl1-1*, *lfy-1*, *lfy-2*, *lfy-12*) used in this study have recessive loss-of-function alleles generated by EMS mutagenesis and are able to produce mRNA with mutations (*15*, *26*). *tfl1-1* is a strong missense mutation (*15*). *lfy-1* and *lfy-12* have the same strong nonsense mutation, while *lfy-2* contains a missense mutation and shows weaker mutant phenotype compared to *lfy-1* (*26*). The *lfy-1* allele was maintained using traffic lines (*49*, *50*). *tfl1-1* heterozygotes were obtained by crossing to wild-type Col-0. gTFL1-GFP *lfy-1* was obtained by crossing gTFL1-GFP *tfl1-1* to *lfy-1* heterozygotes. 35S:LFY-GR (*29*) was in Landsberg *erecta* background. Genotyping primers are listed in table S1. Plants were grown on soil in long day (LD) conditions (22°C, 110-120 µmol/m^2/s, 16-hour light/8-hour dark), in short day (SD) conditions (22°C, 110-120 µmol/m^2/s, 8-hour light/16-hour dark), or treated with far-red light enriched long-day photoperiod (FRP) (red:far-red ratio = 0.08, 22°C, 110-120 µmol/m^2/s). For 24-hour FRP treatments, I1 phase plants from SD conditions (fig. S19A) or I2 phase plants from LD conditions (fig. S21) were grown under constant FRP light for 24 hours (*7*, *8*). For fig. S16A, vegetative phase plants (5 LD) were treated by 16-hour FRP/8-hour dark cycles for 5 days.

Phenotyping

Rosette leaf number (at 1 cm bolt) or branch number on the primary inflorescence were used to measure the duration of the vegetative or I1 phase, respectively. Determinacy/indeterminacy (presence/absence of terminal flowers) was scored at the end of inflorescence development (start of senescence). For determinate inflorescences, flowers formed on the primary inflorescence were counted to measure the length of the I2 phase. Photos were taken with a Canon EOS Rebel T5 digital camera.

Identification of TFL1 *regulatory regions*

Phylogenetic shadowing was performed using mVista (*51*, *52*) alignment program Shuffle-LAGAN (*53*) with default settings on *TFL1* genomic sequences from *Arabidopsis thaliana* (TAIR10, Chr5:1020101-1028600), *Arabidopsis halleri* (FJVB01000049.1, 621687-631371), *Arabidopsis lyrata* (NW_003302550.1, 1210060-1219981), *Capsella bursa-pastoris* (KX139002.1) (*21*), and *Capsella rubella* (NW_006238918.1, 1006052-1021998). Transcription factor occupancy based on ChIP-seq or DAP-seq is from the ReMap 2022 database (*23*). *cis*-regulatory regions studied are (V Chr5:1023389-1023844, VI Chr5:1022489-1023188, VII Chr5:1021587-1022113). LFY ChIP-seq (*14*) and MNase-seq before and after LFY binding (*14*) was obtained from the GEO repository (GSE141704 and GSE141705 bigWig files) and displayed using the integrative genomics viewer (*54*). LFY binding sites in region VII were determined by MORPHEUS (*27*, *28*) using a score limit of -20.

Transgenic plants

TFL1 (AT5G03840) genomic constructs consist of 3229-bp 5′ intergenic and *TFL1* genomic sequence (Chr5:1024763-1027991), mEGFP with a GGGTPGL linker (5′-GGAGGAGGTACCCCCGGGCTC-3′) (*55*), 4613-bp wild-type *TFL1* 3′ intergenic sequences (Chr5:1020147-1024759) (for gTFL1-mEGFP), or *TFL1* 3′ intergenic sequences with regulatory region deletions (for dV, dVI, dVII gTFL1-mEGFP), or LFY binding site mutations (for mLFYBS gTFL1-mEGFP) in pCAMBIA1300; mLFYBS region VII was synthesized (GENEWIZ). Resulting constructs were transformed into *tfl1-1*, and T1 primary transformants were selected on half strength Murashige and Skoog medium (1/2MS) containing 15-25 µg/mL hygromycin B. At least two independent T2 lines with single transgene-insertion-site showing 3:1 segregation for hygromycin

resistance (binomial exact test, *p*-value>0.4) and median expression levels were selected and propagated to obtain homozygous T3 or T4 offspring. To investigate transgene expression level in wild-type morphology plants (Fig. 4E and figs. S6 and S16), the transgenic plants in *tfl1* background were backcrossed to wild-type Col-0, and F1 plants (*tfl1*/+) were used for analyses.

The dexamethasone-inducible amiRLFY construct is comprised of the driver module (pTFL1-GR-LhG4) of 2195-bp 5′ *TFL1* promoter (Chr5:1025797-1027991), the coding sequence of the synthetic transcription factor GR-LhG4 (*56*), 4613-bp wild-type *TFL1* 3′ intergenic sequences (Chr5:1020147-1024759) plus the E9 terminator and the effector module (pOp6-amiRLFY) of pOp6 containing six lac operators and a minimal 35S promoter, artificial microRNA amir-lfy-1 (*57*) targeting *LFY* (AT5G61850), and the NOS terminator (from nopaline synthase gene). pTFL1-GR-LhG4_pOp6-amiRLFY in pCAMBIA1300 was transformed into gGLFY *lfy-1*. For dexamethasone-inducible FT (AT1G65480) overexpression, the UBQ10 promoter (Chr4:2716559-2718558) was used to drive the expression of GR-LhG4, and pOp6 drives TMV Ω translational enhancer (*58*) and the coding sequences of FT (AT1G65480.2) fused with mTagBFP2. pUBQ10-GR-LhG4_pOp6-FT-mTagBFP2-myc was transformed into Col-0. Transgenic line selection, and identification of single-site-insertion plants for further analysis was as described above, except that T1 plants were screened for inducible reduction of GLFY fluorescence for amiRLFY and increase in mTagBFP2 fluorescence for FT overexpression. Homozygous single-site-insertion T3 plants were used for all analyses. gTFL1-mEGFP response to FT overexpression was assessed in the F1 generation of homozygous pUBQ10-GR-LhG4_pOp6-FT-mTagBFP2-myc crossed to homozygous gTFL1-mEGFP *tfl1-1*, dVII gTFL1-mEGFP *tfl1-1*, and mLFYBS gTFL1-mEGFP *tfl1-1*.

To construct the estradiol-inducible GFP degron, the anti-GFP nanobody LaG16 (*59*) fused with the BTB domain of SPOP (*60*) (LaG16-SPOP) was driven by the pOlexA promoter in the pUBQ10-XVE vector (*61*), and the seed fluorescence selection marker pNapA-DsRed (*24*) was added to the construct. The resulting construct pUBQ10-XVE_pOlexA-LaG16-SPOP was transformed into gTFL1-GFP *tfl1-1*. DsRed seed fluorescence were used for T1 transgenic line selection, and transformants were screened for strong estradiol-inducible TFL1-GFP depletion. Inflorescences formed in the axils of rosette leaves of screened T1 transgenic lines were used for phenotypic analyses in fig. S10G. Single-site-insertion T2 or T3 plants were used for RNA FISH analyses.

gLFY (Chr5:24842005-24847234) was cloned into pMCS:GW (*62*) and transformed into Col-0, and T1 transformants were identified on soil by Basta spray (0.1%). Primary inflorescences of T1 plants were examined by RNA FISH from 1 cm shoots, while determinacy was examined in inflorescences formed in the axils of rosette leaves.

CRISPR genome editing

CRISPR genomic deletion constructs for *TFL1* were generated as described (*24*). 20-nt guide RNA spacers for deletion of *TFL1* region VII were designed using CRISPOR (*63*). Two single guide RNA (sgRNA) expression cassettes (U3promoter-spacer-scaffold) were cloned into pFGCI2-Cas9 (*24*) to create pCRISPR_TFL1-VII. After transformation into Col-0, T1 transformants were identified based on seed fluorescence, followed by PCR screen for VII deletion in the T1 population with primers flanking region VII (table S1). One T1 plant (line #13) showed homozygous deletion of VII. In the T2 generation, we selected seeds without Cas9 transgene by seed fluorescence and backcrossed individual T2 plants to Col-0 twice to remove potential off target mutations. The resulting BC1F1 plants #13-1 and #13-4 had different CRISPR deletions and offspring of homozygous second backcross BC2F2 individuals from both were used for all analyses.

For LFY-mScarlet-I gene targeting, we designed one 20-nt guide RNA spacer targeting the *LFY* stop codon (5′-GACGACTT-GCGTTTCTAGTT-3′), followed by cloning into pFGCI2-Cas9 (*24*) as described above. Subsequently, a donor sequence comprised of a left homology arm (Chr5:24842026-24846931), coding sequences of a GGGGS linker, mScarlet-I, a FLAG tag, and a right homology arm (Chr5:24846935-24847855) were cloned into NcoI of pFGCI2-Cas9. After transformation into Col-0, T1 transformants were identified as above except that the PCR screening employed a forward primer from endogenous *LFY* and a reverse primer from mScarlet-I (table S1). In plants with nuclear-localized mScarlet-I fluorescence in the inflorescence apices, the Cas9 transgene was removed as described above and confirmed by PCR tests. Correct targeting of mScarlet-I was confirmed by Sanger sequencing in T3 plant #18-26-1 followed by backcrossed to Col-0 wild type. Experiments were performed in the BC1F1 generation.

Chemical treatments

Dexamethasone inductions employed 5 µM dexamethasone (SIGMA) in 0.1% ethanol 0.015% Silwet-L77 for 35S:LFY-GR nuclear accumulation, amiRLFY expression (pTFL1-GR-LhG4_pOp6-amiRLFY), and FT overexpression (pUBQ10-GR-LhG4_pOp6-FT-mTagBFP2-myc), with 0.1% ethanol 0.015% Silwet-L77 serving as mock control. For the TFL1-GFP degron of pUBQ10-XVE_pOlexA-LaG16-SPOP gTFL1-GFP *tfl1-1*, 10 µM β-estradiol (SIGMA) in 1.1% dimethylsulfoxide (DMSO) 0.015% Silwet-L77 was used, with 1.1% DMSO 0.015% Silwet-L77 serving as mock control. For RNA FISH analyses, 5 µL chemical solution was applied to the center of a 1 cm bolt primary inflorescence apex with a pipette, and treatment duration was overnight (16-20 hours). For phenotypic analyses of amiRLFY and TFL1-GFP degron plants, the inflorescence apex was treated twice, with the second treatment two days after the first treatment to allow continuous depletion of LFY or TFL1.

Dissection of inflorescences

For wholemount RNA FISH, wholemount IHC, and fluorescence microscopy (top-view), primary inflorescences were manually dissected to expose inflorescence meristems before shoot

elongation (I1 or early I2 phases) or at 1 cm bolt (I2 phase). All leaves and older flowers (beyond stage 4) were removed with forceps or needles under a stereomicroscope. For longitudinal inflorescence sections (side-view fluorescence microscopy or "half-mount" FISH), inflorescences were cut with razor blades under a stereomicroscope to make sections of around 300 µm thickness close to the inflorescence meristems.

RNA fluorescence in situ hybridization (FISH)

RNA FISH based on hybridization chain reactions (HCR RNA FISH) for wholemount inflorescences was as described (*64*). "Half-mount" sections were further cleared after FISH. After post-fixing with 4% paraformaldehyde in PBS for 30 min, sections were washed by DPBS buffer twice, and incubated with ClearSee (*65*) at room temperature in dark for at least a week. To stain the cell walls, cleared sections were incubated in ClearSee containing 0.0025% Calcofluor White (SIGMA) for 10-15 min, followed by one wash with ClearSee. Sections were imaged on slides using ClearSee as mounting medium. HCR FISH hybridization probe sets (table S2) were designed and produced by Molecular Instruments, and HCR amplifiers with fluorescent dyes Alexa Fluor 488, Alexa Fluor 514, Alexa Fluor 546 were used for the amplification steps. Co-detection of RNA FISH and fluorescence proteins was conducted as described (*64*).

Wholemount immunohistochemistry (IHC)

Wholemount IHC was performed on dissected inflorescences as in (*66*) with the following modifications. Fixed and permeabilized inflorescences were blocked by incubating with blocking buffer (2% BSA in 1x MTSB) (*66*) on a rotator at 4°C overnight. For LFY IHC, affinity purified rabbit polyclonal anti-LFY primary antibody (*29*) and anti-rabbit-AlexaFluor488 secondary antibody (Invitrogen, A11034) were used at 1:200 dilution in blocking buffer with 0.1% Tween-20 on a rotator at 4°C overnight. After each antibody incubation, samples were washed with 1x MTSB 3 times (5 min + 1 hour + 1 hour) at room temperature with gentle rotation. Combined LFY IHC and *TFL1* RNA FISH was performed as described (*64*) with LFY antibody treatments as above.

Clearing and staining for fluorescent protein reporters

For imaging fluorescent proteins in longitudinal sections of inflorescences at different stages, sections were fixed, cleared, and stained with Calcofluor White as described (*65*). Sections were imaged on slides using ClearSee as mounting medium. For imaging fluorescent proteins in I2 phase inflorescences (top view), primary inflorescences were dissected, and cell walls were stained with 0.1% propidium iodide solution for 5 min as described (*67*). Inflorescences were inserted in 2% agarose gel in a 60-mm petri dish, and samples were imaged using a water immersion lens without coverslips.

Confocal image acquisition

Confocal images were captured using Leica LAS X software on a Leica Stellaris 5 White Light Laser confocal microscope with an HC PL APO CS2 40×/1.10 W objective or on a Leica TCS SP8 multiphoton confocal microscope with an HC PL APO CS2 20×/0.75 IMM objective. Images (512×512 px or 1024×1024 px) were captured at a bit depth of 8 or 16, and a 0.5, 1, or 2-µm step size was used for acquiring z-stacks. The same laser power and detector gain were used for all samples in the same experiments. Excitation laser wavelength and detection ranges for fluorescent proteins and dyes are listed in table S3.

Confocal image analyses

Maximum intensity projections and longitudinal views of inflorescence confocal z-stacks were generated using FIJI (*68*). For the latter, the z-stack was resliced from top of the image with a 2-µm spacing to obtain a XZ stack. A maximum intensity projection was performed on the ten XZ slices closest to the inflorescence meristem. Single-slice longitudinal sections of LFY-mScarlet-I and GLFY inflorescences were generated in FIJI using "Orthogonal Views". Brightness and contrast of the images were adjusted using FIJI (*68*) or Affinity Designer, with all images of the same experiment adjusted in the identical manner.

Inflorescence developmental stage classification in confocal images was as follows: Inflorescences with shoot apical meristem doming and without flowers were classified as I1 phase, and those with a flower older than stage 3 [flower stages based on (*69*)] as I2 phase. All intervening stages were classified as I1-to-I2 transition.

Quantification of fluorescence or FISH intensity was performed using FIJI (*68*). To quantify the mean intensities in single longitudinal optical sections of fluorescent reporters, a 60-µm-diameter circle at the center of inflorescence meristem (excluding lateral meristems) was selected manually using the oval selection tool, followed by mean intensity measurements for each channel. To quantify the mean intensities of top-view inflorescence confocal images, z-stacks (from the epidermis to 58-µm deep layer) were projected using sum slices. In the z-projection image, a 60-µm-diameter circle at the center of the inflorescence meristem (excluding lateral meristems) was selected manually and the mean intensity was measured for each channel. The distribution of fluorescence and FISH intensities in a top-view confocal images reflects intensities in annuli of different inner and outer radiuses at the center of the inflorescence meristem for each channel in the sum slice z-projection. Mean intensity in each annulus were calculated by dividing the integrated density in the annulus by the area of the annulus.

ChIP assay

ChIP was conducted in F2 plants of 35S:LFY-GR crossed to gTFL1-mEGFP *tfl1-1* or to mLFYBS gTFL1-mEGFP *tfl1-1* grown on 1/2MS plates in long-day conditions treated with 5 µM dexamethasone solution (5 µM dexamethasone 0.1% ethanol) or with mock solution (0.1% ethanol) on day 14. Plants were submerged in the solution for 4 hours and allowed to grow in plates with residual solutions for another 20 hours. 350-450 mg seedlings were

harvested for each biological replicate. ChIP assay was performed as described in (*70*) with rabbit polyclonal anti-LFY antibody (*29*) (1:100 dilution) using primer sets specific to WT or mLFYBS region VII (table S1 and fig. S2E). ChIP signals were normalized to input (*70*).

Reverse transcription (RT)–qPCR

To identify representative transgenic lines for *tfl1-1* mutants rescued by gTFL1-mEGFP constructs, we measured the abundance of *TFL1-mEGFP* transcripts in T2 plant whole inflorescences. Since independent transgenic lines showed wide variations in flowering time, we synchronized the plants by growing them in short day conditions for 14 days, followed by transfer to long-day conditions for 6 days. RNA was extracted from whole inflorescences (including inflorescence meristems and lateral meristems) after trimming leaves longer than 5 mm. 10-15 inflorescences from each transgenic line were harvested per replicate. To compare the *TFL1* levels in whole inflorescences of Col-0 wild type and criVII lines, plants were grown in long-day conditions, and inflorescences (5 inflorescences per replicate) were harvested as described above on day 16. To test whether the deletion or mutations of LFY binding sites affects the response to LFY overexpression in the whole inflorescences, long-day-grown F1 plants of gTFL1-mEGFP *tfl1-1*, dVII gTFL1-mEGFP *tfl1-1*, or mLFYBS gTFL1-mEGFP *tfl1-1* crossed to 35S:LFY-GR were treated on day 16 with dexamethasone or mock solution for 24 hours and ten inflorescences per replicate were harvested as described above.

RNA was extracted using the RNeasy kit with on-column deoxyribonuclease digestion (Qiagen), and complementary DNA was synthesized by SuperScript III first-strand synthesis system (Invitrogen). Quantitative PCR was performed using PowerUp SYBR master mix (Applied Biosystems) on a QuantStudio 3 machine. *TFL1* (or *mEGFP*) expression level was normalized to the internal control *ACTIN 2* (*ACT2*), and the 2^-ddCt method (*71*) was used to normalize the expression level of the treated sample to the mock control. Primers used are listed in table S1.

Statistical analyses

For phenotypic analyses, means of rosette leaf number or branch number were compared between genotypes by unpaired two-tailed Welch's *t*-test, and differences in determinate proportions of two populations were tested by the Fisher's exact test. To compare gene expression levels (RT-qPCR, fluorescence intensity, or RNA FISH intensity), unpaired two-tailed Welch's *t*-tests were used to compare two groups. Kruskal-Wallis test followed by Dunn's test (significance level 0.05) was used to compare the Sobol' indices in the global sensitivity analyses of our computer models. All statistical analyses were performed in R or Microsoft Excel.

REFERENCES AND NOTES

1. Y. Zhu, D. Wagner, Plant Inflorescence Architecture: The Formation, Activity, and Fate of Axillary Meristems. *Cold Spring Harb. Perspect. Biol.* **12**, a034652 (2020). doi:10.1101/cshperspect.a034652 Medline
2. Y. Eshed, Z. B. Lippman, Revolutions in agriculture chart a course for targeted breeding of old and new crops. *Science* **366**, eaax0025 (2019). doi:10.1126/science.aax0025 Medline
3. R. Claßen-Bockhoff, K. Bull-Hereñu, Towards an ontogenetic understanding of inflorescence diversity. *Ann. Bot. (Lond.)* **112**, 1523–1542 (2013). doi:10.1093/aob/mct009 Medline
4. R. Benlloch, A. Berbel, A. Serrano-Mislata, F. Madueño, Floral initiation and inflorescence architecture: A comparative view. *Ann. Bot. (Lond.)* **100**, 659–676 (2007). doi:10.1093/aob/mcm146 Medline
5. O. J. Ratcliffe, I. Amaya, C. A. Vincent, S. Rothstein, R. Carpenter, E. S. Coen, D. J. Bradley, A common mechanism controls the life cycle and architecture of plants. *Development* **125**, 1609–1615 (1998). doi:10.1242/dev.125.9.1609 Medline
6. F. D. Hempel, P. C. Zambryski, L. J. Feldman, Photoinduction of flower identity in vegetatively biased primordia. *Plant Cell* **10**, 1663–1676 (1998). doi:10.1105/tpc.10.10.1663 Medline
7. Y. Zhu, S. Klasfeld, C. W. Jeong, R. Jin, K. Goto, N. Yamaguchi, D. Wagner, TERMINAL FLOWER 1-FD complex target genes and competition with FLOWERING LOCUS T. *Nat. Commun.* **11**, 5118 (2020). doi:10.1038/s41467-020-18782-1 Medline
8. F. D. Hempel, D. Weigel, M. A. Mandel, G. Ditta, P. C. Zambryski, L. J. Feldman, M. F. Yanofsky, Floral determination and expression of floral regulatory genes in Arabidopsis. *Development* **124**, 3845–3853 (1997). doi:10.1242/dev.124.19.3845 Medline
9. S. Balasubramanian, S. Sureshkumar, J. Lempe, D. Weigel, Potent induction of Arabidopsis thaliana flowering by elevated growth temperature. *PLOS Genet.* **2**, e106 (2006). doi:10.1371/journal.pgen.0020106 Medline
10. C. Ibañez, Y. Poeschl, T. Peterson, J. Bellstädt, K. Denk, A. Gogol-Döring, M. Quint, C. Delker, Ambient temperature and genotype differentially affect developmental and phenotypic plasticity in Arabidopsis thaliana. *BMC Plant Biol.* **17**, 114 (2017). doi:10.1186/s12870-017-1068-5 Medline
11. X. Ma, N. L. Sukiran, H. Ma, Z. Su, Moderate drought causes dramatic floral transcriptomic reprogramming to ensure successful reproductive development in Arabidopsis. *BMC Plant Biol.* **14**, 164 (2014). doi:10.1186/1471-2229-14-164 Medline
12. L. Corbesier, C. Vincent, S. Jang, F. Fornara, Q. Fan, I. Searle, A. Giakountis, S. Farrona, L. Gissot, C. Turnbull, G. Coupland, FT protein movement contributes to long-distance signaling in floral induction of Arabidopsis. *Science* **316**, 1030–1033 (2007). doi:10.1126/science.1141752 Medline
13. P. Prusinkiewicz, Y. Erasmus, B. Lane, L. D. Harder, E. Coen, Evolution and development of inflorescence architectures. *Science* **316**, 1452–1456 (2007). doi:10.1126/science.1140429 Medline
14. R. Jin, S. Klasfeld, Y. Zhu, M. Fernandez Garcia, J. Xiao, S.-K. Han, A. Konkol, D. Wagner, LEAFY is a pioneer transcription factor and licenses cell reprogramming to floral fate. *Nat. Commun.* **12**, 626 (2021). doi:10.1038/s41467-020-20883-w Medline
15. S. Shannon, D. R. Meeks-Wagner, A Mutation in the Arabidopsis TFL1 Gene Affects Inflorescence Meristem Development. *Plant Cell* **3**, 877–892 (1991). doi:10.2307/3869152 Medline
16. D. Bradley, O. Ratcliffe, C. Vincent, R. Carpenter, E. Coen, Inflorescence commitment and architecture in Arabidopsis. *Science* **275**, 80–83 (1997). doi:10.1126/science.275.5296.80 Medline
17. L. Conti, D. Bradley, TERMINAL FLOWER1 is a mobile signal controlling Arabidopsis architecture. *Plant Cell* **19**, 767–778 (2007). doi:10.1105/tpc.106.049767 Medline
18. M. Cerise, V. da Silveira Falavigna, G. Rodríguez-Maroto, A. Signol, E. Severing, H. Gao, A. van Driel, C. Vincent, S. Wilkens, F. R. Iacobini, P. Formosa-Jordan, A. Pajoro, G. Coupland, Two modes of gene regulation by TFL1 mediate its dual function in flowering time and shoot determinacy of Arabidopsis. *Development* **150**, dev202089 (2023). doi:10.1242/dev.202089 Medline
19. D. Goretti, M. Silvestre, S. Collani, T. Langenecker, C. Méndez, F. Madueño, M. Schmid, TERMINAL FLOWER1 Functions as a Mobile Transcriptional Cofactor in the Shoot Apical Meristem. *Plant Physiol.* **182**, 2081–2095 (2020). doi:10.1104/pp.19.00867 Medline
20. K. Kaufmann, F. Wellmer, J. M. Muiño, T. Ferrier, S. E. Wuest, V. Kumar, A.

Serrano-Mislata, F. Madueño, P. Krajewski, E. M. Meyerowitz, G. C. Angenent, J. L. Riechmann, Orchestration of floral initiation by APETALA1. *Science* **328**, 85–89 (2010). doi:10.1126/science.1185244 Medline
21. A. Serrano-Mislata, P. Fernández-Nohales, M. J. Doménech, Y. Hanzawa, D. Bradley, F. Madueño, Separate elements of the TERMINAL FLOWER 1 cis-regulatory region integrate pathways to control flowering time and shoot meristem identity. *Development* **143**, 3315–3327 (2016). doi:10.1242/dev.135269 Medline
22. A. Serrano-Mislata, K. Goslin, B. Zheng, L. Rae, F. Wellmer, E. Graciet, F. Madueño, Regulatory interplay between LEAFY, APETALA1/CAULIFLOWER and TERMINAL FLOWER1: New insights into an old relationship. *Plant Signal. Behav.* **12**, e1370164 (2017). doi:10.1080/15592324.2017.1370164 Medline
23. F. Hammal, P. de Langen, A. Bergon, F. Lopez, B. Ballester, ReMap 2022: A database of Human, Mouse, Drosophila and Arabidopsis regulatory regions from an integrative analysis of DNA-binding sequencing experiments. *Nucleic Acids Res.* **50** (D1), D316–D325 (2022). doi:10.1093/nar/gkab996 Medline
24. T. Bieluszewski, M. Szymanska-Lejman, W. Dziegielewski, L. Zhu, P. A. Ziolkowski, Efficient Generation of CRISPR/Cas9-Based Mutants Supported by Fluorescent Seed Selection in Different Arabidopsis Accessions. *Methods Mol. Biol.* **2484**, 161–182 (2022). doi:10.1007/978-1-0716-2253-7_13 Medline
25. D. Weigel, O. Nilsson, A developmental switch sufficient for flower initiation in diverse plants. *Nature* **377**, 495–500 (1995). doi:10.1038/377495a0 Medline
26. E. A. Schultz, G. W. Haughn, LEAFY, a Homeotic Gene That Regulates Inflorescence Development in Arabidopsis. *Plant Cell* **3**, 771–781 (1991). doi:10.2307/3869271 Medline
27. E. G. Minguet, S. Segard, C. Charavay, F. Parcy, MORPHEUS, a Webtool for Transcription Factor Binding Analysis Using Position Weight Matrices with Dependency. *PLOS ONE* **10**, e0135586 (2015). doi:10.1371/journal.pone.0135586 Medline
28. E. Moyroud, E. G. Minguet, F. Ott, L. Yant, D. Posé, M. Monniaux, S. Blanchet, O. Bastien, E. Thévenon, D. Weigel, M. Schmid, F. Parcy, Prediction of regulatory interactions from genome sequences using a biophysical model for the Arabidopsis LEAFY transcription factor. *Plant Cell* **23**, 1293–1306 (2011). doi:10.1105/tpc.111.083329 Medline
29. D. Wagner, R. W. Sablowski, E. M. Meyerowitz, Transcriptional activation of APETALA1 by LEAFY. *Science* **285**, 582–584 (1999). doi:10.1126/science.285.5427.582 Medline
30. M. A. Blázquez, L. N. Soowal, I. Lee, D. Weigel, LEAFY expression and flower initiation in Arabidopsis. *Development* **124**, 3835–3844 (1997). doi:10.1242/dev.124.19.3835 Medline
31. X. Wu, J. R. Dinneny, K. M. Crawford, Y. Rhee, V. Citovsky, P. C. Zambryski, D. Weigel, Modes of intercellular transcription factor movement in the Arabidopsis apex. *Development* **130**, 3735–3745 (2003). doi:10.1242/dev.00577 Medline
32. A. Sessions, M. F. Yanofsky, D. Weigel, Cell-cell signaling and movement by the floral transcription factors LEAFY and APETALA1. *Science* **289**, 779–782 (2000). doi:10.1126/science.289.5480.779 Medline
33. F. Parcy, O. Nilsson, M. A. Busch, I. Lee, D. Weigel, A genetic framework for floral patterning. *Nature* **395**, 561–566 (1998). doi:10.1038/26903 Medline
34. D. S. Glass, X. Jin, I. H. Riedel-Kruse, Nonlinear delay differential equations and their application to modeling biological network motifs. *Nat. Commun.* **12**, 1788 (2021). doi:10.1038/s41467-021-21700-8 Medline
35. S. Shannon, D. R. Meeks-Wagner, Genetic Interactions That Regulate Inflorescence Development in Arabidopsis. *Plant Cell* **5**, 639–655 (1993). doi:10.2307/3869807 Medline
36. Y. H. Song, A. Kubota, M. S. Kwon, M. F. Covington, N. Lee, E. R. Taagen, D. Laboy Cintrón, D. Y. Hwang, R. Akiyama, S. K. Hodge, H. Huang, N. H. Nguyen, D. A. Nusinow, A. J. Millar, K. K. Shimizu, T. Imaizumi, Molecular basis of flowering under natural long-day conditions in Arabidopsis. *Nat. Plants* **4**, 824–835 (2018). doi:10.1038/s41477-018-0253-3 Medline
37. S. Y. Kim, X. Yu, S. D. Michaels, Regulation of CONSTANS and FLOWERING LOCUS T expression in response to changing light quality. *Plant Physiol.* **148**, 269–279 (2008). doi:10.1104/pp.108.122606 Medline
38. S.-J. Kim, S. M. Hong, S. J. Yoo, S. Moon, H. S. Jung, J. H. Ahn, Post-Translational Regulation of FLOWERING LOCUS T Protein in Arabidopsis. *Mol. Plant* **9**, 308–311 (2016). doi:10.1016/j.molp.2015.11.001 Medline
39. M. A. Félix, M. Barkoulas, Pervasive robustness in biological systems. *Nat. Rev. Genet.* **16**, 483–496 (2015). doi:10.1038/nrg3949 Medline
40. S. B. Gelvin, Integration of Agrobacterium T-DNA into the Plant Genome. *Annu. Rev. Genet.* **51**, 195–217 (2017). doi:10.1146/annurev-genet-120215-035320 Medline
41. A. R. Plackett, S. J. Conway, K. D. Hewett Hazelton, E. H. Rabbinowitsch, J. A. Langdale, V. S. Di Stilio, *LEAFY* maintains apical stem cell activity during shoot development in the fern *Ceratopteris richardii*. *eLife* **7**, e39625 (2018). doi:10.7554/eLife.39625 Medline
42. C. Sayou, M. Monniaux, M. H. Nanao, E. Moyroud, S. F. Brockington, E. Thévenon, H. Chahtane, N. Warthmann, M. Melkonian, Y. Zhang, G. K.-S. Wong, D. Weigel, F. Parcy, R. Dumas, A promiscuous intermediate underlies the evolution of LEAFY DNA binding specificity. *Science* **343**, 645–648 (2014). doi:10.1126/science.1248229 Medline
43. N. N. Rao, K. Prasad, P. R. Kumar, U. Vijayraghavan, Distinct regulatory role for RFL, the rice LFY homolog, in determining flowering time and plant architecture. *Proc. Natl. Acad. Sci. U.S.A.* **105**, 3646–3651 (2008). doi:10.1073/pnas.0709059105 Medline
44. K. Ikeda-Kawakatsu, M. Maekawa, T. Izawa, J. Itoh, Y. Nagato, ABERRANT PANICLE ORGANIZATION 2/RFL, the rice ortholog of Arabidopsis LEAFY, suppresses the transition from inflorescence meristem to floral meristem through interaction with APO1. *Plant J.* **69**, 168–180 (2012). doi:10.1111/j.1365-313X.2011.04781.x Medline
45. D. Bradley, R. Carpenter, L. Copsey, C. Vincent, S. Rothstein, E. Coen, Control of inflorescence architecture in Antirrhinum. *Nature* **379**, 791–797 (1996). doi:10.1038/379791a0 Medline
46. R. Carpenter, L. Copsey, C. Vincent, S. Doyle, R. Magrath, E. Coen, Control of flower development and phyllotaxy by meristem identity genes in antirrhinum. *Plant Cell* **7**, 2001–2011 (1995). Medline
47. F. Parcy, K. Bomblies, D. Weigel, Interaction of LEAFY, AGAMOUS and TERMINAL FLOWER1 in maintaining floral meristem identity in Arabidopsis. *Development* **129**, 2519–2527 (2002). doi:10.1242/dev.129.10.2519 Medline
48. K. Goslin, B. Zheng, A. Serrano-Mislata, L. Rae, P. T. Ryan, K. Kwaśniewska, B. Thomson, D. S. Ó'Maoiléidigh, F. Madueño, F. Wellmer, E. Graciet, Transcription Factor Interplay between LEAFY and APETALA1/CAULIFLOWER during Floral Initiation. *Plant Physiol.* **174**, 1097–1109 (2017). doi:10.1104/pp.17.00098 Medline
49. G. Wu, G. Rossidivito, T. Hu, Y. Berlyand, R. S. Poethig, Traffic lines: New tools for genetic analysis in Arabidopsis thaliana. *Genetics* **200**, 35–45 (2015). doi:10.1534/genetics.114.173435 Medline
50. R. S. Poethig, W. L. Cullina, E. Doody, T. Floyd, J. P. Fouracre, T. Hu, M. Xu, J. Zhao, Short-interval traffic lines: Versatile tools for genetic analysis in Arabidopsis thaliana. *G3* **12**, jkac202 (2022). doi:10.1093/g3journal/jkac202 Medline
51. C. Mayor, M. Brudno, J. R. Schwartz, A. Poliakov, E. M. Rubin, K. A. Frazer, L. S. Pachter, I. Dubchak, VISTA : Visualizing global DNA sequence alignments of arbitrary length. *Bioinformatics* **16**, 1046–1047 (2000). doi:10.1093/bioinformatics/16.11.1046 Medline
52. K. A. Frazer, L. Pachter, A. Poliakov, E. M. Rubin, I. Dubchak, VISTA: Computational tools for comparative genomics. *Nucleic Acids Res.* **32**, W273–W279 (2004). doi:10.1093/nar/gkh458 Medline
53. M. Brudno, S. Malde, A. Poliakov, C. B. Do, O. Couronne, I. Dubchak, S. Batzoglou, Glocal alignment: Finding rearrangements during alignment. *Bioinformatics* **19** (Suppl 1), i54–i62 (2003). doi:10.1093/bioinformatics/btg1005 Medline
54. J. T. Robinson, H. Thorvaldsdóttir, W. Winckler, M. Guttman, E. S. Lander, G. Getz, J. P. Mesirov, Integrative genomics viewer. *Nat. Biotechnol.* **29**, 24–26 (2011). doi:10.1038/nbt.1754 Medline
55. S. Hanano, K. Goto, Arabidopsis TERMINAL FLOWER1 is involved in the regulation of flowering time and inflorescence development through transcriptional repression. *Plant Cell* **23**, 3172–3184 (2011). doi:10.1105/tpc.111.088641 Medline

56. A.-K. Schürholz, V. López-Salmerón, Z. Li, J. Forner, C. Wenzl, C. Gaillochet, S. Augustin, A. V. Barro, M. Fuchs, M. Gebert, J. U. Lohmann, T. Greb, S. Wolf, A Comprehensive Toolkit for Inducible, Cell Type-Specific Gene Expression in Arabidopsis. *Plant Physiol.* **178**, 40–53 (2018). doi:10.1104/pp.18.00463 Medline
57. R. Schwab, S. Ossowski, M. Riester, N. Warthmann, D. Weigel, Highly specific gene silencing by artificial microRNAs in Arabidopsis. *Plant Cell* **18**, 1121–1133 (2006). doi:10.1105/tpc.105.039834 Medline
58. D. R. Gallie, D. E. Sleat, J. W. Watts, P. C. Turner, T. M. Wilson, Mutational analysis of the tobacco mosaic virus 5′-leader for altered ability to enhance translation. *Nucleic Acids Res.* **16**, 883–893 (1988). doi:10.1093/nar/16.3.883 Medline
59. P. C. Fridy, Y. Li, S. Keegan, M. K. Thompson, I. Nudelman, J. F. Scheid, M. Oeffinger, M. C. Nussenzweig, D. Fenyö, B. T. Chait, M. P. Rout, A robust pipeline for rapid production of versatile nanobody repertoires. *Nat. Methods* **11**, 1253–1260 (2014). doi:10.1038/nmeth.3170 Medline
60. E. Sorge, D. Demidov, I. Lermontova, A. Houben, U. Conrad, Engineered degradation of EYFP-tagged CENH3 via the 26S proteasome pathway in plants. *PLOS ONE* **16**, e0247015 (2021). doi:10.1371/journal.pone.0247015 Medline
61. A. Y. Husbands, A. Feller, V. Aggarwal, C. E. Dresden, A. S. Holub, T. Ha, M. C. P. Timmermans, The START domain potentiates HD-ZIPIII transcriptional activity. *Plant Cell* **35**, 2332–2348 (2023). doi:10.1093/plcell/koad058 Medline
62. M. Michniewicz, E. M. Frick, L. C. Strader, Gateway-compatible tissue-specific vectors for plant transformation. *BMC Res. Notes* **8**, 63 (2015). doi:10.1186/s13104-015-1010-6 Medline
63. J. P. Concordet, M. Haeussler, CRISPOR: Intuitive guide selection for CRISPR/Cas9 genome editing experiments and screens. *Nucleic Acids Res.* **46** (W1), W242–W245 (2018). doi:10.1093/nar/gky354 Medline
64. T. Huang, B. Guillotin, R. Rahni, K. D. Birnbaum, D. Wagner, A rapid and sensitive, multiplex, whole mount RNA fluorescence in situ hybridization and immunohistochemistry protocol. *Plant Methods* **19**, 131 (2023). doi:10.1186/s13007-023-01108-9 Medline
65. D. Kurihara, Y. Mizuta, Y. Sato, T. Higashiyama, ClearSee: A rapid optical clearing reagent for whole-plant fluorescence imaging. *Development* **142**, 4168–4179 (2015). doi:10.1242/dev.127613 Medline
66. T. Pasternak, O. Tietz, K. Rapp, M. Begheldo, R. Nitschke, B. Ruperti, K. Palme, Protocol: An improved and universal procedure for whole-mount immunolocalization in plants. *Plant Methods* **11**, 50 (2015). doi:10.1186/s13007-015-0094-2 Medline
67. O. Hamant, P. Das, A. Burian, *Plant Cell Morphogenesis: Methods and Protocols*, V. Žárský, F. Cvrčková, Eds. (Humana Press, 2014), pp. 111–119.
68. J. Schindelin, I. Arganda-Carreras, E. Frise, V. Kaynig, M. Longair, T. Pietzsch, S. Preibisch, C. Rueden, S. Saalfeld, B. Schmid, J.-Y. Tinevez, D. J. White, V. Hartenstein, K. Eliceiri, P. Tomancak, A. Cardona, Fiji: An open-source platform for biological-image analysis. *Nat. Methods* **9**, 676–682 (2012). doi:10.1038/nmeth.2019 Medline
69. D. R. Smyth, J. L. Bowman, E. M. Meyerowitz, Early flower development in Arabidopsis. *Plant Cell* **2**, 755–767 (1990). Medline
70. N. Yamaguchi, C. M. Winter, M.-F. Wu, C. S. Kwon, D. A. William, D. Wagner, PROTOCOLS: Chromatin Immunoprecipitation from Arabidopsis Tissues. *Arabidopsis Book* **12**, e0170 (2014). doi:10.1199/tab.0170 Medline
71. K. J. Livak, T. D. Schmittgen, Analysis of relative gene expression data using real-time quantitative PCR and the 2(-Delta Delta C(T)) Method. *Methods* **25**, 402–408 (2001). doi:10.1006/meth.2001.1262 Medline
72. C. Hodgens, T. Huang, LFY-TFL1 negative feedback loop model, Zenodo (2025); https://doi.org/10.5281/zenodo.14343022.
73. M. Endo, M. Yoshida, Y. Sasaki, K. Negishi, K. Horikawa, Y. Daimon, K.-I. Kurotani, M. Notaguchi, M. Abe, T. Araki, Re-Evaluation of Florigen Transport Kinetics with Separation of Functions by Mutations That Uncouple Flowering Initiation and Long-Distance Transport. *Plant Cell Physiol.* **59**, 1621–1629 (2018). doi:10.1093/pcp/pcy063 Medline
74. L. F. Shampine, S. Thompson, J. A. Kierzenka, G. D. Byrne, Non-negative solutions of ODEs. *Appl. Math. Comput.* **170**, 556–569 (2005). doi:10.1016/j.amc.2004.12.011
75. K. Cranmer, J. Brehmer, G. Louppe, The frontier of simulation-based inference. *Proc. Natl. Acad. Sci. U.S.A.* **117**, 30055–30062 (2020). doi:10.1073/pnas.1912789117 Medline
76. M. A. Beaumont, W. Zhang, D. J. Balding, Approximate Bayesian computation in population genetics. *Genetics* **162**, 2025–2035 (2002). doi:10.1093/genetics/162.4.2025 Medline
77. C. Hodgens, D. T. Flaherty, A.-M. Pullen, I. Khan, N. J. English, L. Gillan, M. Rojas-Pierce, B. S. Akpa, Model-based inference of a dual role for HOPS in regulating guard cell vacuole fusion. *In Silico Plants* **6**, diae015 (2024). doi:10.1093/insilicoplants/diae015 Medline
78. X. Y. Zhang, M. N. Trame, L. J. Lesko, S. Schmidt, Sobol Sensitivity Analysis: A Tool to Guide the Development and Evaluation of Systems Pharmacology Models. *CPT Pharmacometrics Syst. Pharmacol.* **4**, 69–79 (2015). doi:10.1002/psp4.6 Medline
79. M. Shibata, C. Breuer, A. Kawamura, N. M. Clark, B. Rymen, L. Braidwood, K. Morohashi, W. Busch, P. N. Benfey, R. Sozzani, K. Sugimoto, GTL1 and DF1 regulate root hair growth through transcriptional repression of *ROOT HAIR DEFECTIVE 6-LIKE 4* in *Arabidopsis*. *Development* **145**, dev159707 (2018). doi:10.1242/dev.159707 Medline
80. F. Khorashadi Zadeh, J. Nossent, F. Sarrazin, F. Pianosi, A. van Griensven, T. Wagener, W. Bauwens, Comparison of variance-based and moment-independent global sensitivity analysis approaches by application to the SWAT model. *Environ. Model. Softw.* **91**, 210–222 (2017). doi:10.1016/j.envsoft.2017.02.001
81. U. Alon, *An introduction to systems biology: Design principles of biological circuits* (CRC Press, 2019).
82. J. Bezanson, A. Edelman, S. Karpinski, V. B. Shah, Julia: A Fresh Approach to Numerical Computing. *SIAM Rev.* **59**, 65–98 (2017). doi:10.1137/141000671
83. C. Rackauckas, Q. Nie, DifferentialEquations.jl – A Performant and Feature-Rich Ecosystem for Solving Differential Equations in Julia. *J. Open Res. Softw.* **5**, 15 (2017). doi:10.5334/jors.151
84. S. Christ, D. Schwabeneder, C. Rackauckas, M. K. Borregaard, T. Breloff, Plots.jl – A User Extendable Plotting API for the Julia Programming Language. *J. Open Res. Softw.* **11**, 5 (2023). doi:10.5334/jors.431
85. E. Tankhilevich, J. Ish-Horowicz, T. Hameed, E. Roesch, I. Kleijn, M. P. H. Stumpf, F. He, GpABC: A Julia package for approximate Bayesian computation with Gaussian process emulation. *Bioinformatics* **36**, 3286–3287 (2020). doi:10.1093/bioinformatics/btaa078 Medline
86. V. K. Dixit, C. Rackauckas, GlobalSensitivity.jl: Performant and Parallel Global Sensitivity Analysis with Julia. *J. Open Source Softw.* **7**, 4561 (2022). doi:10.21105/joss.04561
87. Y. Ma, V. Dixit, M. J. Innes, X. Guo, C. Rackauckas, "A Comparison of Automatic Differentiation and Continuous Sensitivity Analysis for Derivatives of Differential Equation Solutions," 2021 IEEE High Performance Extreme Computing Conference, Waltham, MA, 20 to 24 September 2021 (IEEE, 2021).
88. R Core Team, R: A Language and Environment for Statistical Computing. (2023).
89. H. Wickham, *ggplot2: Elegant Graphics for Data Analysis* (Springer, 2016).
90. A. Kassambara, ggpubr: 'ggplot2' Based Publication Ready Plots (2025).
91. A. Pajoro, P. Madrigal, J. M. Muiño, J. T. Matus, J. Jin, M. A. Mecchia, J. M. Debernardi, J. F. Palatnik, S. Balazadeh, M. Arif, D. S. Ó'Maoiléidigh, F. Wellmer, P. Krajewski, J.-L. Riechmann, G. C. Angenent, K. Kaufmann, Dynamics of chromatin accessibility and gene regulation by MADS-domain transcription factors in flower development. *Genome Biol.* **15**, R41 (2014). doi:10.1186/gb-2014-15-3-r41 Medline

ACKNOWLEDGMENTS

We thank A. Husbands for comments on the manuscript. We thank the Penn CDB Microscopy Core (RRID SCR_022373) for the use of confocal microscopes. We thank J. Caplan for advice on tissue clearing for HCR RNA-FISH. We thank anonymous reviewer 2 for suggesting the inclusion of factor(s) X in the model. **Funding:** This work has been funded by National Science Foundation grant IOS 2319036 (D.W.), NSF PGRP BIO-2112058 (R.S.), Ministerio de Ciencia Innovación y Universidades of Spain (PID2021-

122158NB-I00 and CNS2023-143915 to K.W.), and Severo Ochoa (SO) Program for Centres of Excellence in R&D from the Agencia Estatal de Investigación of Spain [grant CEX2020-000999-S (2022 to 2025) to the CBGP].
Author contributions: Conceptualization: D.W., T.H.; Formal analysis: T.H., C.D.H., M.M.; Investigation: T.H., S.P.; Methodology: T.H., C.D.H., M.M.; Software: C.D.H., T.H., R.S., M.M., K.W.; Supervision: D.W., R.S.; Visualization: T.H., D.W.; Writing – original draft: T.H., D.W., C.D.H.; Writing – review and editing: D.W., T.H., C.D.H., R.S., K.W., M.M. **Competing interests:** The authors declare that they have no competing interests. **Data and materials availability:** All codes used in the computer modeling are available on Zenodo (*72*). Other data are available in the main text or the supplementary materials. All reasonable requests for materials will be fulfilled.

SUPPLEMENTARY MATERIALS
science.org/doi/10.1126/science.adv5429
Supplementary Text
Figs. S1 to S25
Tables S1 to S12
References (*73*–*91*)
Reproducibility Checklist

Submitted 23 December 2024; resubmitted 07 August 2025
Accepted 21 October 2025
Published online 22 January 2026
10.1126/science.adv5429

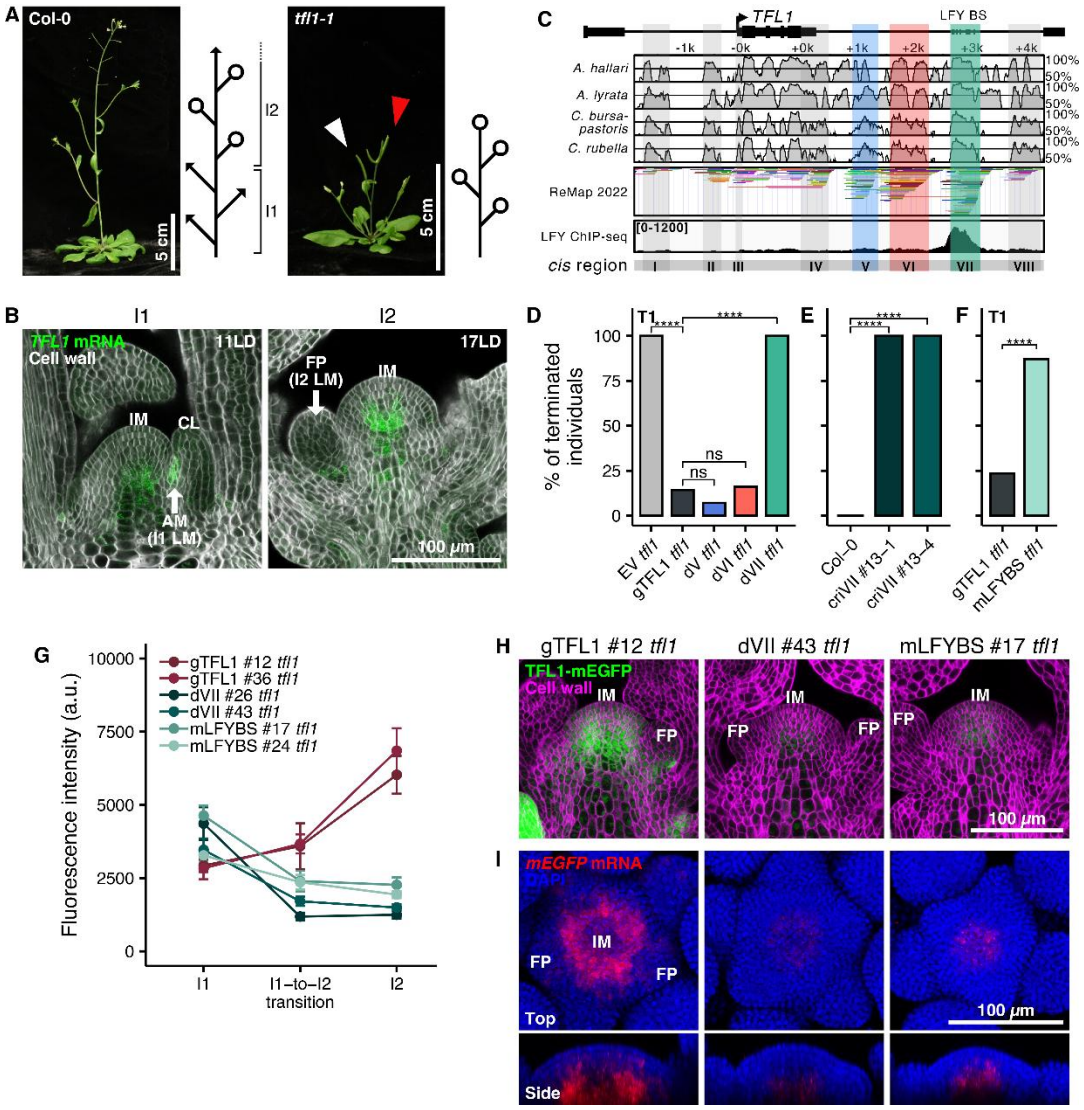

Fig. 1. *TFL1* cis-regulatory region VII and LFY binding sites therein are necessary for *TFL1* up-regulation and inflorescence indeterminacy. (**A**) Indeterminate wild-type (left) and determinate *tfl1-1* (right) inflorescence. Red arrowhead: terminal flower, white arrowhead: flower in lieu of branches. Circles, flowers; arrows, shoots. (**B**) *TFL1* FISH (green) in wild type in I1 (11 LD) and I2 (17 LD) inflorescences (longitudinal sections). Cell wall (Calcofluor-white), white. (**C**) Combined phylogenetic shadowing, ReMap transcription factor binding peaks (*23*), and LFY ChIP-seq (*14*). Sequence conservation with *A. thaliana* (50-100%) is shown for each track (right). Line colors in the ReMap 2022 track represent binding peaks of different transcription factors. Regions tested: V, VI, and VII. (**D**) Determinacy in *tfl1-1* transformed with empty vector (EV, n=28), gTFL1-mEGFP (n=28), or versions thereof with regulatory region deletions: dV (n=28), dVI (n=31), or dVII (n=27). (**E**) Determinacy in wild-type Col-0 and region VII CRISPR deletion lines (n≥10). (**F**) Determinacy in *tfl1-1* transformed with gTFL1 (n=34) or mLFYBS (n=31). [(D) to (F)] Fisher's exact test *p*-values: ns >0.05, **** <0.0001. (**G** and **H**) Quantification (G) and confocal images (H) of gTFL1, dVII, and mLFYBS fluorescence. (G) Mean ± SEM (gTFL1 #12 n_{total}=36, gTFL1 #36 n_{total}=37, dVII #26 n_{total}=45, dVII #43 n_{total}=51, mLFYBS #17 n_{total}=47, mLFYBS #24 n_{total}=55). (H) I2 phase inflorescences (longitudinal sections). mEGFP, green; cell wall (Calcofluor-white), magenta. A.u., arbitrary units. (**I**) Wholemount *mEGFP* FISH (red) in I2 phase gTFL1, dVII, and mLFYBS *tfl1-1* inflorescence meristems (top, maximum intensity projection; bottom, xz longitudinal view). Nuclei (DAPI), blue. IM, inflorescence meristem; LM, lateral meristem; AM, axillary meristem; FP, flower primordium; CL, cauline leaf; LD, long day growth.

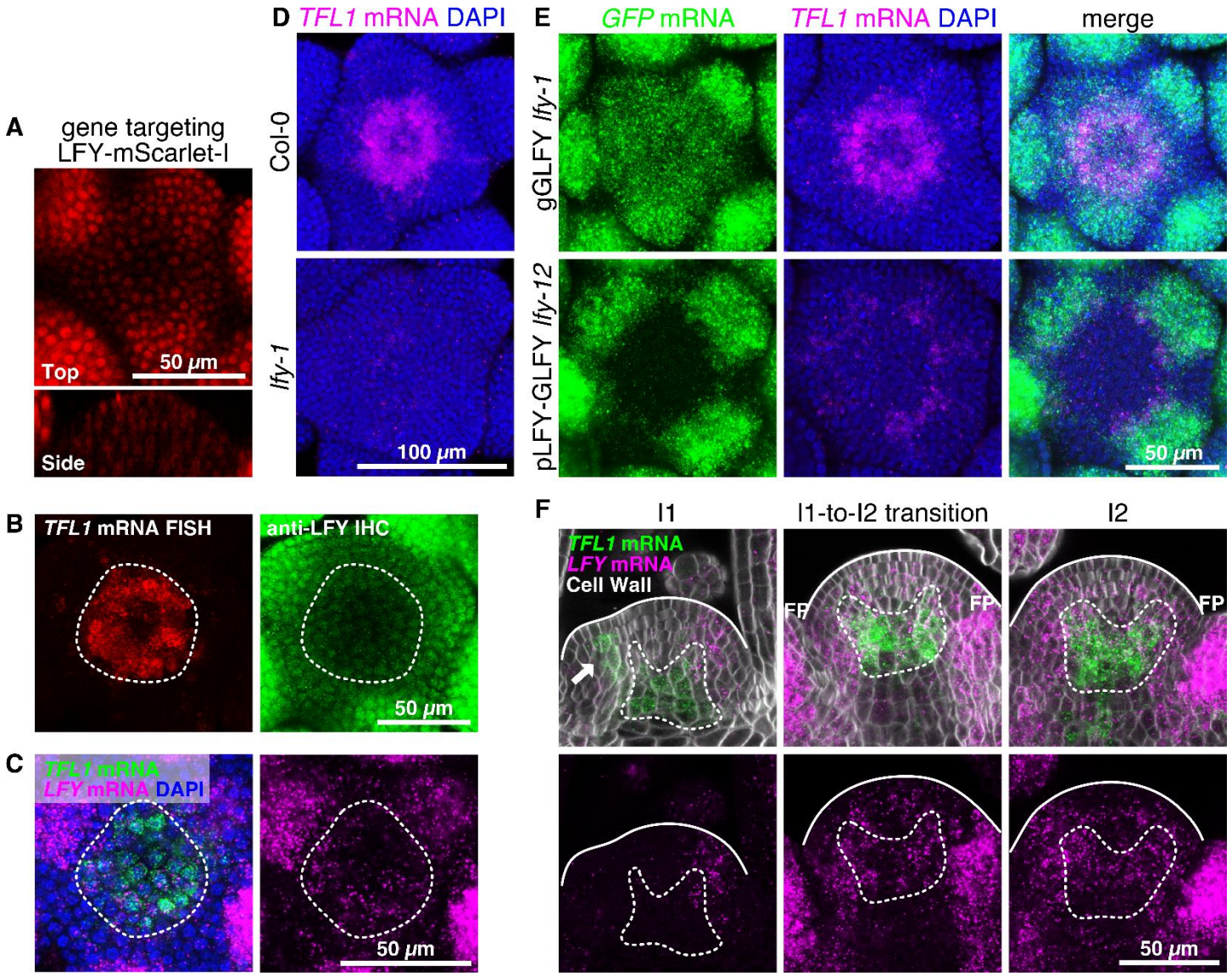

Fig. 2. LFY protein and RNA is present in the center of I2 stage inflorescence meristems in the *TFL1* domain. (**A**) CRISPR gene targeted LFY-mScarlet-I I2 phase inflorescence meristem (top, single optical section; bottom, xz longitudinal view). (**B**) Combined wholemount *TFL1* FISH (left) and LFY immunohistochemistry (right) in wild-type I2 inflorescence meristem center, single optical section. (**C**) Wholemount RNA FISH for *TFL1* (green) and *LFY* (magenta) in wild-type I2 inflorescence meristem center, single optical section. Nuclei (DAPI), blue; left, merged channels; right, *LFY* channel; white dashed lines, *TFL1* expression domain. (**D**) Wholemount *TFL1* FISH (magenta) in I2 phase inflorescences of wild-type Col-0 and *lfy-1* mutant (maximum intensity projections). Nuclei (DAPI), blue. (**E**) Wholemount *GFP* (green) and *TFL1* (magenta) FISH in different LFY translational reporters (maximum intensity projections). Nuclei (DAPI), blue. (**F**) Developmental timeseries RNA FISH for *TFL1* (green) and *LFY* (magenta) in wild-type inflorescence meristems (longitudinal view: top, merged channels; bottom, *LFY* channel). Cell wall (Calcofluor-white), white; arrow, *TFL1* in axillary meristem; solid lines, inflorescence shoot apices; dashed lines, *TFL1* expression domain; FP, flower primordium.

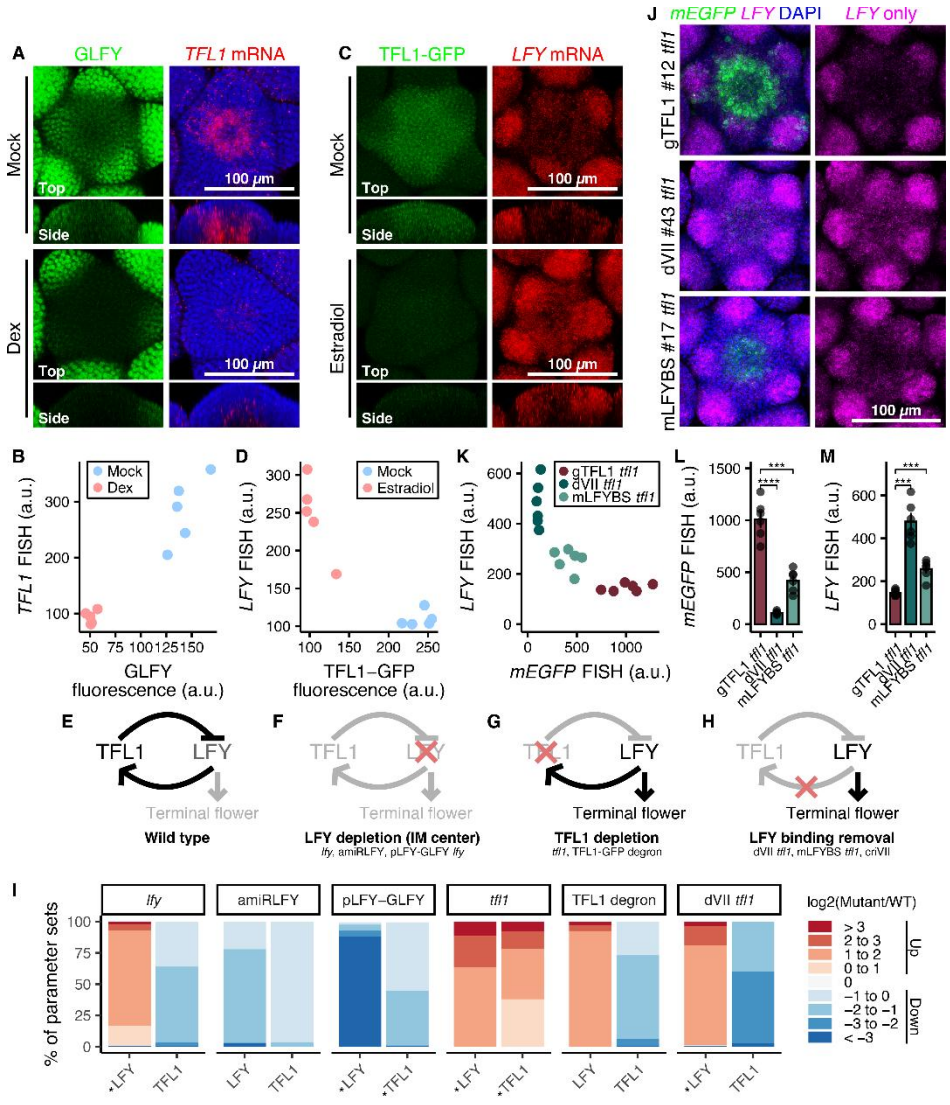

Fig. 3. *TFL1* and *LFY* engage in a negative feedback loop in I2 phase inflorescence meristems. (**A** and **B**) Fluorescence and wholemount FISH in gGLFY *lfy-1* inflorescence meristems expressing an inducible artificial *LFY* miRNA in the *TFL1* domain (A) and quantification (B). LFY, green; *TFL1*, red; nuclei (DAPI), blue. Induction by dexamethasone (Dex) or mock treatment for 20 hours. (**C** and **D**) Fluorescence and wholemount FISH in gTFL1-GFP *tfl1-1* inflorescence meristems after inducible GFP degradation (C) and quantification (D). TFL1, green; *LFY*, red; nuclei (DAPI), blue. Induction by estradiol or mock treatment for 20 hours. [(A) and (C)] Top, maximum intensity projections; bottom, xz longitudinal view. [(B) and (D)] Quantification of fluorescence and FISH intensity in the inflorescence meristem center. Datapoints represent individual inflorescences (n=5). (**E** to **H**) Schematics of the LFY-TFL1 negative feedback loop model in wild-type (E) and mutant [(F) to (H)] inflorescence meristems and observed (in)determinacy outputs. (**I**) Log2 fold changes of LFY and TFL1 values in mutants relative to wild type simulated by the 2-node LFY-TFL1 negative feedback loop model. Shown are log2 fold change distributions across all accepted parameter sets (n=20000). *lfy* and *tfl1* mutants express nonfunctional LFY and TFL1, respectively. Mutant model outcomes labeled by asterisks are predictions made by the model, unlabeled model outcomes were constrained by parameterization criteria. (**J** to **M**) Wholemount *mEGFP* and *LFY* FISH in I2 stage inflorescence meristems of gTFL1-mEGFP *tfl1-1* and mutant versions thereof (dVII, mLFYBS). (J) Top-view maximum intensity projections. Left, merged channels; right, *LFY* channel. *mEGFP*, green; *LFY*, magenta; nuclei (DAPI), blue. [(K) to (M)] Quantification of *mEGFP* and *LFY* FISH intensity in the inflorescence meristem center. Datapoints represent individual inflorescences. [(L) and (M)] mean ± SEM (n=6). Two-tailed Welch's *t*-test; ***P <0.001; ****P <0.0001.

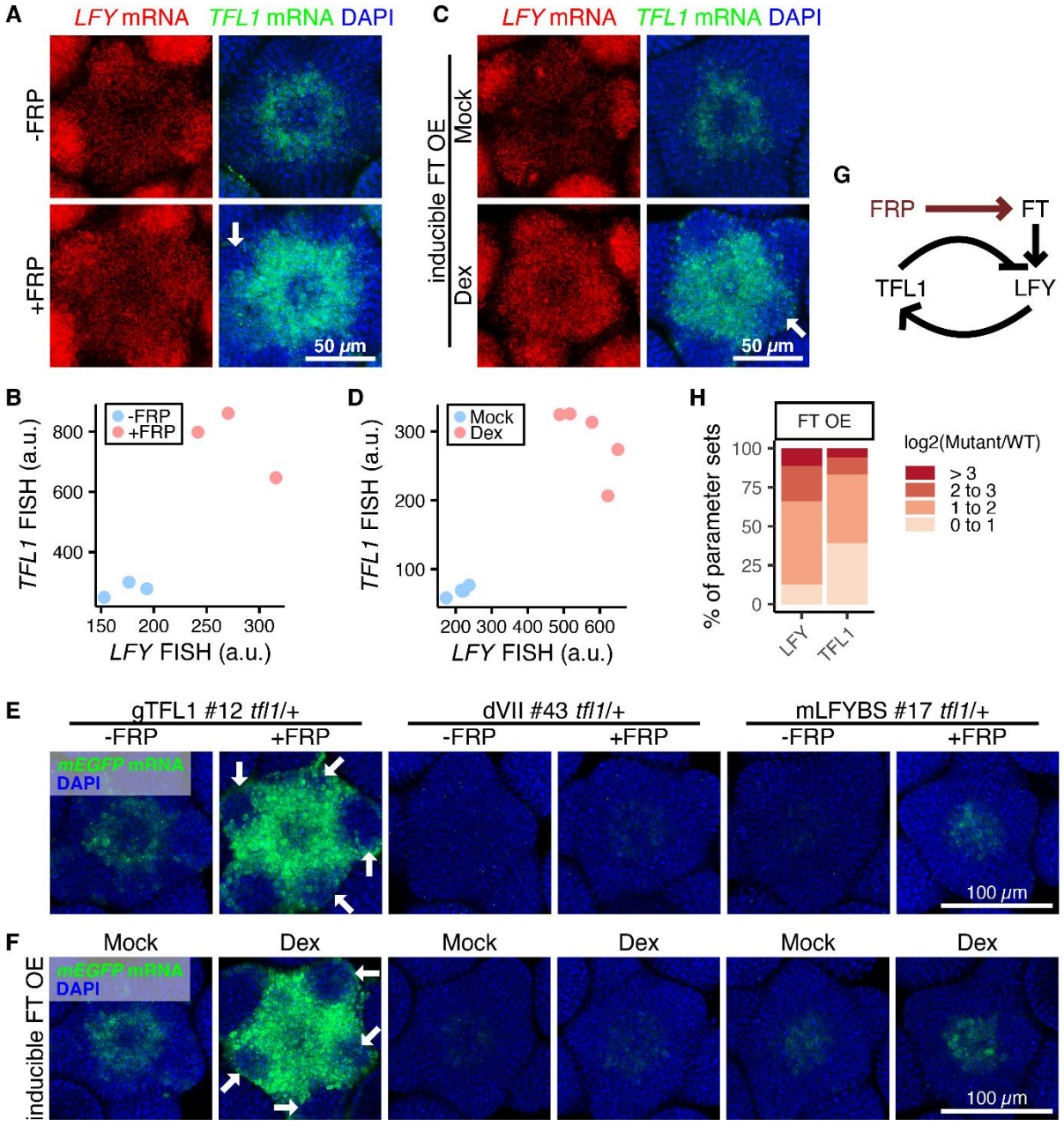

Fig. 4. Floral inductive cues and FT promote *TFL1* accumulation via LFY. (**A** and **B**) Wholemount FISH (A) and quantification (B) of *LFY* (red) and *TFL1* (green) in wild-type I2 inflorescences with or without a 24-hour far-red-enriched photoperiod (FRP). (**C** and **D**) Wholemount FISH (C) and quantification (D) of *LFY* (red) and *TFL1* (green) after inducible FT overexpression in I2 inflorescence meristems (Dex) or treatment with mock solution for 16 hours. [(B) and (D)] Quantification of RNA FISH intensity in the inflorescence meristem center. Datapoints represent individual inflorescence samples. n≥3. (**E** and **F**) *mEGFP* mRNA (green) expression in gTFL1-mEGFP or mutant versions thereof (dVII, mLFYBS) in response to FRP treatment (E) or FT overexpression (F). *mEGFP* expression were examined in wildtype morphology inflorescences (*tfl1-1*/+ background). [(A), (C), (E), and (F)] Nuclei (DAPI), blue. Shown are maximum intensity projections. Arrows, early flower primordia lacking *TFL1* expression. (**G**) Working model for activation of the negative feedback loop by floral inductive cues/systemic FT (input). (**H**) The distribution of log2 fold changes of simulated LFY and TFL1 values upon inducible FT overexpression compared to the wild type across all accepted parameter sets (n=20000).

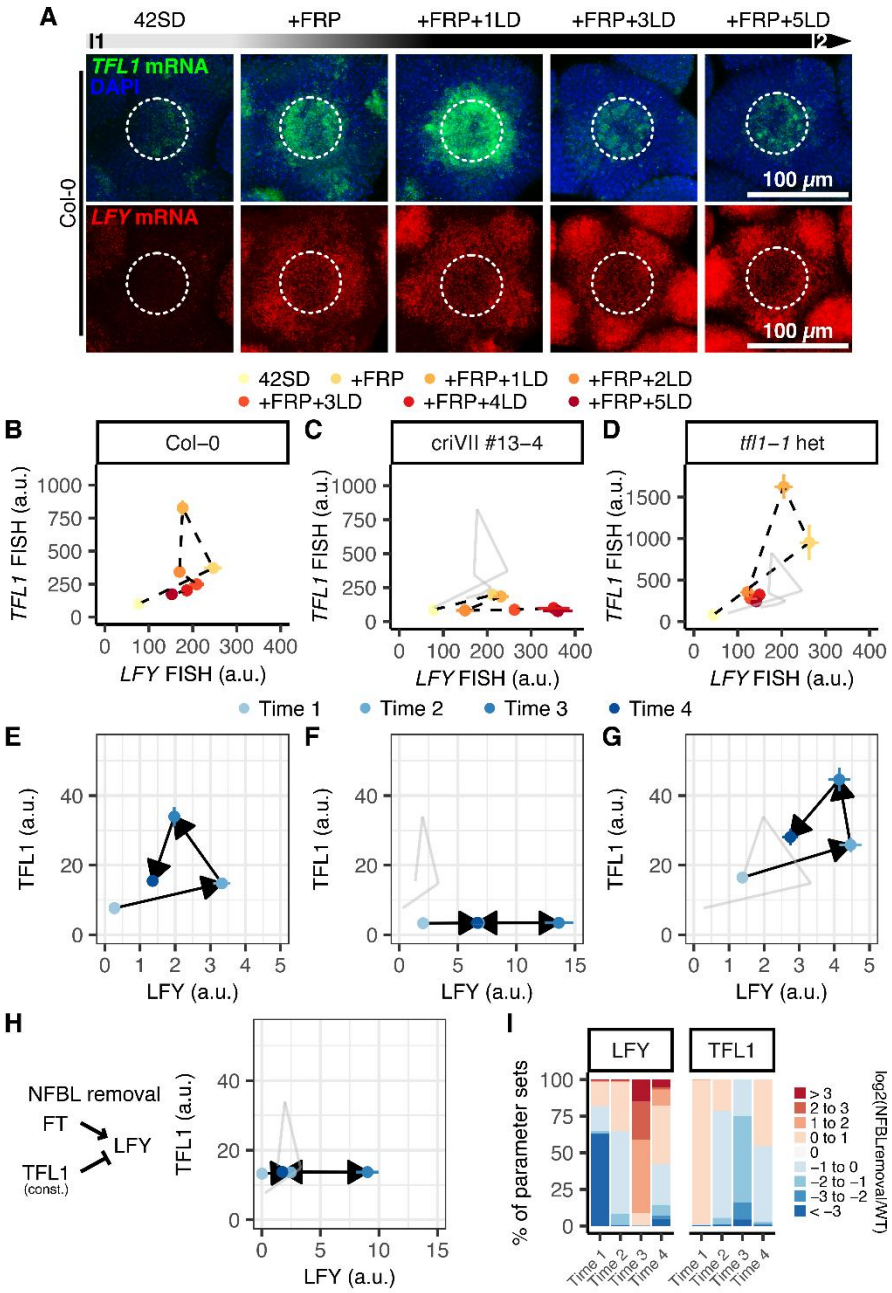

Fig. 5. *TFL1* up-regulation buffers *LFY* accumulation under strong floral inductive signals. (**A** to **D**) Time-course wholemount FISH of *TFL1* and *LFY* expression in inflorescence meristems of wild-type Col-0 [(A) and (B)], criVII (C), and *tfl1-1* heterozygotes (D) before and after FRP induction. I1 phase inflorescences grown in short days for 42 days (42SD) were treated with 24-hour FRP (+FRP) followed by transfer to long-day (LD). (A) FISH in wild-type Col-0 (maximum intensity projections). *LFY*, red; *TFL1*, green; nuclei (DAPI), blue. [(B) to (D)] Quantification of *TFL1* and *LFY* FISH intensity in the inflorescence meristem center (mean ± SEM, n≥4). (D) comprises wild-type and mutant *TFL1* mRNA. (**E** to **H**) Simulations of the 3-node computer model in response to a strong pulsed FT input in wild type (E), criVII (F), *tfl1-1* heterozygote (G) scenarios as indicated in (B) to (D), and the negative feedback loop (NFBL) removal scenario (H). Shown are the means of simulated LFY and TFL1 using accepted parameter sets (n=1617), and the error bars indicate SEM. Time 1-4 corresponds to 42SD, +FRP, +FRP+1LD, and +FRP+2LD. (H) NFBL removal: elevated constitutive *TFL1* expression without feedback by LFY. [(C), (D), (F), (G), and (H)] Gray lines, response of the wild type. (**I**) Distributions of simulated LFY and TFL1 log2 fold changes in NFBL removal relative to the wild type across all accepted parameter sets (n=1617).

Science
AAAS

Supplementary Materials for

A negative feedback loop between TERMINAL FLOWER1 and LEAFY protects inflorescence indeterminacy

Tian Huang *et al.*

Corresponding author(s): Rosangela Sozzani, ross_sozzani@ncsu.edu; Doris Wagner, wagnerdo@sas.upenn.edu

DOI: 10.1126/science.adv5429

The PDF file includes:

Other Supplementary Material for this manuscript includes the following:

Supplementary Text

Computer modeling overview

We developed and characterized a series of models describing the regulatory interactions between LFY, TFL1, FT and factor X in simulated indeterminate or terminating Arabidopsis inflorescence meristems. We presented these models in a unitless (non-dimensionalized) form and evaluated each model for its ability to recapitulate empirical biological observations based on parameterization studies. Within the parameter range identified by the parameterization, we performed sensitivity analyses for each model and studied the oscillation tendency.

Two-node model equations

We begin with a simple 2-node LFY-TFL1 model (Fig. 3E) using a delay differential equation model (*34*) to describe the abundance of LFY and TFL1 species over time:

$$\frac{d[LFY]}{dt} = \max\left(0, bLFY - tfl1bs * hill([TFL1]_{t-d}, k_{TFL1}, n_{TFL1})\right) - dLFY * [LFY] \quad (1)$$

$$\frac{d[TFL1]}{dt} = bTFL1 + lfybs * hill([LFY]_{t-d}, k_{LFY}, n_{LFY}) - dTFL1 * [TFL1] \quad (2)$$

$$hill(C, k, n) = \frac{1}{1 + \left(\frac{k}{C}\right)^n} \quad (3)$$

Where $[LFY]_{t-d}$ indicates the amount of LFY species present at time *t-d* where *t* is the current time and *d* is the delay (0.5 units in all models), and $[LFY]$ indicates the amount of LFY species present at time *t*. Each parameter starting with "b" denotes the basal production rate of a corresponding species. Each parameter starting with "k" denotes the concentration of the corresponding species when the promoter of the other species is half occupied, and parameters starting with "n" are Hill coefficients. Each parameter ending with "bs" indicates the maximum effect of the corresponding species on the other species. Parameters starting with "d" are degradation rates. The maximum function ensures a non-negative total production rate of [LFY] - sufficiently strong repression blocks the new production of [LFY] but cannot alter the basal degradation of extant [LFY].

Three-node model equations

We expand our model to include FT as an input for the negative feedback loop (Fig. 4G), representing the influence of FT in either standard growth conditions (e.g. long-day conditions) or a far-red-enriched long-day photoperiod (FRP) treatment.

$$\frac{d[LFY]}{dt} = \max(0, bLFY - tfl1bs * hill([TFL1]_{bound}, k_{TFL1}, n_{TFL1}) + ftbs * hill([FT]_{bound}, k_{FT}, n_{FT})) - dLFY * [LFY] \quad (4)$$

$$\frac{d[TFL1]}{dt} = bTFL1 + lfybs * hill([LFY]_{t-d}, k_{LFY}, n_{LFY}) - dTFL1 * [TFL1] \quad (5)$$

Where the competition between FT and TFL1 for access to the promoter of *LFY* are described as:

$$[TFL1]_{bound} = [TFL1]_{t-d} * e^{-[FT]_{apparent} * pExp} \quad (6)$$

$$[FT]_{bound} = [FT]_{apparent} * e^{-[TFL1]_{t-d} * pExp} \quad (7)$$

The Hill function noted above is described in equation #3. The $[FT]_{apparent}$ input over time is described below.

Four-node model equations

We extend the model to consider terminating inflorescence meristem cells that exits from the negative feedback loop (fig. S23G). Recapitulating the experimental observations from terminating inflorescence meristem cells (fig. S23, A to C) requires the introduction of an additional hypothesized "factor X" species which is induced by [LFY] and represses [TFL1]:

$$\frac{d[LFY]}{dt} = \max(0, bLFY - tfl1bs * hill([TFL1]_{bound}, k_{TFL1}, n_{TFL1}) + ftbs * hill([FT]_{bound}, k_{FT}, n_{FT})) - dLFY * [LFY] \quad (8)$$

$$\frac{d[TFL1]}{dt} = \max(0, bTFL1 + lfybs * hill([LFY]_{t-d}, k_{LFY}, n_{LFY}) - tfl1xbs * hill([X]_{t-d}, k_{TFL1X}, n_{TFL1X})) - dTFL1 * [TFL1] \quad (9)$$

$$\frac{d[X]}{dt} = bX + xlfybs * hill([LFY]_{t-d}, k_{XLFY}, n_{XLFY}) - dX * [X] \quad (10)$$

The Hill function noted above and the expressions for competitive binding of TFL1 and FT are described in equations #3, #6, and #7.

FT abundance over time

Two types of FT input dynamics are specified in the 3-node and 4-node models to recapitulate experiments according to whether they were subject to invariable or varying floral inductive cues.

For growth conditions with invariable floral inductive cues (e.g. long-day conditions), the rate of change of [FT] is set to 0.0 to reflect constant [FT]:

$$\frac{d[FT]}{dt} = 0.0 \quad (11)$$

Model solutions are initialized with a positive abundance of [FT] at the starting time (t0):

$$[FT]_{t0} = 2.0 \quad (12)$$

To describe the varying floral inductive cues in a time-course FRP experiment, we estimated a pulsed [FT] profile based on our experimental design (fig. S19A). The desired [FT] profile consists of an initial abundance of zero [FT] to reflect the short-day conditions before the experiment, a large increase of [FT] during the simulation to reflect the FRP treatment, and a steady positive final value to reflect ongoing long-day conditions. Considering the known kinetics of FT protein in response to photoperiod shifts (*38*) and the kinetics of FT protein transportation from leaves to shoot apices (*73*), a delay is added between the photoperiod shift and the changes in the FT level in the shoot apices. For example, in our experiment, the initial accumulation of FT in the inflorescence meristem can be estimated 12 hours after the plants are transferred from the short-day condition to the FRP condition. Based on these estimates above, the desired [FT] profile was simulated using combined derivatives of Gaussian and sigmoid functions:

$$\frac{d[FT]}{dt} = \frac{2}{scalePar} * d\sigma\left(\frac{t - tc}{scalePar}\right) - \frac{heightPar}{peakWidth^2} * (t - tc) * e^{\frac{-(tc-t)^2}{2*peakWidth^2}} \quad (13)$$

$$d\sigma(x) = \left(\frac{1}{1+e^x}\right) * \left(1 - \frac{1}{1+e^x}\right) \quad (14)$$

Where tc indicates the time at which maximal [FT] is observed. Values for $scalePar$, $peakWidth$, and $heightPar$ were chosen to find the best fit between this function and the observed published data (table S4). The resulting [FT] profile is presented in fig. S22D top panel, where 48, 72, 96, 120 units of time in the simulation correspond to 42SD, +FRP, +FRP+1LD, +FRP+2LD in the FRP experiment (fig. S19A).

Finally, since the relative abundance of [FT] with respect to [LFY] or [TFL1] in inflorescence meristem cells is unknown, we permit each dynamic profile of [FT] to vary by altering the magnitude of perceived [FT] in each parameter set:

$$[FT]_{apparent} = [FT] * FTmod \quad (15)$$

Where the parameter $FTmod$ is a constant multiplier of [FT] abundance. This permits the $[FT]_{apparent}$ curve to achieve a different amplitude based on the parameter $FTmod$, while the dynamic changes are kept the same.

Positive domain mitigations

As these models represent discrete biological objects (LFY, TFL1, FT, and the hypothesized factor(s) X), their concentrations are only valid in the positive domain. However, some combinations of parameter values may cause the model system to take small negative values during the solution. Therefore, we constrained our model to the positive domain with the following mitigations. First, when examining the abundance of any model species, negative values are treated as zero values. Second, as suggested by (*74*), if any object in the model has negative abundance during a timestep, the derivative for that timestep is restricted to non-negative values.

Representation of mutations

Given any parameter set, biological mutations are represented in our simulations by performing the indicated modifications (table S5) and re-evaluating the model solution. Each mutation is presented as an ablation of model functionality (setting a relevant parameter value to zero, as in knockout mutants) or a relative modification of the parameter's value (e.g. [LFY] degradation rate (the dLFY parameter) is increased five-fold over the wild-type value in the amiRLFY mutant). Since our representations of *lfy* mutant and mLFYBS *tfl1* in 2-node and 3-node models are identical, only *lfy* mutant were shown. For Sobol' sensitivity analysis, the lower and upper bounds of the parameter range were modified to represent each mutant (e.g. if the dLFY range in wild type is between 0.01 and 1, the corresponding dLFY bounds in the amiRLFY mutant were 5 fold higher (0.05 to 5)).

Model outcomes

Final values of [LFY], [TFL1], and [X] are calculated and used as the outputs of each model simulation. Final values are defined by examining the final 10% of each simulation's timespan by the following procedure:

1. Interpolate values for [LFY], [TFL1], and [X] within the final 10% of the simulation every 0.1 units of time
2. Identify the minimum and maximum values for [LFY], [TFL1], and [X] within that region of time, clamped to [0, ∞]
3. Final values of [LFY], [TFL1], and [X] are calculated as the midpoints of the minimum (Min) and maximum (Max) values: $\frac{Min+Max}{2}$

The derived final values of [LFY], [TFL1], and [X] were used in parameterization studies, Sobol' sensitivity analyses, and for calculating [LFY] or [TFL1] fold changes in mutant relative to wild-type simulations.

Model parameterization

We tested the ability of our models to recapitulate empirical observations using a simulation-based inference strategy, Approximate Bayesian Computation (*75*-*77*). ABC methods use a simulation-based-inference approach to estimate the posterior distribution of parameter likelihoods. This technique allows us to identify regions of parameter space sufficient to satisfy (or *satisfice*) expected model behaviors (fig. S13A). Sets of criteria for the 2-node, 3-node, and 4-node models are defined based on our experimental data (tables S6 to S9). These criteria facilitate filtering parameter space using an ABC rejection algorithm (*76*).

Our criteria are expressed as thresholds defining the minimum fold change in a mutant simulation relative to a WT simulation (tables S6 to S9). For example, biological evidence suggests that depletion of LFY (amiRLFY) causes TFL1 to decrease approximately 3-fold (Fig. 3B), so we set a minimum 1.5-fold decrease of [TFL1] (i.e. $\leq \frac{2}{3}$ relative to WT) for the *in silico* experiment. We model an amiRLFY mutant by increasing dLFY (the degradation rate of [LFY]) and expect this to result in a decrease of [TFL1] final value compared to the WT case where dLFY is unmodified. If the fold-change value $[TFL1]_{amiRLFY}$ / $[TFL1]_{WT}$ is less than $\frac{2}{3}$, Criterion #4 is assigned a value of 0.0. Otherwise, a non-zero value is returned, and the parameter set is rejected. This process repeats for every criterion. Only parameter sets simultaneously satisficing all applicable criteria (total criteria score == 0.0) are accepted for further studies.

Notably, two independent parameterizations were performed for the 3-node model. The first parameterization searched for parameter sets that recapitulate experimental observations presented in Figs. 1 to 4 (table S7), and the simulations employed constant FT values as input. The results are presented in fig. S18A. The second parameterization additionally included the dynamic changes in LFY and TFL1 observed in the WT during a time-course FRP experiment (Fig. 5, A and B) as criteria (table S8), and the pulsed FT profile, rather than constant FT, was used as an input for the simulation. The results are presented in fig. S22A.

The 4-node model is treated as an extension of the 3-node model. This parameterization only searched for X-related parameters (table S9). Parameters unrelated to factor X were fixed by selecting the 3-node parameter set closest to the centroid of the 3-node parameterization results given pulsed FT (fig. S22A).

Parameterizations were performed within the default bounds listed in tables S10 to S12. Parameter bounds are presented in linear space (e.g. bLFY takes values between 0.0005 and 20) for simplicity, but algorithmic sampling is performed in log space to ensure that all regions of parameter space are equally accessible. Two independent replicate parameterizations were performed, assessed for concordance and the two replicates were pooled for data presentations.

Model oscillation

Delay differential equation systems such as ours—with two species regulating each other in opposite fashions—are capable of oscillation (*34*). For all parameter sets accepted by parameterizations, we analyzed the presence and strength of [LFY] and [TFL1] oscillation in the wild type and mutant with an intact negative feedback loop (fig. S13B). We investigated the relative oscillation in 2-node and 3-node models only, as the 4-node model extends the 3-node model and is expected to have the same behavior in the inflorescence meristem simulations. We calculated the relative oscillation (defined as the ratio of peak-to-peak amplitude to the midpoint value of the species) by the following procedure:

1. Interpolate the values for [LFY], [TFL1], and [X] within final 25% and 10% of the simulation every 0.1 units of time
2. Access the monotonicity in the final 25%, and relative oscillation of monotonic species is set to 0.0
3. For non-monotonic species, identify the minimum (Min) and maximum (Max) values in the final 10% of the simulation, clamped to [0, ∞]
4. For non-monotonic species, calculate relative oscillation as:

$$Relative\ Oscillation = 2 * \frac{Max - Min}{Max + Min} \tag{16}$$

The derived relative oscillation ranges from 0 to 2, with 0.2 denoting 10% deviation from the midpoint.

Model sensitivity analysis

We used a Sobol' Sensitivity Index approach to determine sensitivity of the model to parameter perturbation (fig. S14C, fig. S18E, fig. S22G, fig. S24E). This method estimates the proportion of variance of a model's output due to either single (first order/S1) or combined (total order/ST) contributions of the different parameters (*77*-*79*). Sensitivity analyses were performed for each model within the parameter space defined by the parameterization results, with two independent 3-node model Sobol' sensitivity analyses conducted in parameter spaces from the separate 3-node parameterizations (fig. S18E and fig. S22G). Simulations of 3-node and 4-node models were performed using constant FT inputs. The sensitivity analysis of each mutant in each model has 5 technical replicates and a Sobol' sequence length of 2^{15} (for the 2-node model) or 2^{16} (all other models) parameter sets. As a negative control and a tool for distinguishing low-sensitivity parameters from truly insensitive parameters, we implemented a dummy parameter with no effect on model outcomes (*80*). The sensitivity indices calculated for this dummy parameter were used in a series of non-parametric Kruskal-Wallis tests ($\alpha = 0.05$) to identify statistically significant sensitivity indices in replicated sensitivity analyses.

Promoter occupancy analysis

Using parameter sets identified using the 3-node model parameterization with pulsed FT (fig. S22A), we investigated the LFY and TFL1 promoter occupancy in LFY overexpression mutants with various bLFY levels. The promoter occupancy is defined as the probability that the binding site on the promoter is occupied and calculated using Hill equations (*81*) based on the final value of [LFY] ($[LFY]_{final}$) and the final value of [TFL1] ($[TFL1]_{final}$):

$$Occupancy_{LFY-to-pTFL1} = hill\left([LFY]_{final}, k_{LFY}, n_{LFY}\right) \tag{17}$$

$$Occupancy_{TFL1-to-pLFY} = hill\left([TFL1]_{finalbound}, k_{TFL1}, n_{TFL1}\right) \tag{18}$$

Where

$$[TFL1]_{finalbound} = [TFL1]_{final} * e^{-[FT]_{apparent} * pExp} \tag{19}$$

[FT] is a constant in the LFY overexpression mutant simulation, and

$$[FT]_{apparent} = [FT]_{t0} * ftmod = 2 * ftmod \quad (20)$$

Software

Models were implemented using Julia (*82*) and the following packages: DifferentialEquations.jl package (*83*), Plots.jl (*84*), GpABC.jl (*85*), and GlobalSensitivity.jl (*86, 87*). Data were analyzed and visualized using R (*88*) with ggplot2 (*89*) and ggpubr (*90*).

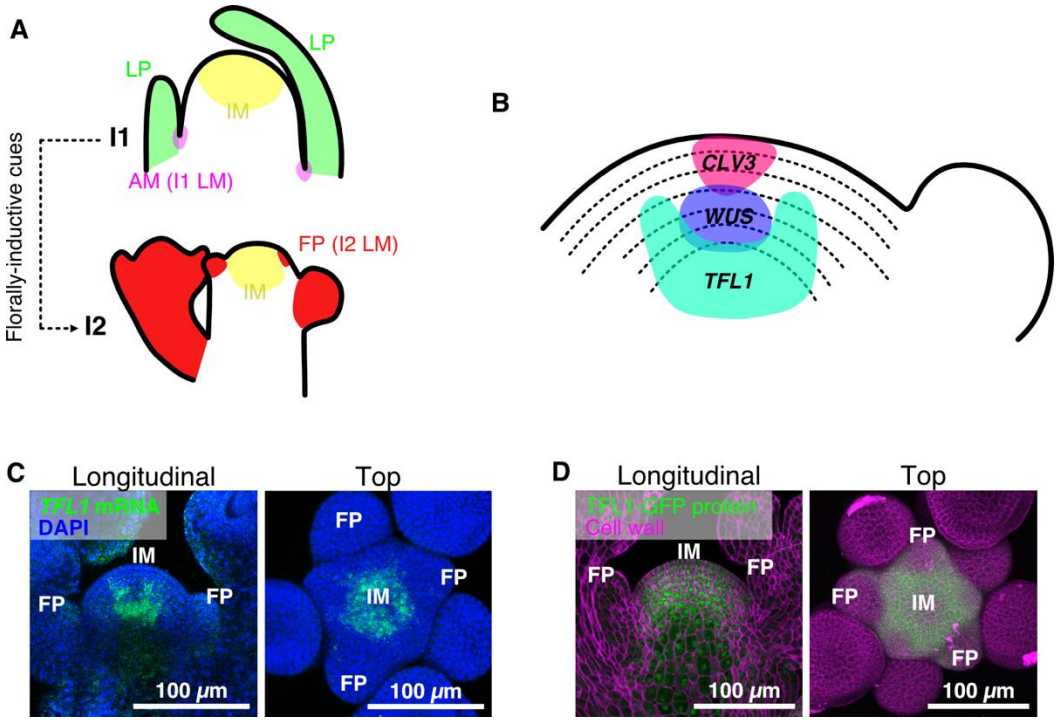

Fig. S1. TFL1 mRNA and protein pattern during inflorescence development. (**A**) The identities and developmental trajectories of all meristems before (I1) and after (I2) the inflorescence starts to produce flowers. (**B**) *TFL1* mRNA expression domain relative to that of *WUS* and *CLV3* in I2 phase inflorescence meristems. (**C** and **D**) *TFL1* mRNA (C) and protein (D) accumulation in I2 phase inflorescences. Longitudinal sections (left) and top-view maximum intensity projections (right). (C) *TFL1* mRNA FISH (green). Nuclei (DAPI): blue. (D) gTFL1-GFP *tfl1-1* fluorescence (green). Cell wall (magenta): Calcofluor-white (left) or PI (right). IM: inflorescence meristem, LM: lateral meristem, AM: axillary meristem, FP: flower primordium, LP: leaf primordium.

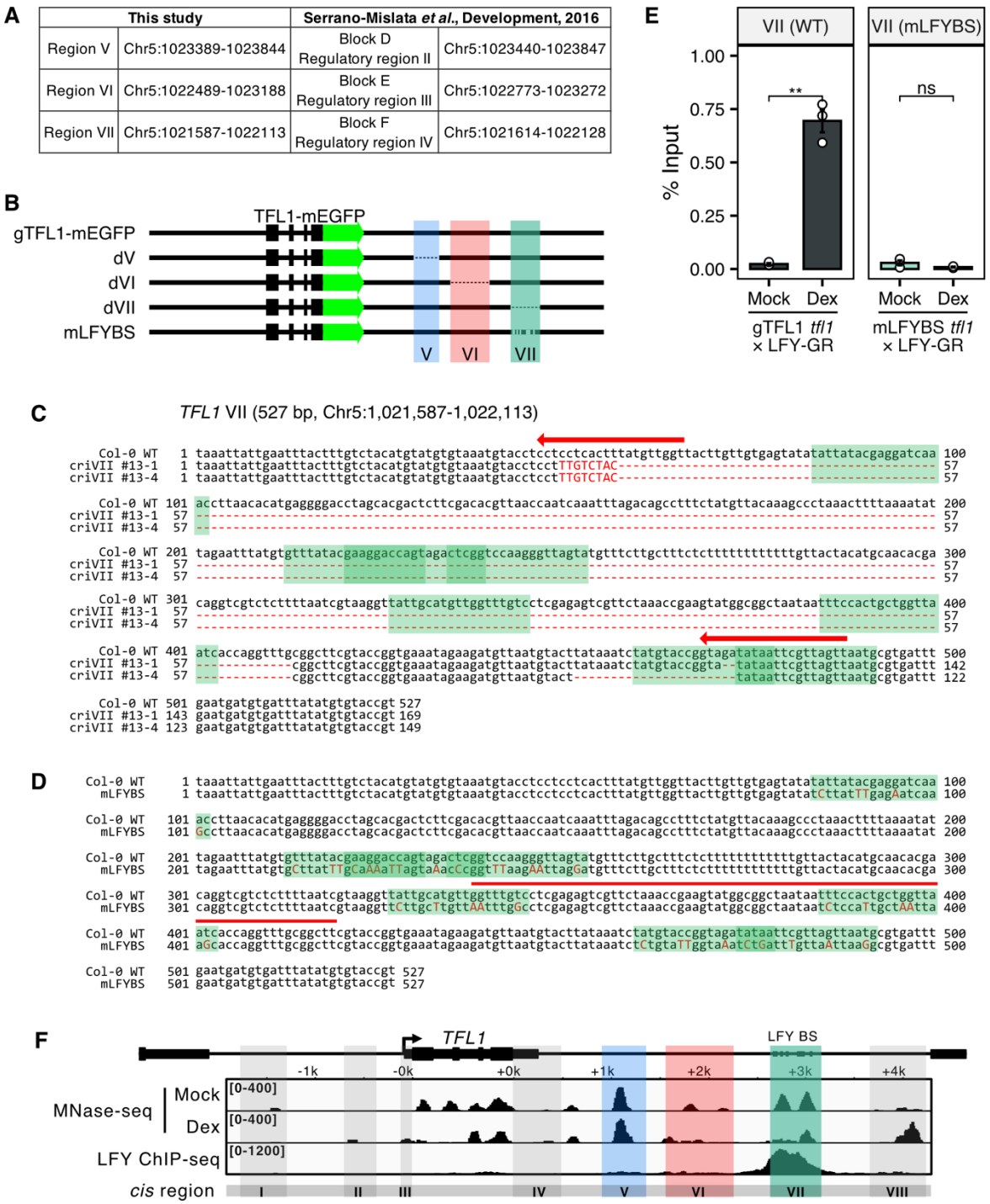

Fig. S2. Constructs and sequences of transgenic and CRISPR deletion lines. (**A**) Comparisons of *TFL1 cis*-regulatory regions identified in this study and (*21*). Coordinates are based on TAIR10. (**B**) Genomic *TFL1* (gTFL1-mEGFP) containing wild-type *TFL1* intergenic regulatory sequences, with individual regulatory region deletions (dV, dVI, dVII), or LFY binding site mutations (mLFYBS). mLFYBS is identical in length to the gTFL1-mEGFP control. (**C** and **D**) Sequence alignments of wild-type *TFL1* cis-regulatory region VII and region VII with CRISPR deletions (criVII) (C) or mLFYBS (D). The 19-bp LFY binding sites are highlighted in green. (C) Red arrows: CRISPR guide RNA targeting sites. (D) Red horizontal line: amplicon for

ChIP-qPCR in D. Point mutations in LFY binding sites are marked in red. (**E**) LFY-GR ChIP-qPCR for wild-type region VII (WT) or mLFYBS region VII after treatment with dexamethasone (Dex) or mock solution. Mean ± SEM (n=3). Two-tailed Welch's *t*-test *p*-values: ns >0.05, ** <0.01. (**F**) MNase-seq (*14*) peaks denote nucleosomes at the *TFL1* locus prior to (Mock) and after (Dex) LFY binding, with LFY occupancy below (*14*).

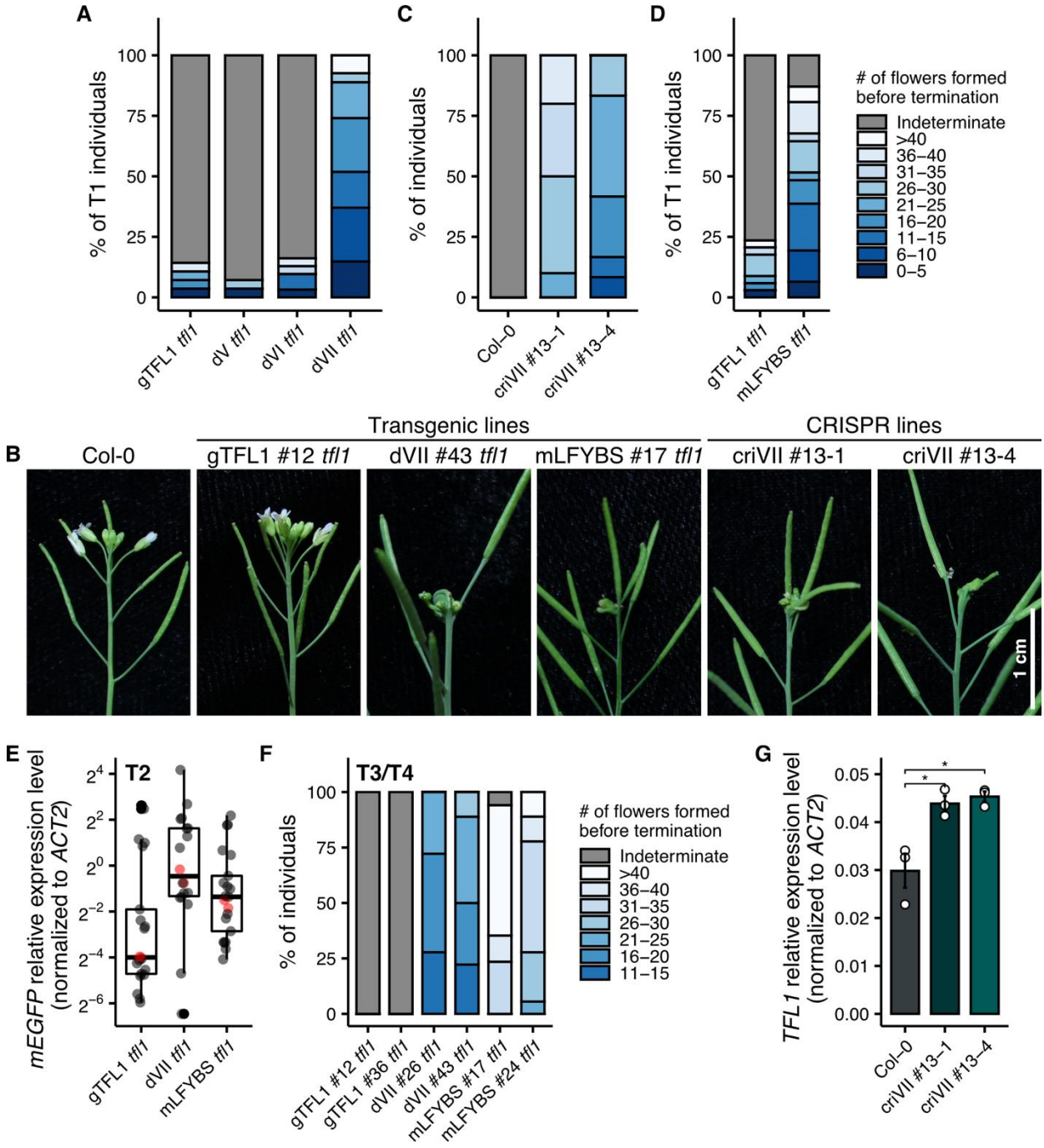

Fig. S3. Terminal flower phenotypes of gTFL1-mEGFP *tfl1-1* transgenic plants and region VII CRISPR deletion mutants. (**A** to **D**) Quantification of flowers formed before termination (A, C, D) and representative inflorescence images (B) for gTFL1-mEGFP (gTFL1), dV, dVI, or dVII *tfl1-1* T1 plants (A), wild-type Col-0, criVII (C), and gTFL1 or mLFYBS *tfl1-1* T1 plants (D). (**E**) Selection of representative median-expression-level transgenic lines (red dots) by qRT-PCR. Datapoints represent independent T2 transgenic lines. (**F**) Quantification of flowers formed before termination in homozygous T3 or T4 populations of all representative lines (n ≥ 17). (**G**) *TFL1* expression measured by RT-qPCR in entire inflorescences of wild-type (Col-0) and criVII at the I1-to-I2 transition. Mean ± SEM (n=3). Two-tailed Welch's *t*-test *p*-value: * <0.05.

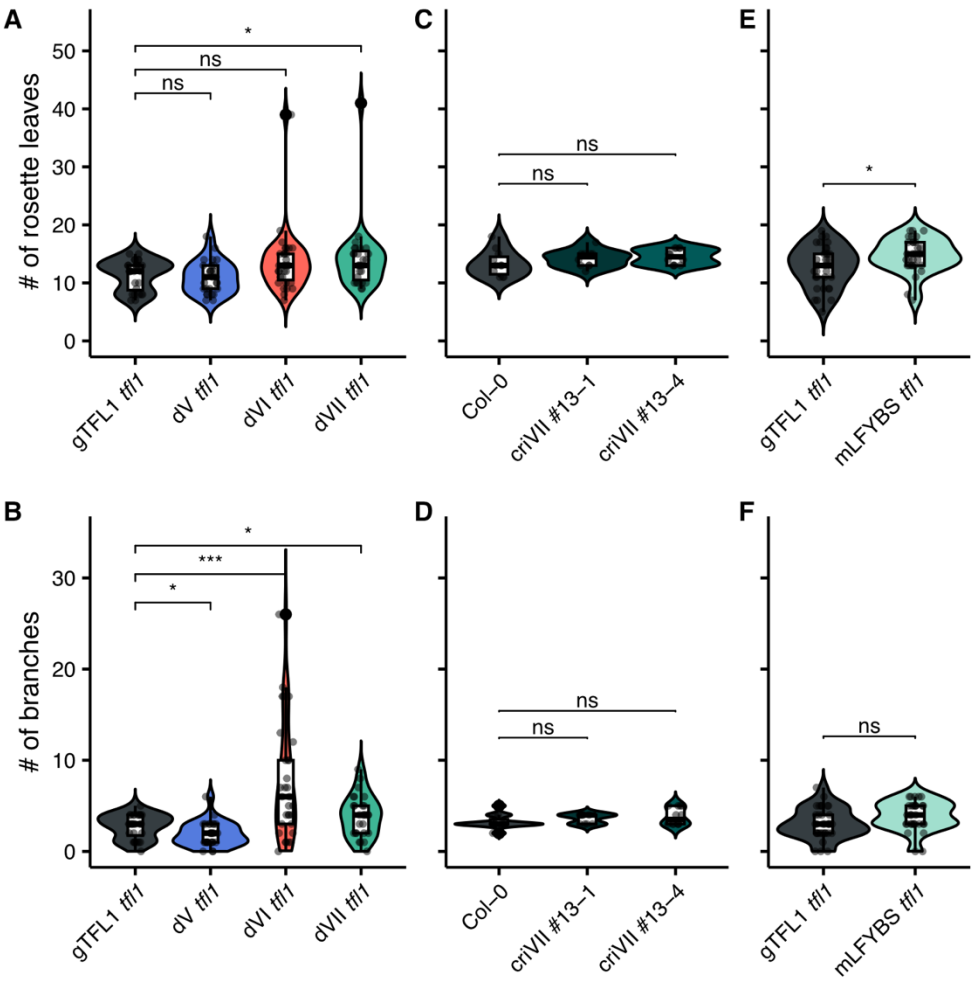

Fig. S4. Phenotypes of gTFL1-mEGFP *tfl1-1* transgenic plants and region VII CRISPR deletion mutants in the vegetative and I1 phase. (**A**, **C**, **E**) Rosette leaves produced in gTFL1-mEGFP (gTFL1), dV, dVI, or dVII *tfl1-1* T1 plants (A), wild-type Col-0, criVII (C), gTFL1, mLFYBS *tfl1-1* T1 plants (E). (**B**, **D**, **F**) Primary branches produced in the same genotypes. Two-tailed Welch's *t*-test *p*-values: ns >0.05, * <0.05, *** <0.001.

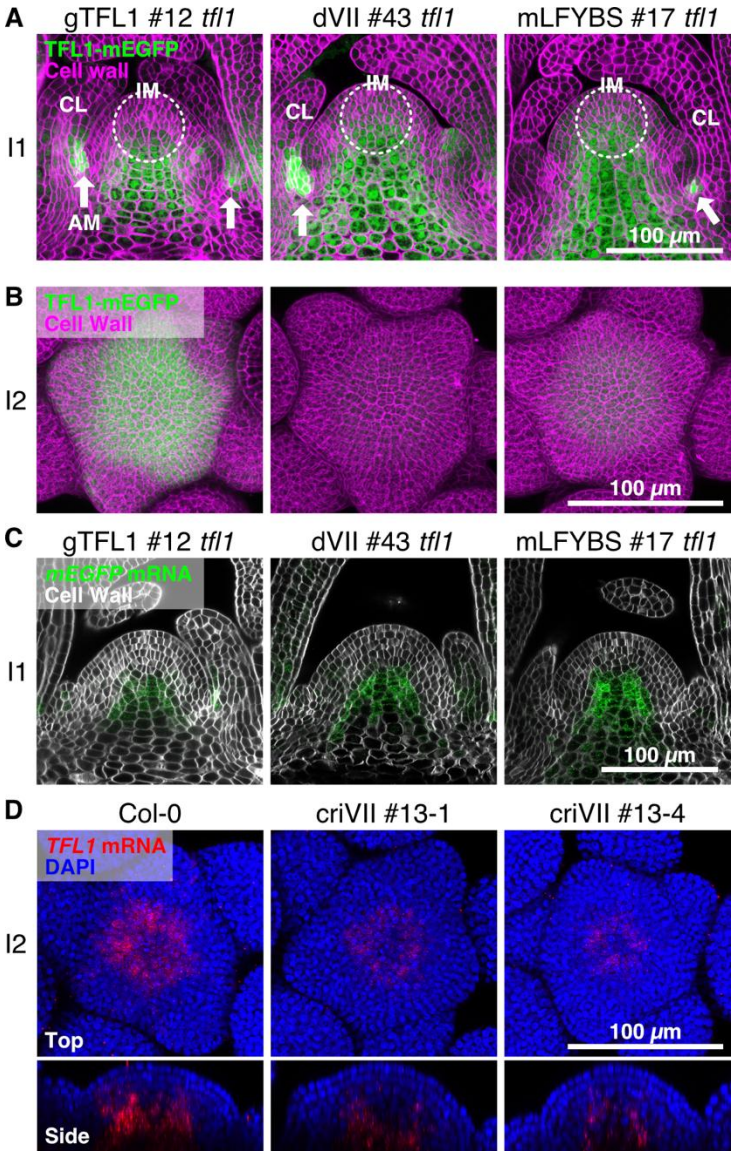

Fig. S5. Spatiotemporal expression of wild-type and binding site mutated *TFL1*. (**A**) Confocal images of the I1 phase inflorescences (longitudinal sections) quantified in Fig. 1G. mEGFP: green, cell wall (Calcofluor-white): magenta. IM: inflorescence meristem, AM: axillary meristem, CL: cauline leaf. Arrows: *TFL1* in AMs. (**B**) Confocal images of TFL1-mEGFP protein (green) expression in I2 phase gTFL1-mEGFP (gTFL1), dVII, and mLFYBS *tfl1-1* inflorescences (top-view maximum intensity projections). Cell wall (PI): magenta. (**C**) *mEGFP* mRNA FISH (green) in I1 phase inflorescences of gTFL1, dVII, and mLFYBS *tfl1-1* (longitudinal sections). Cell wall (Calcofluor-white): white. (A and C) Region VII deletion or mutation results in elevated TFL1 accumulation below its normal site of expression in the I1 phase, suggesting presence of a repressor element. (**D**) Wholemount *TFL1* FISH (red) in I2 phase inflorescences of wild-type Col-0 and criVII (top: top-view maximum intensity projections, bottom: xz longitudinal view). Nuclei (DAPI): blue.

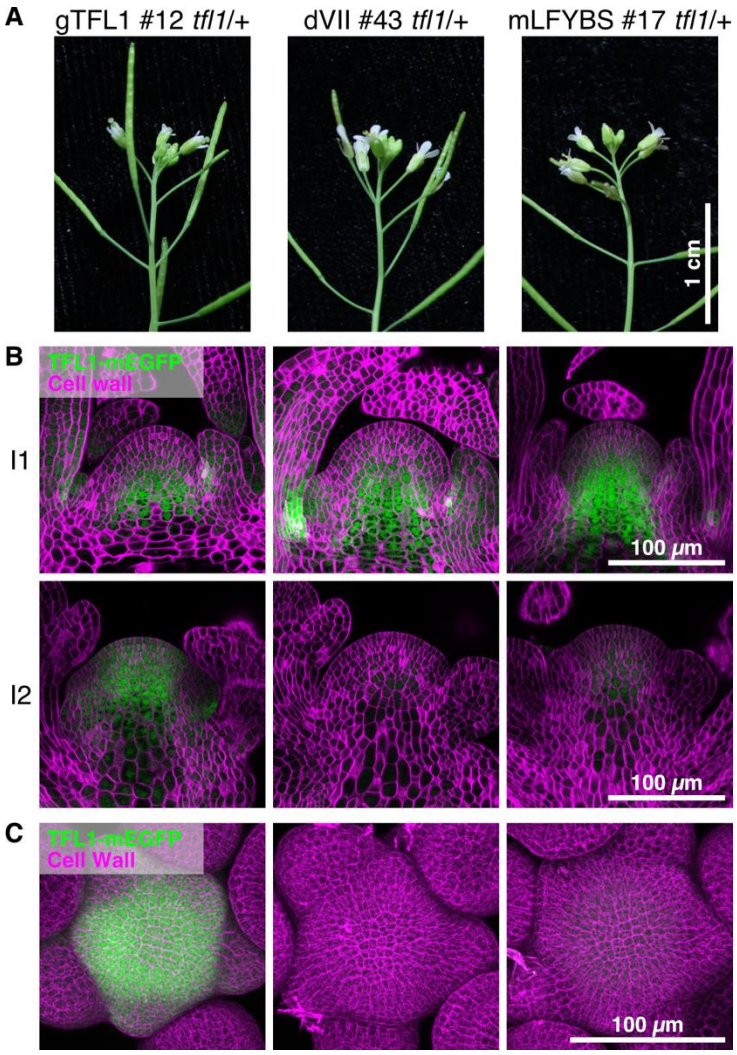

Fig. S6. Spatiotemporal expression of transgenic rescue constructs in *tfl1-1*/+ heterozygous plants. (**A**) Inflorescence indeterminacy of gTFL1-mEGFP (gTFL1), dVII, mLFYBS in *tfl1-1*/+. (**B**) gTFL1-mEGFP protein (green) in the inflorescence meristems of gTFL1, dVII, and mLFYBS *tfl1-1*/+ before and after the I1-to-I2 transition. Cell wall (Calcofluor-white): magenta. (**C**) gTFL1-mEGFP fluorescence (green) in I2 phase *tfl1-1*/+ inflorescences. Shown are top-view maximum intensity projections. Cell wall (PI): magenta.

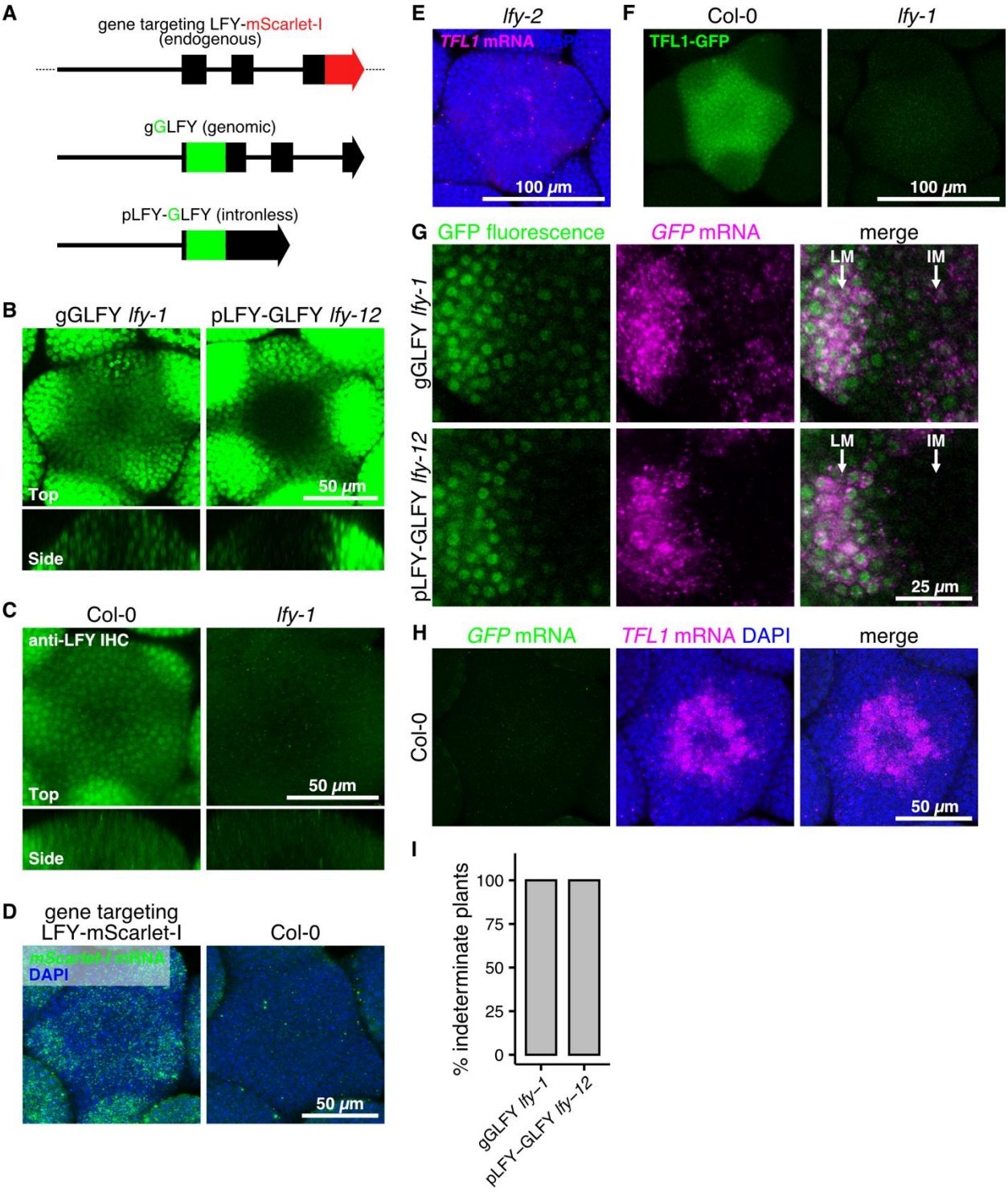

Fig. S7. *LFY* mRNA and protein accumulate in the I2 inflorescence meristem center. (**A**) Diagrams of different LFY reporters. In the CRISPR gene targeting LFY-mScarlet-I, mScarlet-I was integrated at endogenous *LFY* locus at the LFY C terminus. In transgene gGLFY and pLFY-GLFY, GFP was inserted right after the 31st codon of *LFY* (*7, 31*). gGLFY contains all genomic *LFY* sequences, while pLFY-GLFY lacks the intronic sequences. (**B**) gGLFY *lfy-1* and pLFY-GLFY *lfy-12* protein expression (top: top-view maximum intensity projections, bottom: xz

longitudinal views). (**C**) Wholemount immunohistochemistry using anti-LFY antibody in the wild-type and in *lfy-1* inflorescences (top: single optical sections, bottom: xz longitudinal view). (**D**) Wholemount *mScarlet-I* FISH (green) in inflorescences of CRISPR knock-in LFY-mScarlet-I plants and wild-type control. (**E**) Wholemount *TFL1* FISH (magenta) in I2 phase inflorescences of the weak *lfy-2* mutant. (**F**) gTFL1-GFP protein expression in I2 phase inflorescences of wild-type Col-0 and *lfy-1* null mutant. (**G**) Combined GFP fluorescence (green) and GFP FISH (magenta) in I2 phase inflorescences of gGLFY *lfy-1* and pLFY-GLFY *lfy-12*. Shown are single optical sections at the IM-LM boundary. No GLFY protein movement from the LM to the IM was detected in pLFY-GLFY *lfy-12*. LM: lateral flower meristem, IM: inflorescence meristem. (**H**) Wholemount *GFP* (green) and *TFL1* (magenta) FISH in wild-type control I2 phase inflorescences. (D, E, F, H) Shown are top-view maximum intensity projections. Nuclei (DAPI): blue. (**I**) gGLFY *lfy-1* (n=8) and pLFY-GLFY *lfy-12* (n=9) formed indeterminate inflorescences.

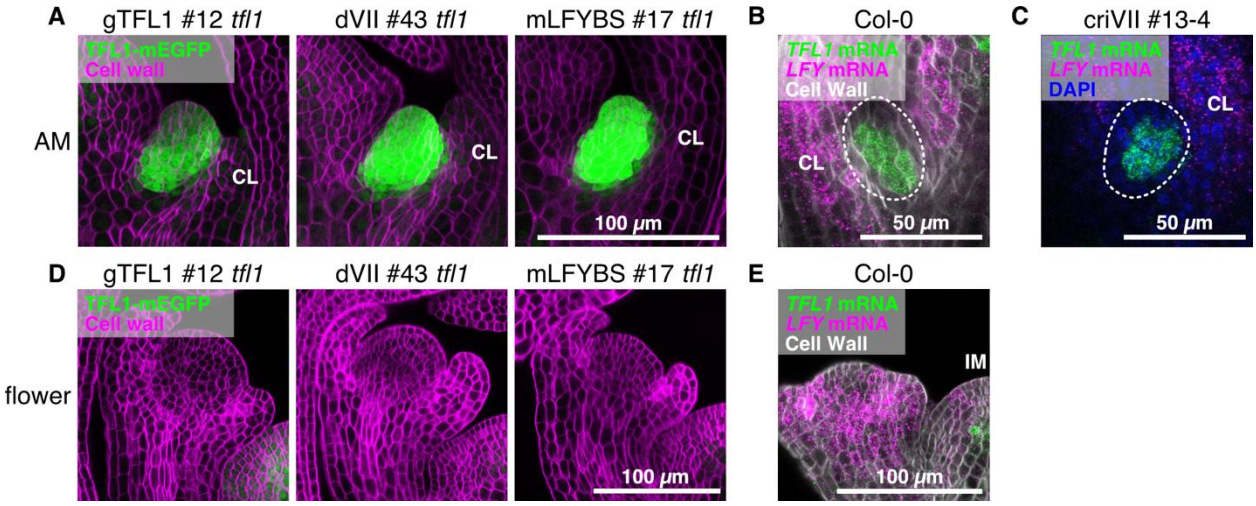

Fig. S8. *TFL1* and *LFY* expression in axillary meristems and flowers in the wild type and mutants. (**A**) gTFL1-mEGFP protein (green) expression is not reduced in axillary meristems (AMs) upon deletion or mutation of region VII. (**B** and **C**) *TFL1* mRNA (green) is present and *LFY* mRNA (magenta) absent from AMs based on FISH. (**D**) gTFL1-mEGFP protein (green) is absent in developing flowers. (**E**) *LFY*, but not *TFL1* is strongly expressed in developing flowers. (A and D) Cell wall (Calcofluor-white): magenta. (B and E) Cell wall (Calcofluor-white): white. (C) Nuclei (DAPI): blue. (B and C) The white dashed line marks the AM where *LFY* expression is absent. IM: inflorescence meristem, CL: cauline leaf.

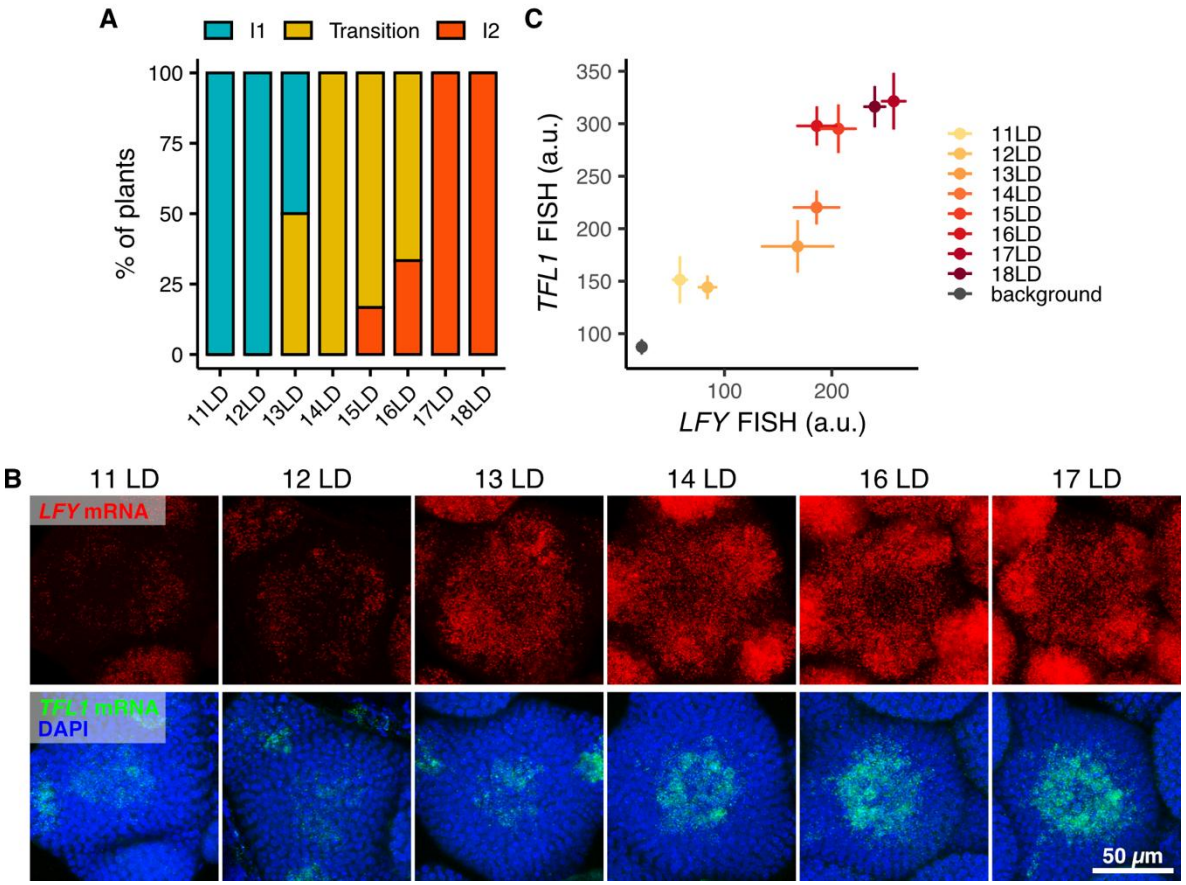

Fig. S9. Temporal accumulation of *LFY* and *TFL1* mRNA during the I1-to-I2 transition in long days. (**A**) Developmental stage of long-day-grown plant samples at different plant age. (**B** and **C**) Wholemount FISH (B) and quantifications (C) of *TFL1* (green) and *LFY* (red) in wild-type inflorescences at different timepoints during inflorescence development. (B) Top-view maximum intensity projections. Nuclei (DAPI): blue. (C) FISH intensity in the center of inflorescence meristems (mean ± SEM, n≥5). "Background": FISH without hybridization probes at the same image acquisition settings.

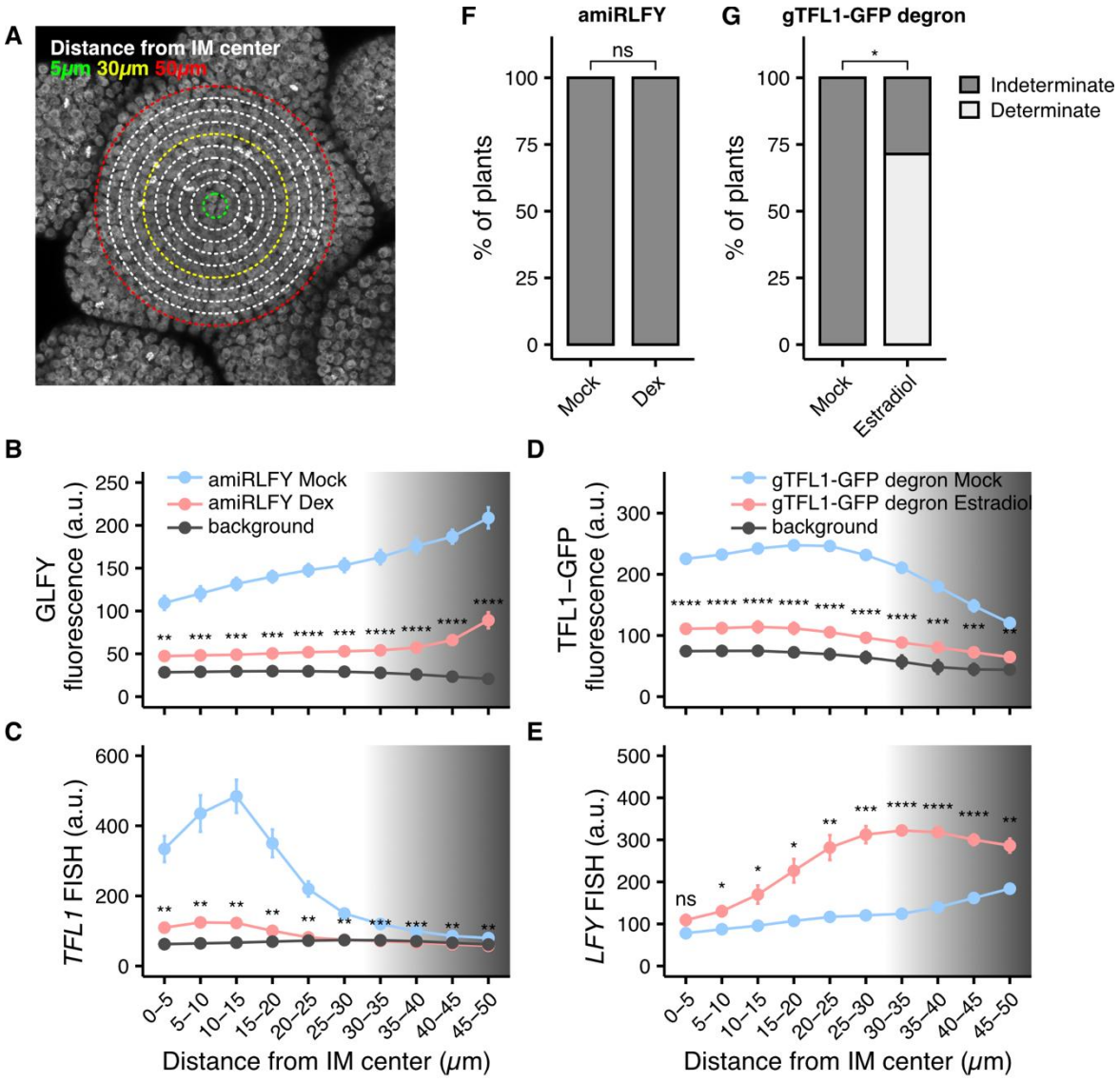

Fig. S10. Image quantification for inducible LFY and TFL1 depletion assays. (**A**) A representative image of an I2 phase inflorescence. The inflorescence meristem center is surrounded by concentric circles separated by 5 μm. Fluorescence intensity was quantified in annulus regions between adjacent circles (B to E). The 30-μm radius circle (yellow) marks the outer boundary of the inflorescence meristem center. (**B** and **C**) Quantification of inducible *LFY* depletion in Fig. 3, A and B. Spatial distribution of GLFY fluorescence (B) and *TFL1* FISH intensity (C) in the inflorescence meristem (mean ± SEM, n=5). "Background": wild type FISH without hybridization probes at the same image acquisition settings. (**D** and **E**) Quantification of the inducible TFL1 depletion in Fig. 3, C and D. Spatial distribution of TFL1-GFP fluorescence (D) and *LFY* FISH intensity (E) in the inflorescences (mean ± SEM, n=5). "Background": Estradiol-treated wild type using the same FISH procedures and image acquisition settings. (B to E) Grayed parts of the plot indicate the bins beyond the inflorescence meristem center that include lateral meristems and flower primordia (between yellow and red circles in A) and were excluded from the fluorescence intensity quantification for the inflorescence meristem center. In each distance bin, means of signal intensity in uninduced (Mock) and induced (Dex or Estradiol) samples were compared by two-tailed Welch's *t*-test. (**F** and **G**) Percentage of plants forming

terminal flowers in response to inducible depletion of LFY (F) or TFL1 (G). n ≥ 7, Fisher's exact test. (B to G) *p*-values: ns >0.05, * <0.05, ** <0.01, *** <0.001, **** <0.0001.

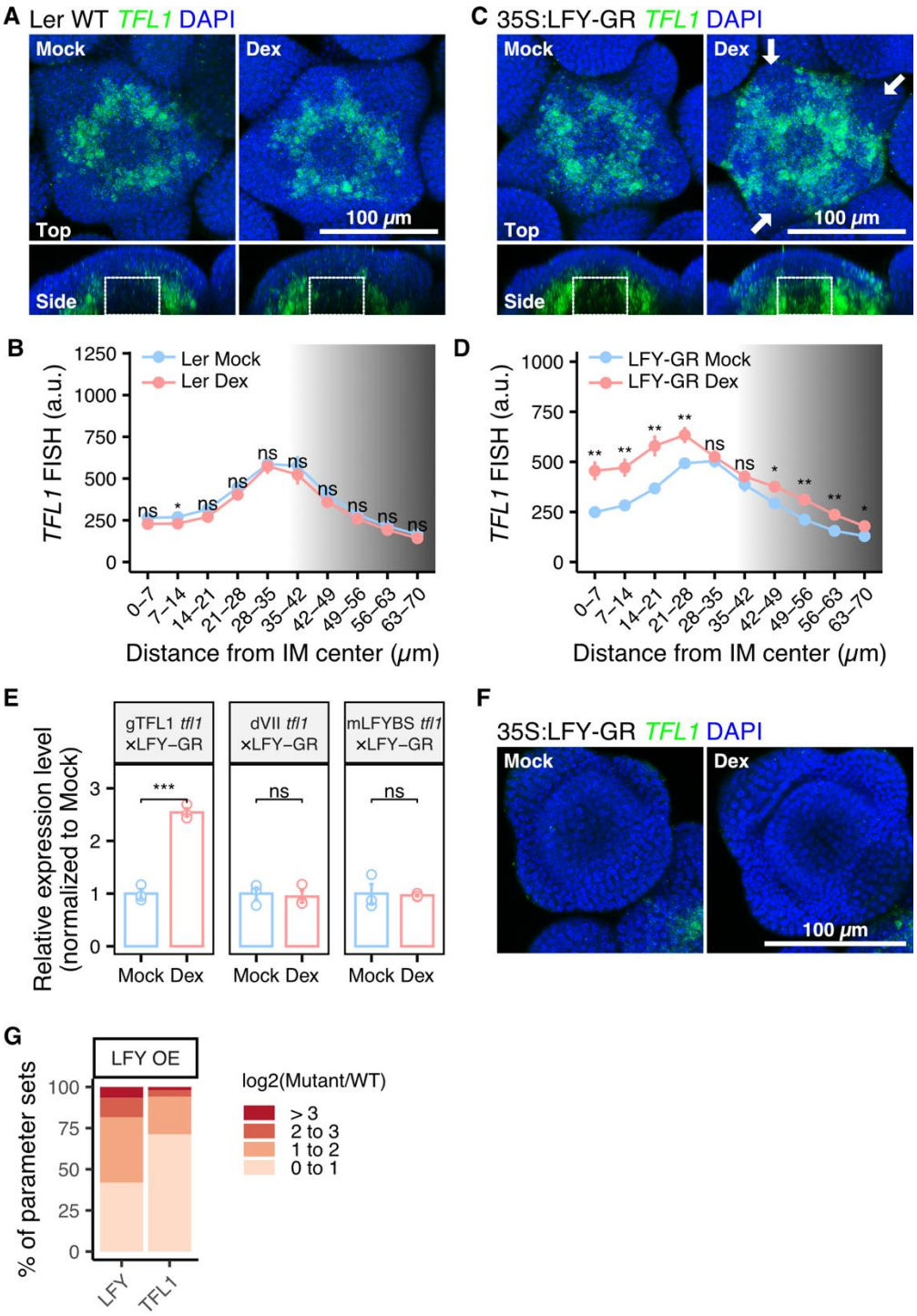

Fig. S11. Induction of 35S:LFY-GR promotes *TFL1* expression in the inflorescence meristem. (**A** to **D**) Wholemount *TFL1* FISH (green) in I2 phase inflorescences of wild-type L*er* (A and B) and 35S:LFY-GR (C and D) treated with 5 μM dexamethasone (Dex) or the mock solution for 20 hours. (A and C) Top-view maximum intensity projections (top) and xz longitudinal view (bottom). Dashed rectangles: the region where *TFL1* expression responds to 35S:LFY-GR induction. Arrows indicate early flower primordia. *TFL1* is not expressed in these tissues after 35S:LFY-GR induction. Nuclei (DAPI): blue. (B and D) Spatial distribution of

TFL1 FISH intensity in the inflorescences (mean ± SEM). L*er* n=3, 35S:LFY-GR n=8. Gray parts of the plot indicate the bins beyond the inflorescence meristem center that include lateral meristems and flower primordia. In each distance bin, means of signal intensity in Mock and Dex samples were compared by two-tailed Welch's *t*-test. Absolute values of FISH intensity in B and D are not comparable due to use of different fluorescent dyes and image acquisition settings. (**E**) *gTFL1*, *dVII*, *mLFYBS gTFL1-mEGFP* expression measured by RT-qPCR after inducing LFY-GR with 5 µM dexamethasone solution (Dex) or mock solution (Mock) in entire inflorescences. Mean ± SEM (n=3). (B, D, E) Two-tailed Welch's *t*-test *p*-values: ns >0.05, * <0.05, ** <0.01, *** <0.001, **** <0.0001. (**F**) Wholemount *TFL1* FISH (green) in stage 4 flowers of 35S:LFY-GR treated with dexamethasone (Dex) or mock solution (maximum intensity projections). *TFL1* upregulation was not observed in Dex-treated flowers. Nuclei (DAPI): blue. (**G**) Distribution of log2 fold changes of simulated increases in LFY and TFL1 accumulation in response to inducible LFY overexpression compared to the wild type across all accepted parameter sets (n=20000).

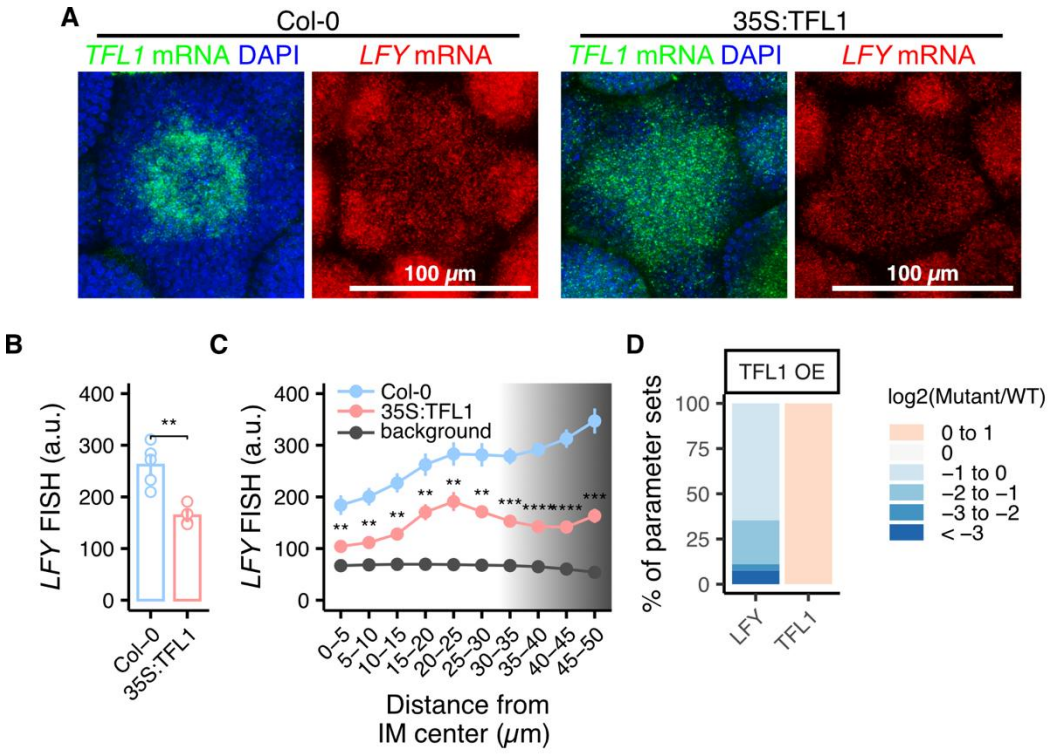

Fig. S12. Ectopic expression of *TFL1* in the inflorescence meristem represses *LFY* expression. (**A** to **C**) Wholemount FISH (A) and quantification (B and C) of *TFL1* (green) and *LFY* (red) in stage-matched I2 inflorescences of wild-type Col-0 and 35S:TFL1 (maximum intensity projections). Nuclei (DAPI): blue. n≥4. (B) Shown are mean ± SEM. Two-tailed Welch's *t*-test *p*-value: ** <0.01. (C) Spatial distribution of *LFY* FISH intensity in the inflorescences (mean ± SEM). "Background": wild-type Col-0 without FISH hybridization probes using same image acquisition settings. Gray parts of the plot indicate bins beyond the inflorescence meristem center that are excluded from fluorescence intensity quantification for the inflorescence meristem center as they comprise lateral meristems and flower primordia. In each distance bin, means were compared by two-tailed Welch's *t*-test. *p*-values: ns >0.05, * <0.05, ** <0.01, *** <0.001, **** <0.0001. (**D**) Distribution of log2 fold changes for simulated LFY and TFL1 levels in TFL1 overexpression relative to the wild type across all accepted parameter sets (n=20000).

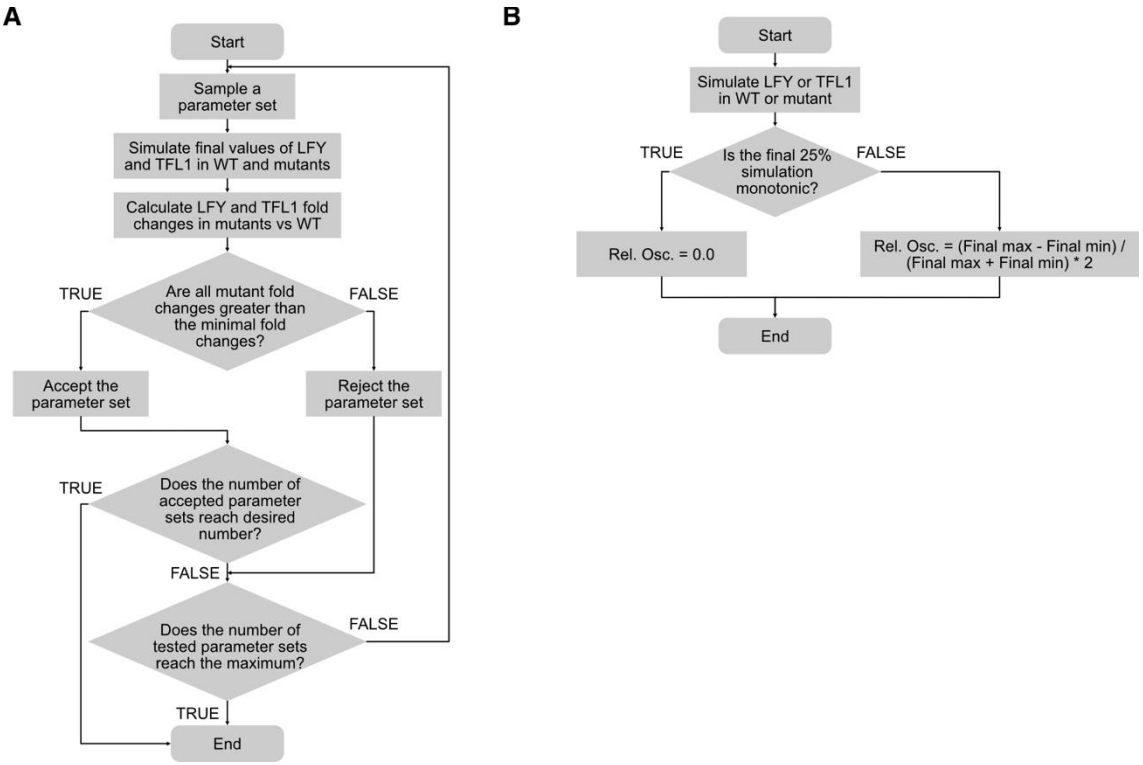

Fig. S13. Flowchart of computer model parameterization and oscillation studies. (**A**) Model parameterization. The midpoint of the maximum and minimum values in the final 10% timespan of each simulation was used as LFY and TFL1 final values (model outcome) to calculate the expression fold changes for mutants compared to the wild type. (**B**) Quantification of oscillation frequency for all accepted parameter sets. First, the final 25% timespan of the LFY or TFL1 simulations were used for assessing monotonicity. If simulations were not monotonic, the maximum (final max) and minimum (final min) values of LFY or TFL1 in the final 10% of the simulations were used for calculating the relative oscillation of non-monotonic simulations. For example, a relative oscillation of 0.2 indicates a 10% deviation from the midpoint.

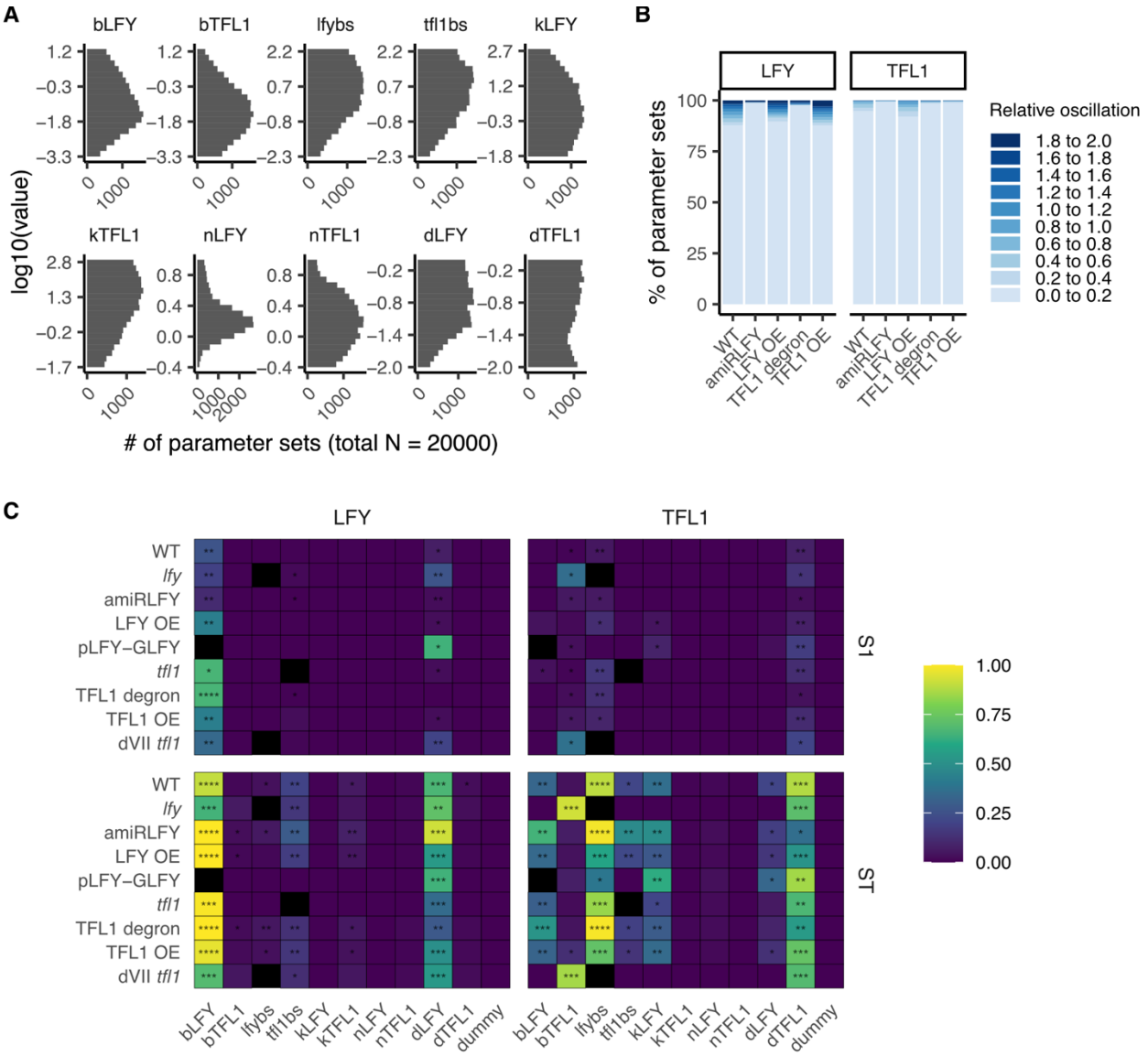

Fig. S14. Parameterization, test of oscillation and Sobol' sensitivity analyses for the 2-node LFY-TFL1 model. (**A**) Distribution of parameters accepted by the parameterization for basal production rate (bLFY, bTFL1), activity (lfybs, tfl1bs), concentration of LFY when the promoter of TFL1 is half occupied and vice versa (kLFY, kTFL1), Hill coefficient (nLFY, nTFL1) and degradation rate (dLFY, dTFL1). 20000 parameter sets were accepted at an acceptance rate of approximately 1 per 4500. (**B**) Relative oscillations of LFY and TFL1 in 2-node model simulations with accepted parameter sets. Shown are simulated wild type or mutants with an intact negative feedback loop. Parameter sets with relative oscillation > 0.2 (deviating 10% from the final value) were rare. (**C**) Global sensitivity analysis for 2-node model outcomes (LFY and TFL1 final values). The heatmaps (mean of 5 technical replicates) of first-order (S1) and total-order (ST) Sobol' indices show the contribution of each parameter to the variance of the model outcome. S1 shows the contribution of each parameter on its own, while ST shows combined contributions of each parameter and its interactions with other parameters. The dummy parameter serves as a control that does not contribute to the model outcomes. Kruskal-Wallis followed by Dunn's test were used to compare the Sobol' indices of parameters in each mutant

(or wild type). Asterisks indicate the Sobol' indices that are statistically distinguishable from the dummy parameter and contribute more than >0.1% to the variance. Adjusted *p*-values: * <0.05, ** <0.01, *** <0.001, **** <0.0001.

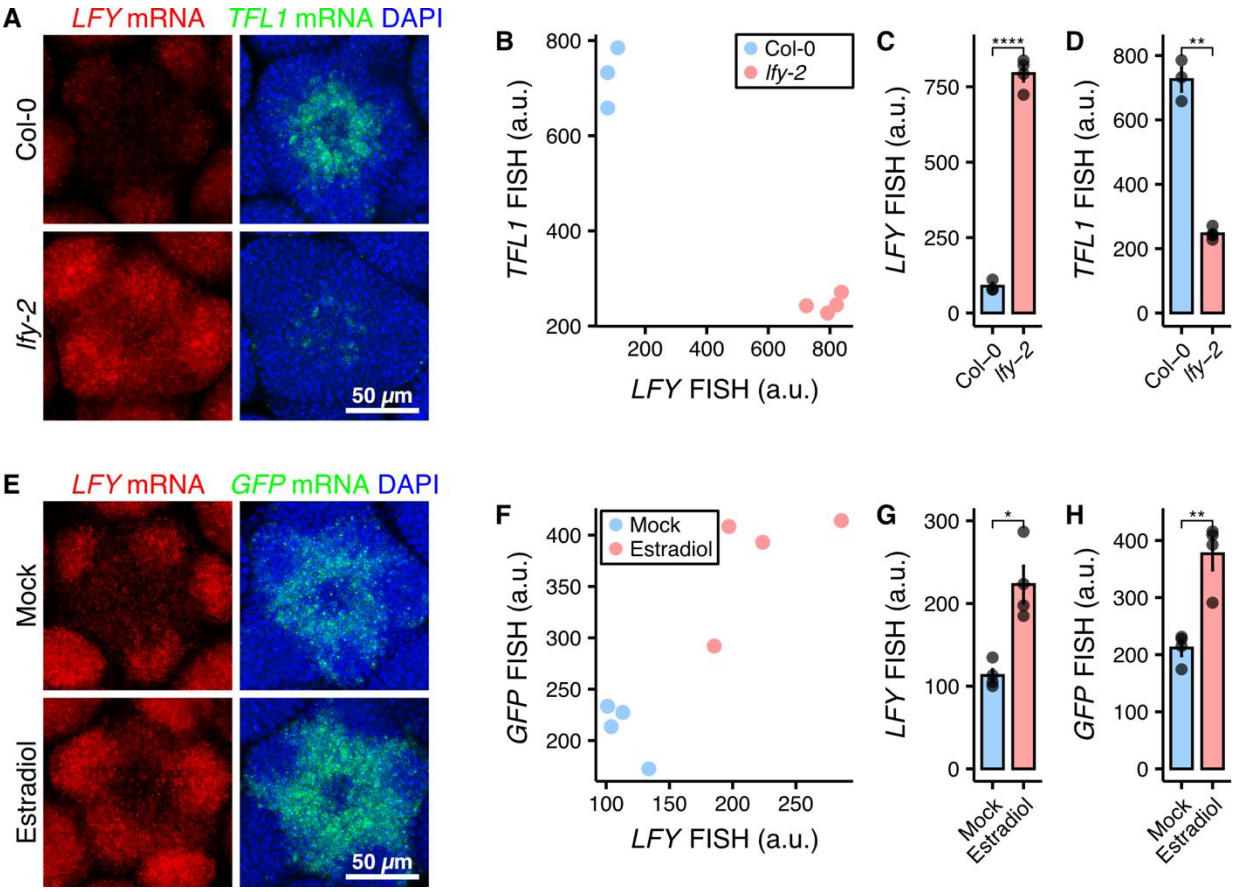

Fig. S15. Effect of TFL1 protein depletion or LFY protein mutation on *TFL1* and *LFY* mRNA levels as a result of the negative feedback loop. (**A** to **D**) Wholemount FISH (A) and quantification (B to D) of *LFY* and *TFL1* in I2 phase inflorescences of wild-type Col-0 and the *lfy-2* mutant. (A) Top-view maximum intensity projections (*LFY*: red, *TFL1*: green). Probes detect mRNA from wild-type and mutant alleles of *LFY*. Reduction of LFY activity triggers reduced *TFL1* accumulation, this in turn leads to increased *LFY* accumulation. (B to D) RNA FISH intensity in the inflorescence meristem center. Datapoints represent individual inflorescence samples (n≥3). (**E** to **H**) Wholemount FISH (E) and quantification (F to H) of *LFY* and *TFL1-GFP* in I2 phase gTFL1-GFP *tfl1-1* inflorescences after inducing GFP degradation (Estradiol) or treatment with mock solution for 20 hours. (E) Top-view maximum intensity projections (*LFY*: red, *TFL1-GFP*: green). TFL1 protein depletion triggers an increase in *LFY* accumulation and hence *TFL1* accumulation**.** (F to H) RNA FISH intensity in the inflorescence meristem center. Datapoints represent individual inflorescence samples (n=4). (C, D, G, H) Mean ± SEM. Means were compared by two-tailed Welch's *t*-test. *p*-values: * <0.05, ** <0.01, **** <0.0001.

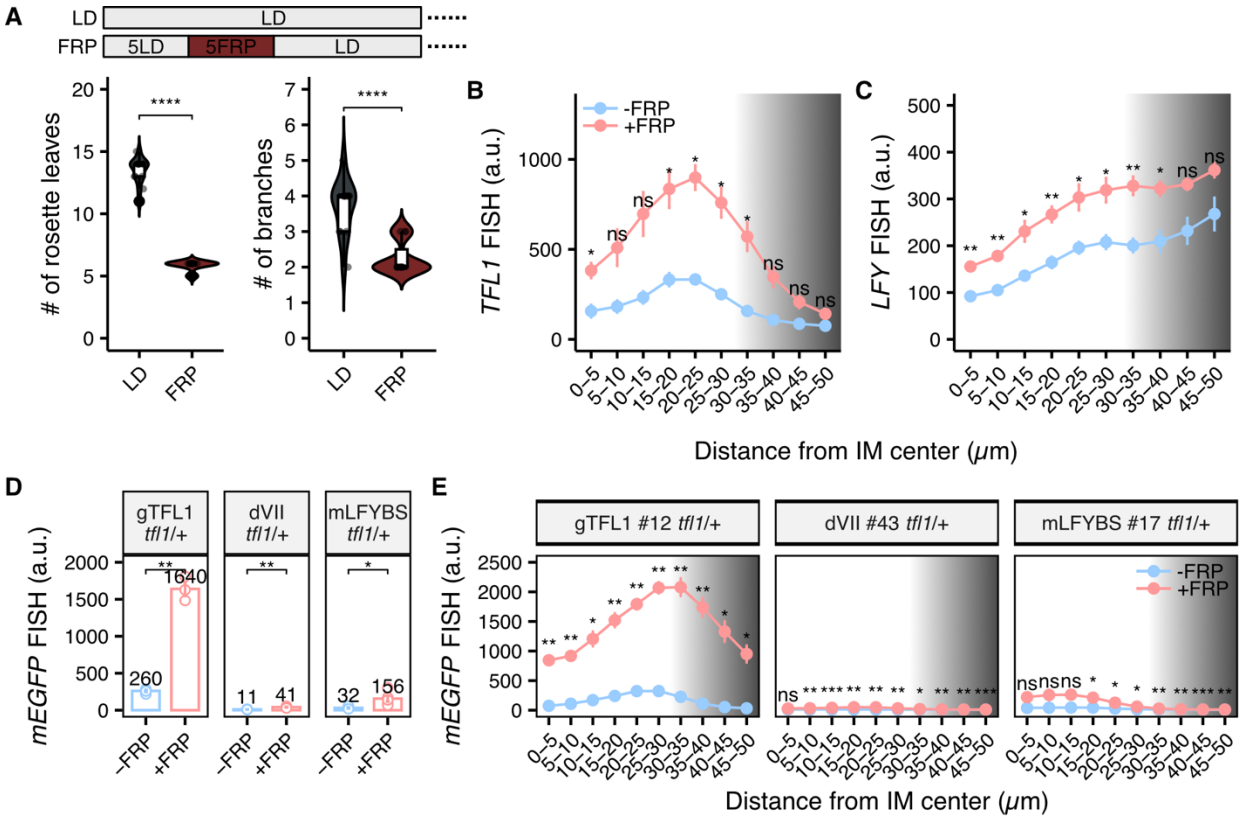

Fig. S16. FRP induces *TFL1* via LFY in I2 phase inflorescence meristems. (**A**) FRP is a very strong floral inductive signal that accelerates developmental transitions relative to long-day growth. Rosette leaves (left) and primary branches (right) produced in wild type grown for 5 days in long-day photoperiod (LD) or in long day supplemented with far-red light (FRP; 16-hour FRP/8-hour dark) treatment. n≥11. The means were compared by two-tailed Welch's *t*-test. *p*-values: **** <0.0001. (**B** and **C**) Quantification of the FRP assay in Fig. 4, A and B. Spatial distribution of *TFL1* (B) and *LFY* (C) FISH intensity in wild-type inflorescences without (-FRP) or with (+FRP) a single continuous 24-hour far-red-enriched treatment (mean ± SEM, n=3). (**D** and **E**) Quantification of response to FRP in the center of inflorescence meristems of wild type and mutants in Fig. 4E. (D) Shown are mean ± SEM (n≥3). Two-tailed Welch's *t*-test *p*-values: * <0.05, ** <0.01. (E) Spatial distribution of *mEGFP* FISH intensity in inflorescences in D treated with (+FRP) or without (-FRP) FRP as described for (B and C). Mean ± SEM, n≥3. (B, C, E) Gray parts of the plot indicate bins beyond the inflorescence meristem center that are excluded from fluorescence intensity quantification for the inflorescence meristem center as they comprise lateral meristems and flower primordia. In each distance bin, means of signal intensity in uninduced (-FRP) and induced (+FRP) samples were compared by two-tailed Welch's *t*-test. *P*-values: ns >0.05, * <0.05, ** <0.01, *** <0.001, **** <0.0001.

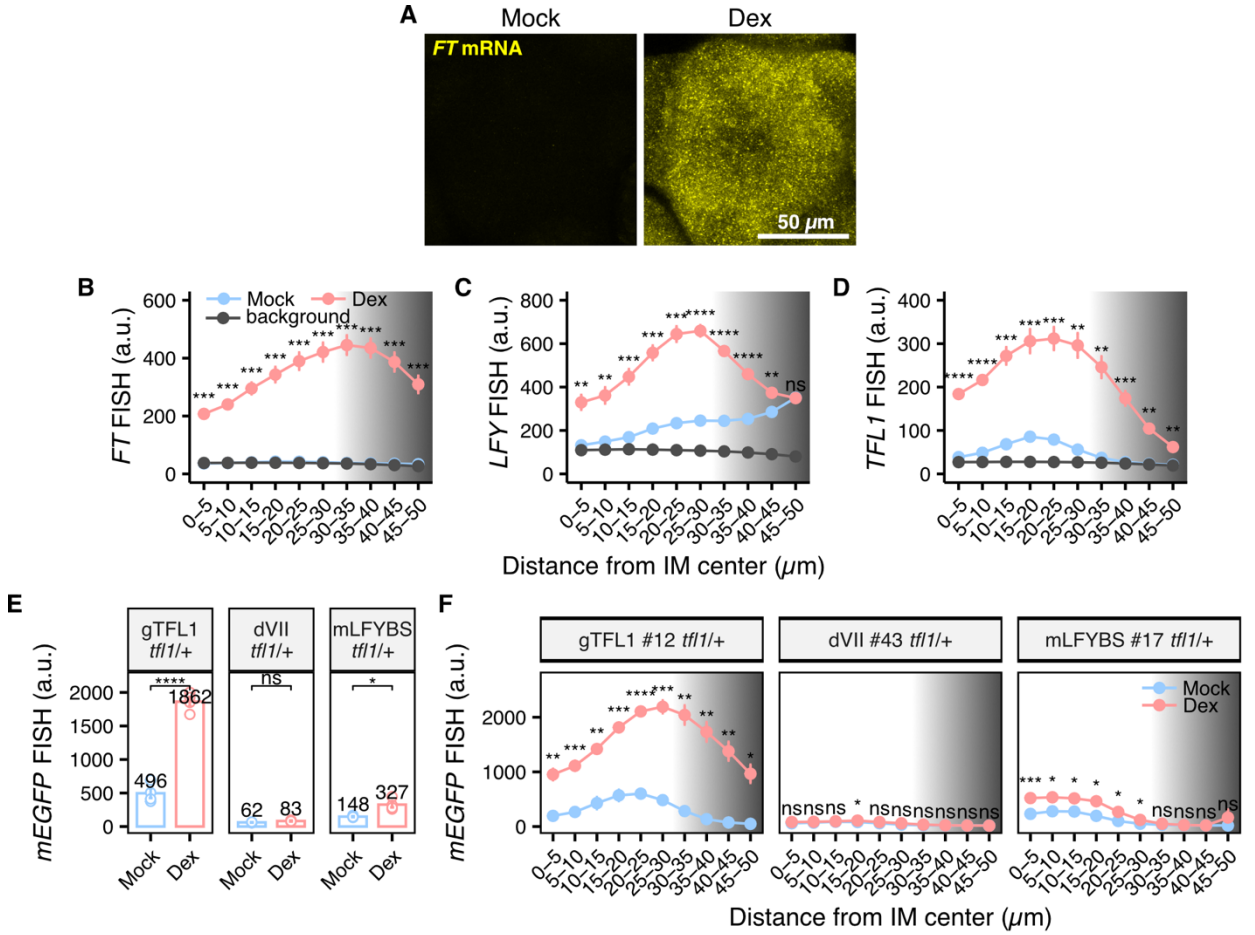

Fig. S17. FT promotes *TFL1* upregulation via LFY. (**A** to **D**) Confocal images (A) and quantification (B to D) of the inducible FT overexpression for the data in Fig. 4, C and D. (A) *FT* (yellow) FISH accumulation in I2 stage inflorescences induced by dexamethasone (Dex) or mock treated for 16 hours (maximum intensity projections). (B to D) Spatial distribution of *FT* (B), *LFY* (C), and *TFL1* (D) transcript levels in inflorescences treated as in A (mean ± SEM, n=5). "Background": wild-type Col-0 (without FISH hybridization probes) using the same image acquisition settings. (**E** and **F**) Quantification of inducible FT overexpression for the data in Fig. 4F comparing gTFL1-mEGFP *tfl1*/+ with versions thereof that lack LFY binding sites (dVII or mLFYBS gTFL1-mEGFP *tfl1*/+). Plants were treated as in (A). (E) Quantification in the inflorescence meristem center (mean ± SEM, n≥3). Two-tailed Welch's *t*-test *p*-values: ns >0.05, * <0.05, **** <0.0001. (F) Spatial distribution of *mEGFP* FISH intensity (mean ± SEM, n≥3). (B, C, D, F) Gray parts of the plot indicate bins beyond the inflorescence meristem center that are excluded from fluorescence intensity quantification for the inflorescence meristem center as they comprise lateral meristems and flower primordia. In each distance bin, means of signal intensity in uninduced (Mock) and induced (Dex) samples were compared by two-tailed Welch's *t*-test. *p*-values: ns >0.05, * <0.05, ** <0.01, *** <0.001, **** <0.0001.

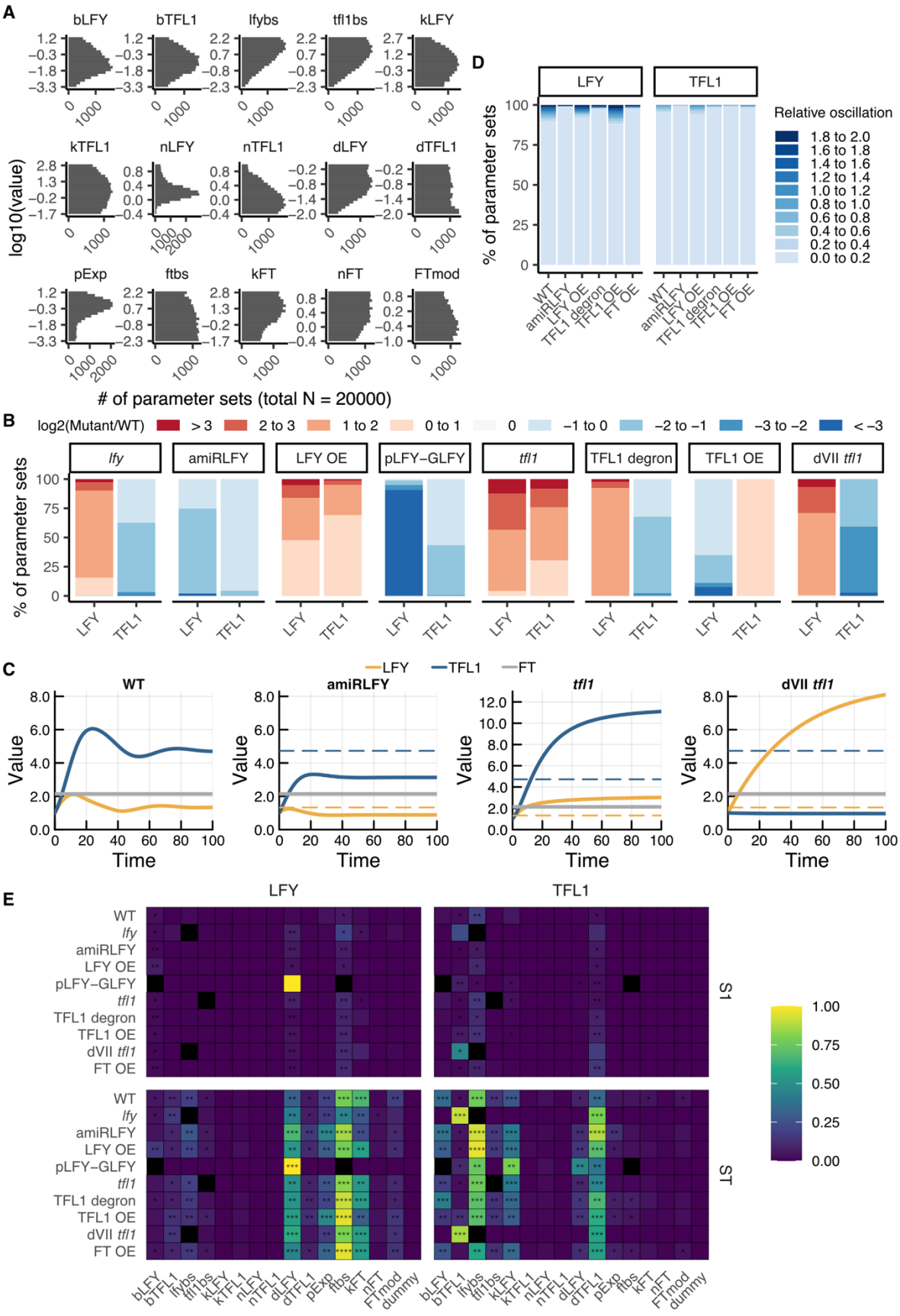
A
bLFY
bTFL1
lfybs
tfl1bs
kLFY
kTFL1
nLFY
nTFL1
dLFY
dTFL1
pExp
ftbs
kFT
nFT
FTmod
log10(value)
# of parameter sets (total N = 20000)
D
LFY
TFL1
% of parameter sets
Relative oscillation
1.8 to 2.0
1.6 to 1.8
1.4 to 1.6
1.2 to 1.4
1.0 to 1.2
0.8 to 1.0
0.6 to 0.8
0.4 to 0.6
0.2 to 0.4
0.0 to 0.2
WT
amiRLFY
LFY OE
TFL1 degron
TFL1 OE
FT OE
B
log2(Mutant/WT)
> 3
2 to 3
1 to 2
0 to 1
0
−1 to 0
−2 to −1
−3 to −2
< −3
lfy
amiRLFY
LFY OE
pLFY–GLFY
tfl1
TFL1 degron
TFL1 OE
dVII tfl1
% of parameter sets
C
LFY
TFL1
FT
WT
amiRLFY
tfl1
dVII tfl1
Value
Time
E
LFY
TFL1
WT
lfy
amiRLFY
LFY OE
pLFY–GLFY
tfl1
TFL1 degron
TFL1 OE
dVII tfl1
FT OE
S1
ST
1.00
0.75
0.50
0.25
0.00
bLFY
bTFL1
lfybs
tfl1bs
kLFY
kTFL1
nLFY
nTFL1
dLFY
dTFL1
pExp
ftbs
kFT
nFT
FTmod
dummy

Fig. S18. Parameterization, test of oscillation and Sobol' sensitivity analyses for the 3-node model using FT as an input. (**A**) Distributions of parameters accepted by the parameterization. 20000 parameter sets were accepted at an acceptance rate of approximately 1 per 16000. (**B**) Distributions of log2 fold changes for simulated LFY and TFL1 levels in mutants relative to the wild type across all accepted parameter sets. (**C**) Example simulations of LFY, TFL1, and FT accumulation over time in wild type and mutants. Parameter set closest to the centroid of the accepted parameter sets were used to generate the graphs. Dashed lines indicate LFY and TFL1 final values in the wild-type simulation. (**D**) Relative oscillations of LFY and TFL1 in 3-node model simulations with accepted parameter sets. Shown are simulated wild type or mutant with an intact negative feedback loop. Parameter sets with relative oscillation > 0.2 (deviating 10% from the final value) were rare. (**E**) Global sensitivity analysis for 3-node model outcomes (LFY and TFL1 final values). The heatmaps (mean of 5 technical replicates) of first-order (S1) and total-order (ST) Sobol' indices show the contribution of each parameter to the variance of the model outcome. The dummy parameter serves as a control that does not contribute to the model outcomes. Kruskal-Wallis followed by Dunn's test were used to compare the Sobol' indices of parameters in each mutant (or wild type). Asterisks indicate the Sobol' indices that are statistically distinguishable from the dummy parameter and contribute more than >0.1% to the variance. Adjusted *p*-values: * <0.05, ** <0.01, *** <0.001, **** <0.0001.

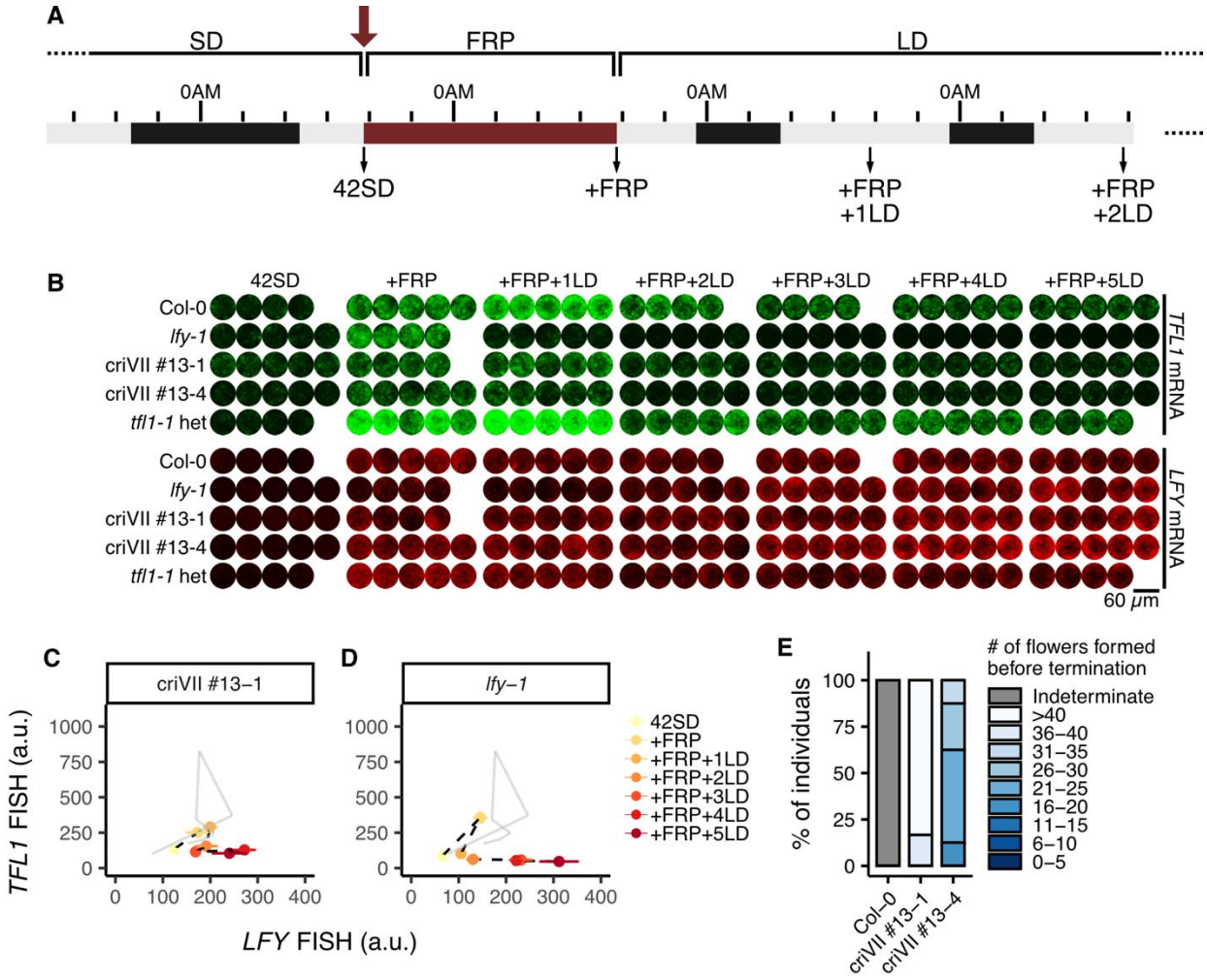

Fig. S19. *TFL1* and *LFY* transcript accumulation in response to FRP treatment. (**A**) Schematic of FRP induction regime (*7, 8*) in Fig. 5, A to D. Plants were grown in non-inductive short-day condition for 42 days, treated with FRP for 24 hours and then transferred to LD. Inflorescences were sampled daily. Red arrow: start of FRP induction. (**B** to **D**) Time-course wholemount FISH for *TFL1* (green) and *LFY* (red) in wild type, *lfy-1*, criVII #13-1, criVII #13-4, and *tfl1-1* heterozygote (*tfl1-1* het) before and after FRP induction. (B) Confocal images of all replicates of the time-course wholemount FISH assay shown in Fig. 5, A to D. 60-µm diameter circles of inflorescence meristem centers for each sample (maximum intensity projections along the z-axis). The *TFL1* (top) and *LFY* (bottom) images at equivalent positions are from separate channels of the same inflorescence. (C and D) Quantification of *TFL1* and *LFY* FISH intensities in the criVII #13-1 line (which retains more LFY binding sites than criVII #13-4) (C) and in the *lfy-1* null mutant (D) (mean ± SEM, n≥4). Gray lines show the data of wild-type Col-0. (B and D) In *lfy-1*, mutant *LFY* mRNA levels were recorded. (**E**) Number of flowers formed before inflorescence meristem termination in wild-type Col-0 and criVII alleles after FRP induction. n≥6. SD: short-day photoperiod, LD: long-day photoperiod, FRP: 24-hour far-red enriched light treatment.

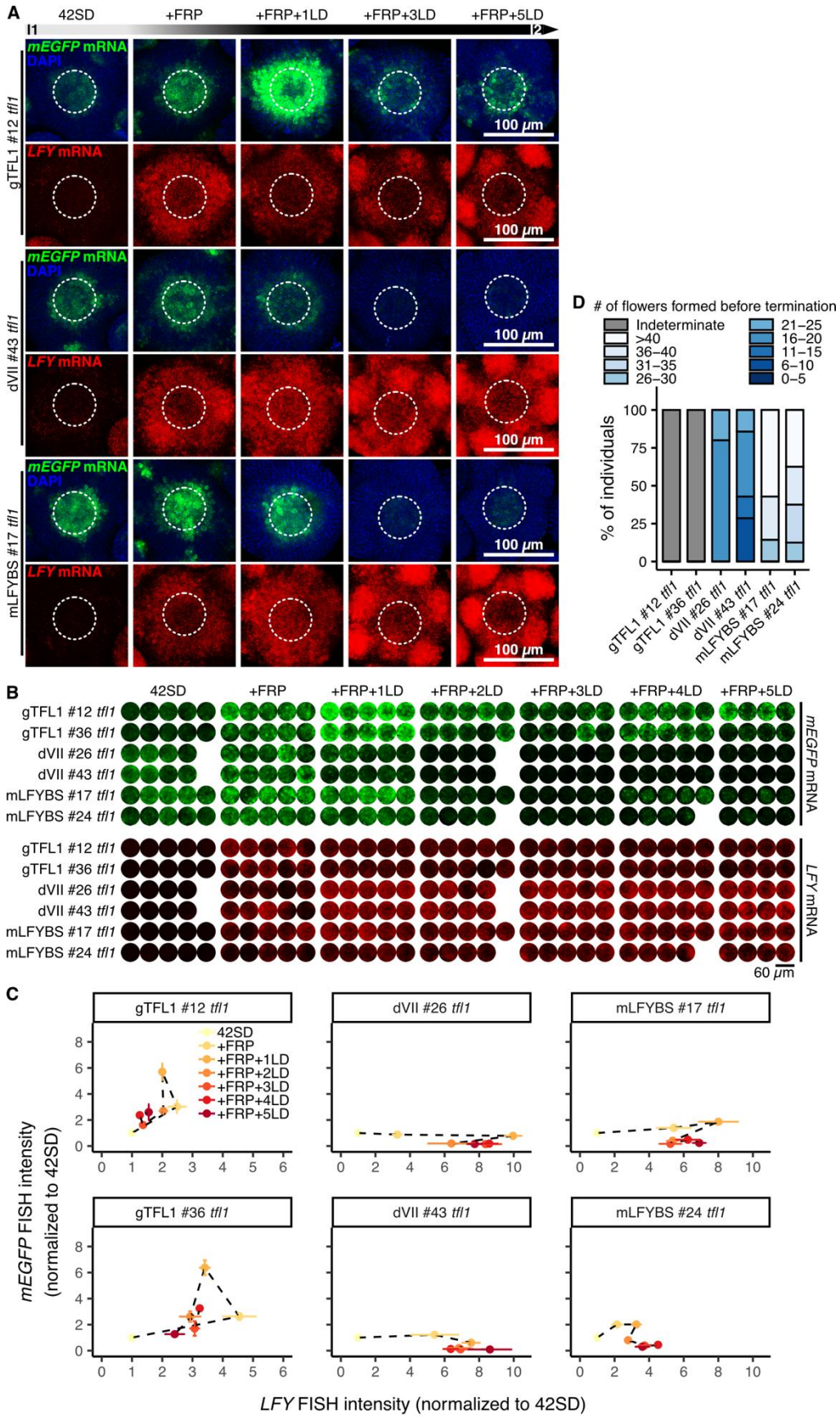
A
42SD
+FRP
+FRP+1LD
+FRP+3LD
+FRP+5LD
I1
I2
mEGFP mRNA
DAPI
LFY mRNA
100 μm
gTFL1 #12 tfl1
dVII #43 tfl1
mLFYBS #17 tfl1
D
# of flowers formed before termination
Indeterminate
>40
36–40
31–35
26–30
21–25
16–20
11–15
6–10
0–5
% of individuals
gTFL1 #12 tfl1
gTFL1 #36 tfl1
dVII #26 tfl1
dVII #43 tfl1
mLFYBS #17 tfl1
mLFYBS #24 tfl1
B
+FRP+2LD
+FRP+4LD
mEGFP mRNA
LFY mRNA
60 μm
C
gTFL1 #12 tfl1
dVII #26 tfl1
mLFYBS #17 tfl1
gTFL1 #36 tfl1
dVII #43 tfl1
mLFYBS #24 tfl1
mEGFP FISH intensity (normalized to 42SD)
LFY FISH intensity (normalized to 42SD)

Fig. S20. *TFL1-mEGFP* and *LFY* transcript accumulation in response to FRP treatment. (**A** to **C**) Time-course wholemount FISH for transgenic rescue lines (gTFL1, dVII, or mLFYBS gTFL1-mEGFP in *tfl1-1*) before and after FRP induction. Experimental design as in fig. S19A. (A) Maximum intensity projections. *mEGFP*: green, *LFY*: red, nuclei (DAPI): blue. (B) 60-µm diameter circles of inflorescence meristem centers for each sample (maximum intensity projections along the z-axis). *mEGFP* (top) and *LFY* (bottom) images at equivalent positions are from separate channels of the same inflorescence. (C) Quantification of *mEGFP* and *LFY* FISH intensity in the time-course experiment (mean ± SEM, n≥4). (**D**) Number of flowers formed before inflorescence meristem termination in the rescue lines after FRP induction. n≥6. SD: short-day photoperiod, LD: long-day photoperiod, FRP: far-red-enriched long-day photoperiod.

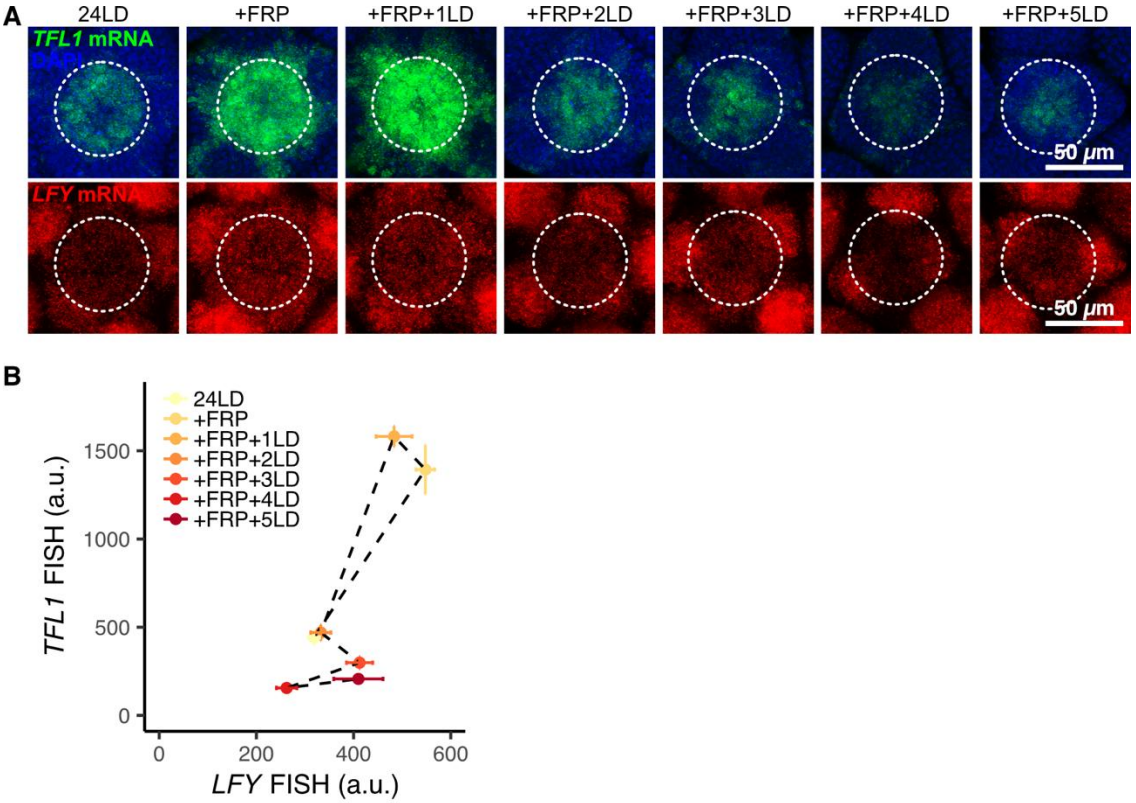

Fig. S21. *TFL1* and *LFY* response to perturbation by FRP in I2 inflorescence meristems, after the reproductive transition. (**A** and **B**) Time-course wholemount FISH for *TFL1* (green) and *LFY* (red) in wild-type inflorescence meristems before and after FRP induction. Inflorescences (24LD) were treated with 24-hour FRP (+FRP) followed by return to LD. (A) Shown are maximum intensity projections. *TFL1*: green, *LFY*: red, nuclei (DAPI): blue. (B) Quantification of *TFL1* and *LFY* FISH intensity in the time-course experiment (mean ± SEM, n=5).

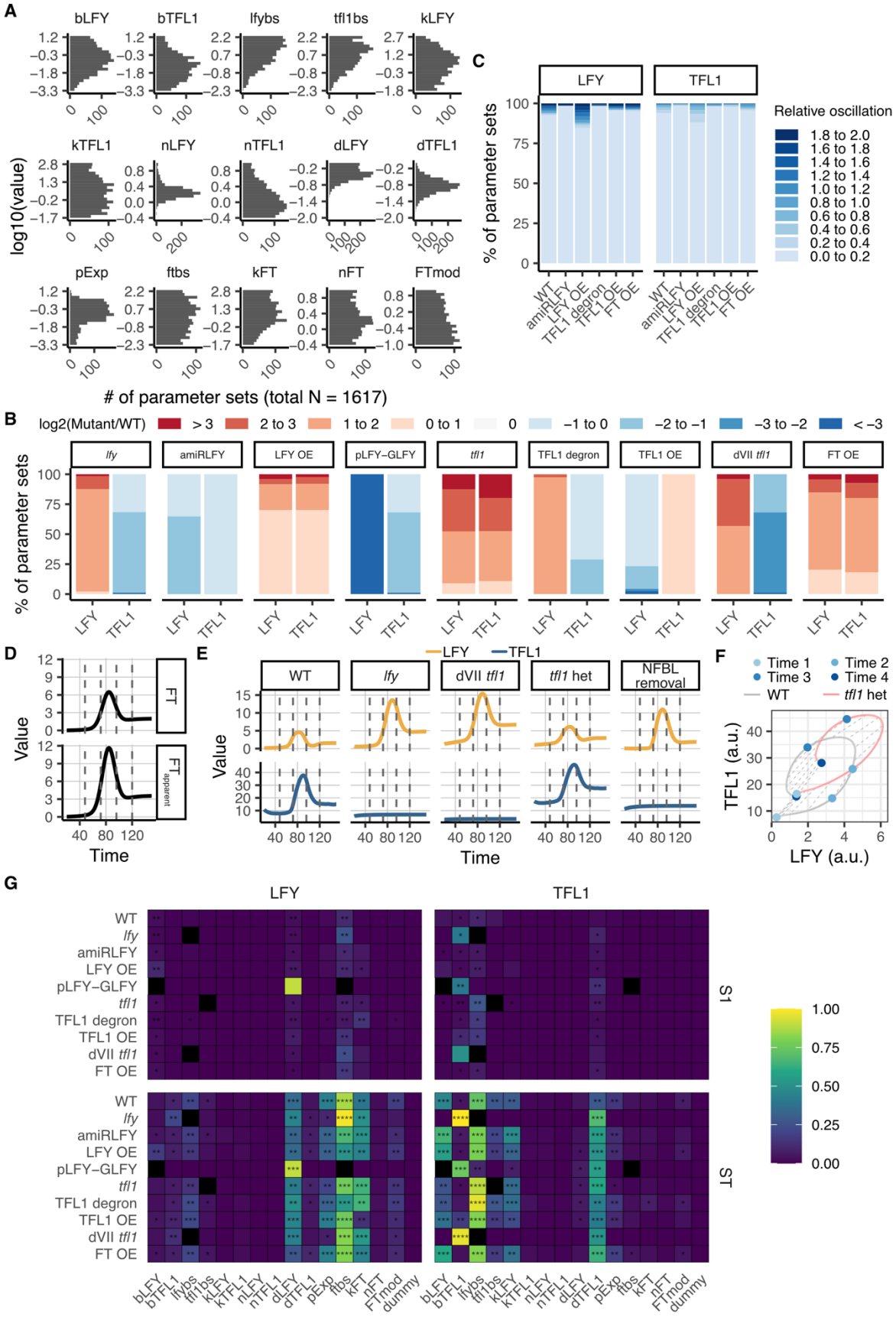
A
bLFY
bTFL1
lfybs
tfl1bs
kLFY
kTFL1
nLFY
nTFL1
dLFY
dTFL1
pExp
ftbs
kFT
nFT
FTmod
log10(value)
# of parameter sets (total N = 1617)
C
LFY
TFL1
% of parameter sets
Relative oscillation
1.8 to 2.0
1.6 to 1.8
1.4 to 1.6
1.2 to 1.4
1.0 to 1.2
0.8 to 1.0
0.6 to 0.8
0.4 to 0.6
0.2 to 0.4
0.0 to 0.2
WT
amiRLFY
LFY OE
pLFY−GLFY
TFL1 degron
TFL1 OE
FT OE
B
log2(Mutant/WT)
> 3
2 to 3
1 to 2
0 to 1
0
−1 to 0
−2 to −1
−3 to −2
< −3
lfy
amiRLFY
LFY OE
pLFY−GLFY
tfl1
TFL1 degron
TFL1 OE
dVII tfl1
FT OE
% of parameter sets
D
FT
FT apparent
Value
Time
E
LFY
TFL1
WT
lfy
dVII tfl1
tfl1 het
NFBL removal
Value
Time
F
Time 1
Time 2
Time 3
Time 4
WT
tfl1 het
TFL1 (a.u.)
LFY (a.u.)
G
LFY
TFL1
WT
lfy
amiRLFY
LFY OE
pLFY−GLFY
tfl1
TFL1 degron
TFL1 OE
dVII tfl1
FT OE
S1
ST
1.00
0.75
0.50
0.25
0.00
bLFY
bTFL1
lfybs
tfl1bs
kLFY
kTFL1
nLFY
nTFL1
dLFY
dTFL1
pExp
ftbs
kFT
nFT
FTmod
dummy

Fig. S22. Parameterization for the 3-node model with changing FT input, test of oscillation study and Sobol' sensitivity analyses. (**A**) Distributions of parameters accepted by the parameterization. 1617 parameter sets were accepted at an acceptance rate of approximately 1 per 1.8 million. Compared to fig. S18A, the dynamic changes of both LFY and TFL1 levels in the wild type at different timepoints of the FRP treatment were included as additional criteria for the parameterization (Fig. 5, A and B). Relative to fig. S18A, a narrow range of degradation rates (dLFY and dTFL1) fit our criteria. (**B**) Distributions of log2 fold changes for simulated LFY and TFL1 levels in mutants relative to the wild type across all accepted parameter sets. (**C**) Relative oscillations of LFY and TFL1 in 3-node model simulations with accepted parameter sets. Shown are simulated wild type or mutants with an intact negative feedback loop. Parameter sets with relative oscillation > 0.2 (deviating 10% from the final value) were rare. (**D** to **F**) Simulations of FT, LFY, and TFL1 in wild type and mutants before and after the simulated FRP treatment. An FT pulse was used to simulate the FRP treatment as shown in fig. S19A. Shown are mean values at different time points of simulations using all accepted parameter sets. (D and E) The vertical dashed lines correspond indicate timepoints 42SD, +FRP, +FRP+1LD, and +FRP+2LD also referred to as Time 1-4 of the FRP treatment experiment. See also (fig. S19A). (D) FT levels over time without (top) or with ($FT_{apparent}$, bottom) the modification by the ftmod parameter (Supplementary Text). (E) Shown are LFY and TFL1 values over time. Simulations with intact negative feedback loops (WT and *tfl1* het) show lower LFY peak and earlier LFY decline. (F) *tfl1* heterozygotes showed similar LFY and TFL1 dynamics as wild type during the simulated FRP treatment and higher LFY and TFL1 values. The gray dashed lines link identical time points between the two curves. (**G**) Global sensitivity analysis for 3-node model outcomes (LFY and TFL1 final values). Analyses were performed within the bounds identified by the parameterization in panel (A). The heatmaps (mean of 5 technical replicates) of first-order (S1) and total-order (ST) Sobol' indices show the contribution of each parameter to the variance of the model outcome. The dummy parameter serves as a control that does not contribute to the model outcomes. Kruskal-Wallis followed by Dunn's test were used to compare the Sobol' indices of parameters in each mutant (or wild type). Asterisks indicate the Sobol' indices that are statistically distinguishable from the dummy parameter and contribute more than >0.1% to the variance. Adjusted *p*-values: * <0.05, ** <0.01, *** <0.001, **** <0.0001. SD: short-day photoperiod, LD: long-day photoperiod, FRP: far-red-enriched long-day photoperiod.

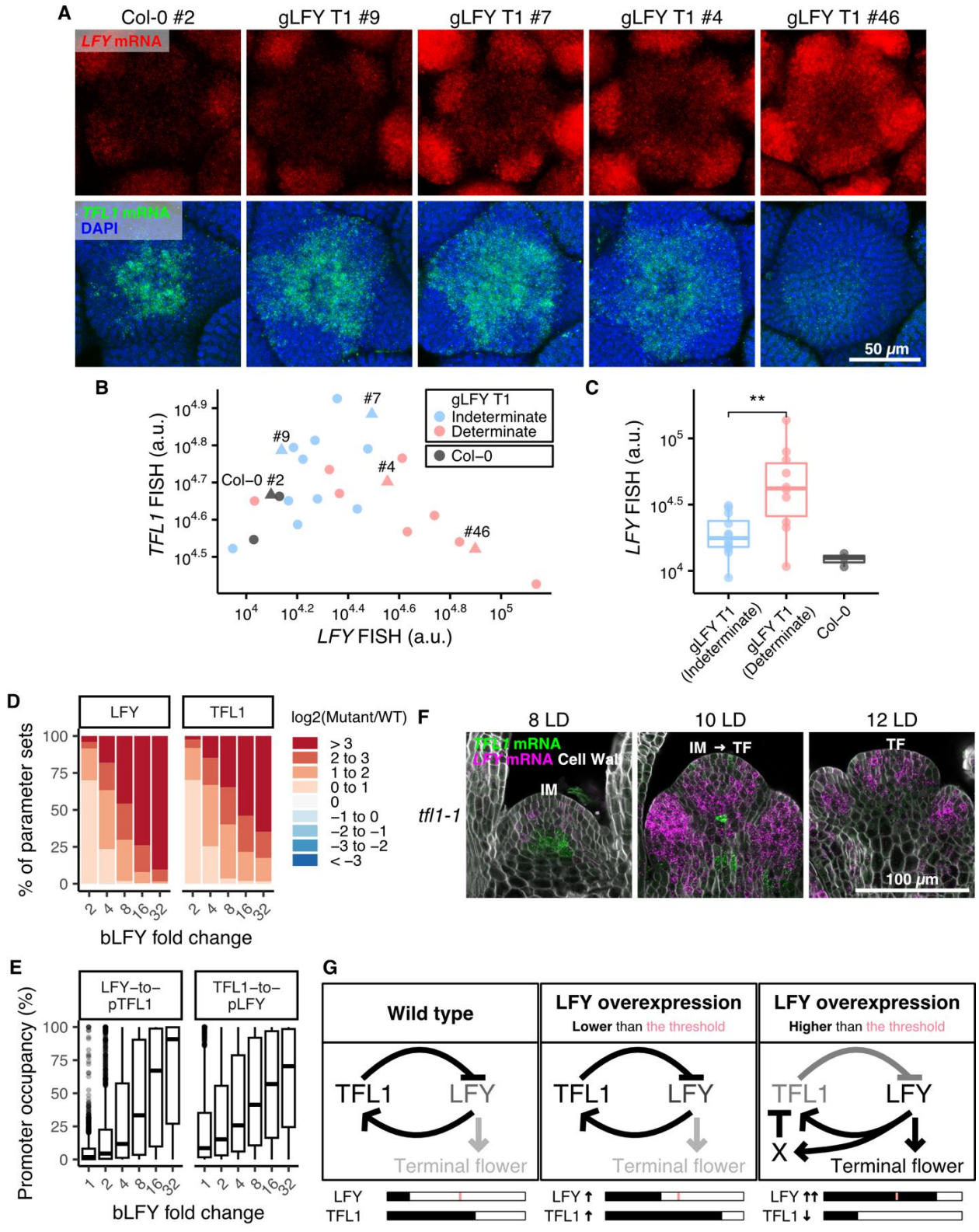

Fig. S23. Sustained *LFY* overaccumulation in the inflorescence meristem overrides the LFY-TFL1 negative feedback loop leading to determinacy. (**A** to **C**) Wholemount FISH (A) and quantification (B and C) for *LFY* (red) and *TFL1* (green) in I2 phase inflorescences of gLFY

T1 transformants. All gLFY T1 samples were assayed at the 1cm bolt stage. (A) Shown are maximum intensity projections. Nuclei (DAPI): blue. (B) Quantification of FISH intensity in the inflorescence meristem center. Datapoints represent individual inflorescence samples. Samples shown in A are depicted as triangles. (C) Quantification of *LFY* FISH intensity in the inflorescence meristem center of indeterminate and determinate gLFY T1 transformants (Col-0 n=3, gLFY n=22). Means were compared by two-tailed Welch's *t*-test. *p*-values: ** <0.01. (**D** and **E**) Predicted distributions of simulated LFY and TFL1 log2 fold changes (D) and predicted promoter occupancy (E) in mutants with increased bLFY across all accepted parameter sets (fig. S22A). (E) Promoter occupancy was calculated using Hill equations based on simulated final values for LFY and TFL1 levels (Supplementary Text). (**F**) Terminating inflorescence meristems loose *TFL1* expression. FISH in *tfl1-1* mutant inflorescences during inflorescence meristem termination (longitudinal sections). *TFL1*: green, *LFY*: magenta. *TFL1* probes detect nonfunctional mRNA. Cell wall (Calcofluor-white): white. IM: inflorescence meristem, TF: terminal flower. (**G**) Schematic for the effect of LFY accumulation on the negative feedback loop. Intact feedback loop in the wild type (left) or in weak overexpression lines (LFY levels ≤ $10^{4.4}$ in (B), center). Terminal flower formation and exit from the negative feedback loop occur when LFY levels exceed a critical threshold. LFY switches from directly promoting *TFL1* to indirectly repressing *TFL1* expression, this likely requires activation of repressors of *TFL1* expression (factor(s) X, right).

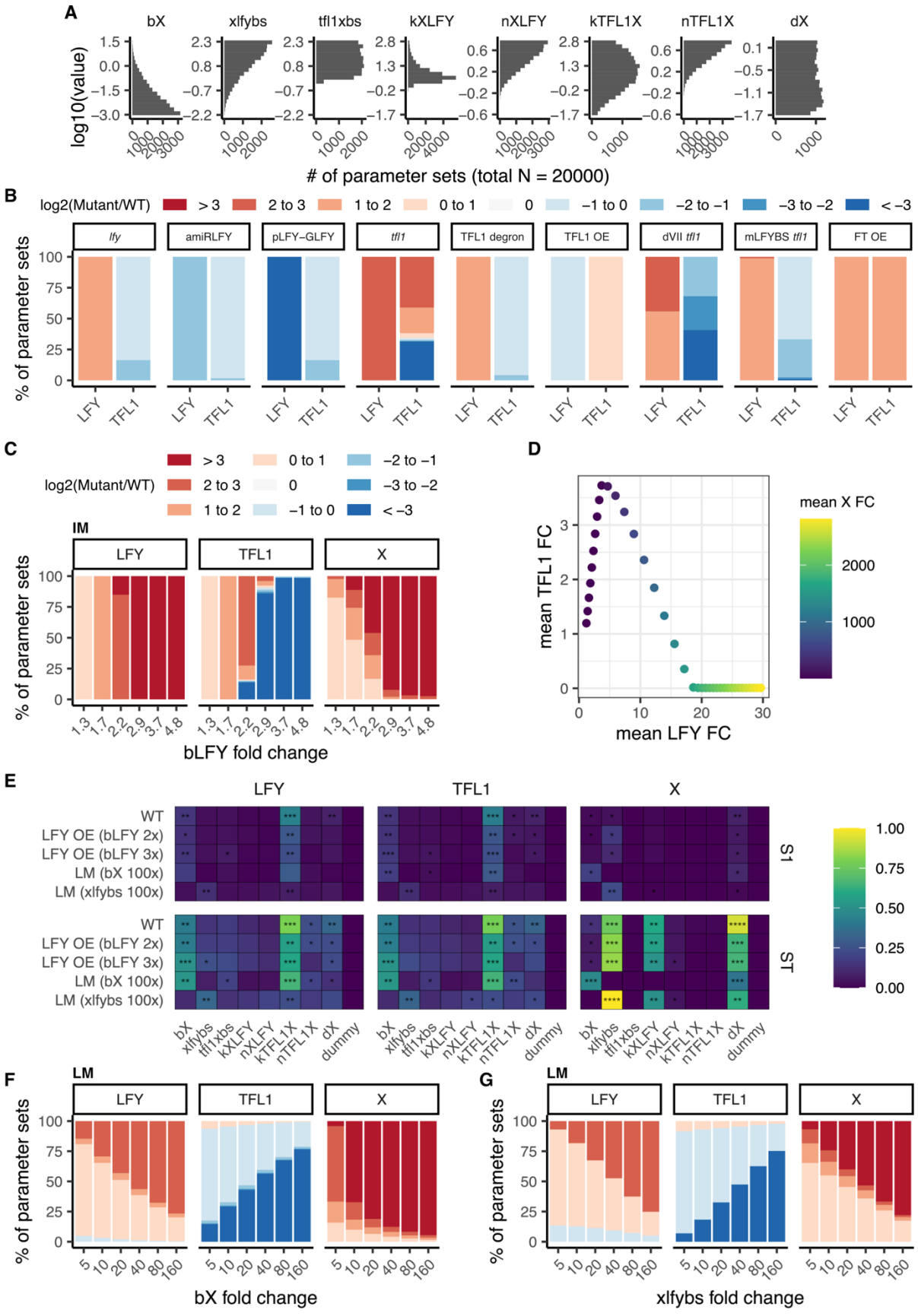
A
bX
xlfybs
tfl1xbs
kXLFY
nXLFY
kTFL1X
nTFL1X
dX
log10(value)
# of parameter sets (total N = 20000)
B
log2(Mutant/WT)
> 3
2 to 3
1 to 2
0 to 1
0
−1 to 0
−2 to −1
−3 to −2
< −3
lfy
amiRLFY
pLFY−GLFY
tfl1
TFL1 degron
TFL1 OE
dVII tfl1
mLFYBS tfl1
FT OE
% of parameter sets
LFY
TFL1
C
IM
LFY
TFL1
X
bLFY fold change
D
mean TFL1 FC
mean LFY FC
mean X FC
E
LFY
TFL1
X
WT
LFY OE (bLFY 2x)
LFY OE (bLFY 3x)
LM (bX 100x)
LM (xlfybs 100x)
S1
ST
dummy
F
LM
bX fold change
G
xlfybs fold change

Fig. S24. Parameterization for factor(s) X in the 4-node model and Sobol' sensitivity analyses in simulated inflorescence meristem and lateral meristems. (**A**) Distribution of X-related parameters accepted by the parameterization. 20000 parameter sets were accepted at an acceptance rate of approximately 1 per 860. Experimental observation in fig. S23A were included as additional criteria for the parameterization. (**B**) Distributions of log2 fold changes for simulated LFY and TFL1 levels in mutants relative to the wild type across all accepted parameter sets. (**C** and **D**) Predicted fold changes of simulated LFY and TFL1 levels in mutants with increased LFY basal production rate bLFY relative to the wild type across all accepted parameter sets. In agreement with our experimental data, weak LFY overexpression (small bLFY increase) upregulated *TFL1*, while strong LFY overexpression (large bLFY increase) promoted an increase in X accumulation, which causes repression of *TFL1* expression. (D) Individual datapoints correspond to increasing bLFY levels in LFY overexpression simulations. Shown are mean simulation fold changes for LFY, TFL1 and X (x, y axes and purple to yellow color, respectively). (**E**) Global sensitivity analysis for 4-node model outcomes (LFY and TFL1 final values). The heatmaps (mean of 5 technical replicates) of first-order (S1) and total-order (ST) Sobol' indices show the contribution of each parameter to the variance of the model outcome. The dummy parameter serves as a control that does not contribute to the model outcomes. Kruskal-Wallis followed by Dunn's test were used to compare the Sobol' indices of parameters in each mutant (or wild type). Asterisks indicate the Sobol' indices that are statistically distinguishable from the dummy parameter and contribute more than >0.1% to the variance. (**F** and **G**) Contribution of factor(s) X to the differential responses to floral inductive cues observed in lateral meristems compared to the inflorescence meristem. Despite LFY upregulation in both meristems, LFY does not activate *TFL1* in lateral meristems. If factor(s) X accumulate to higher levels in lateral meristems than in the inflorescence meristem, due to an increase in basal production rate (higher bX; F) or higher ability of LFY to activate X (higher xlfybs; G), X blocks *TFL1* upregulation in these meristems. Shown are distributions of log2 fold changes for LFY, TFL1 and X in the simulated wild-type lateral meristem relative to the wild-type inflorescence meristem.

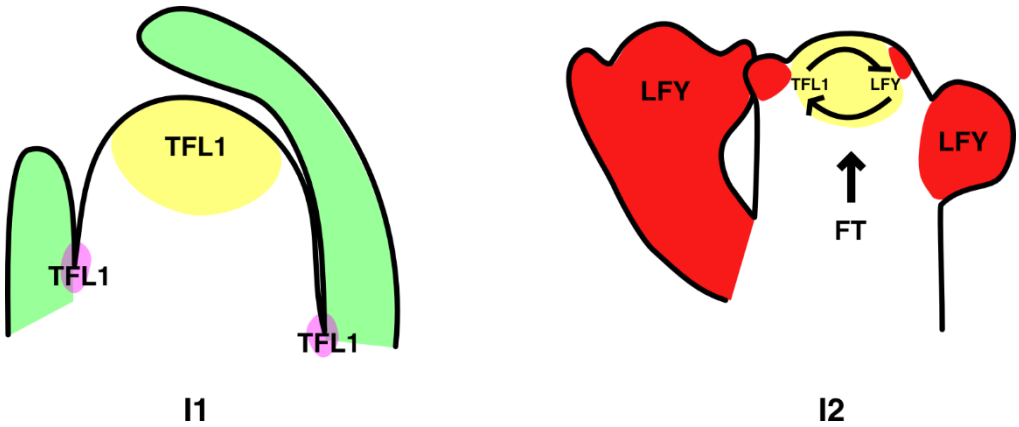

Fig. S25. Mutual exclusion and antagonism versus negative feedback interactions between TFL1 and LFY. Before the inflorescence produces flowers (I1 phase, left), TFL1 accumulates in the axillary meristems (magenta) that give rise to branches and weakly in the inflorescence meristem (yellow) in a LFY-independent manner. LFY is not expressed in the axillary meristem or inflorescence meristem at this stage, but accumulates in very young leaf primordia (not shown). In response to floral inductive cues and increased systemic FT signal *LFY* is upregulated in the inflorescence meristem center, where it triggers the LFY-TFL1 negative feedback loop to protect inflorescence meristem indeterminacy. In lateral meristems or flower primordia (red) at the flanks of the inflorescence meristem, *LFY* is upregulated concomitantly and does not activate the indeterminacy program. Instead, LFY promotes the switch to floral fate by activation of floral meristem identity and homeotic genes. TFL1 is not expressed in lateral meristems or flower primordia in the I2 phase.

Table S1. Primer list

Primers for genotyping			
Mutant	**Direction**	**Sequence (5' to 3')**	**Additional notes**
tfl1-1	Forward	taaaaatatttgcattgtaatctag	dCAPS; XbaI; cut mutant
	Reverse	tgacaatcatgaaactagcg	
lfy-1 and *lfy-12*	Forward	gatcctgaaggtttcacgagtgg	dCAPS; BstAPI; cut wild type
	Reverse	aagcagccgtctgcggtgtcagcagctgtt	
lfy-2	Forward	agagagacagagggaggatc	dCAPS; BamHI; cut wild type
	Reverse	cttggtggggcatttttcgc	
Primers for screening CRISPR edited plants			
CRISPR	**Direction**	**Sequence (5' to 3')**	**Additional notes**
TFL1 VII deletion	Forward	gtgaatcgcatcgaaatgctc	Upstream of region VII
	Reverse	ttgttctaactggaccaatccg	Downstream of region VII
LFY-mScarlet-I gene targeting	Forward	gcgaaaaatgccccaccaag	3' of *LFY* exon 2
	Reverse	ctacttatcgtcatcgtctttg	3' of mScarletI-FLAG
Primers for ChIP-qPCR			
Locus	**Direction**	**Sequence (5' to 3')**	**Additional notes**
TFL1 VII (WT)	Forward	aagccgcaaacctggtgat	
	Reverse	ggtttgtcctcgagagtcgtt	
TFL1 VII (mLFYBS)	Forward	ccgcaaacctggtgcttaat	
	Reverse	tggcctcgagagtcgttcta	
Primers for RT-qPCR			
Gene	**Direction**	**Sequence (5' to 3')**	**Additional notes**
TFL1	Forward	cctgcactggatcgttacaa	Reference (*7*)
	Reverse	tggcaattcatagctcacca	
mEGFP	Forward	atggtgagcaagggcgagg	
	Reverse	cggacacgctgaacttgtgg	
ACT2	Forward	tccctcagcacattccagcagat	Reference (*91*)
	Reverse	aacgattcctggacctgcctcatc	

Table S2. HCR FISH hybridization probe list

Transcript	Amplifier	Probe LOT number
TFL1 (AT5G03840.1)	B3	PRK212, RTK849
LFY (AT5G61850.2)	B1	PRJ831, RTK848
FT (AT1G65480.2)	B2	PRR532
mGFP5	B2	PRO045
mEGFP	B3	PRK551
mScarlet-I	B2	PRN494

Table S3. Excitation and detection settings for confocal microscopy

Stallaris 5		
Dye or fluorescent protein	**Exitation laser line (nm)**	**Detection range (nm)**
Calcofluor White	405	420-490
DAPI	405	425-480
Propidium iodide	549	600-650
Alexa Fluor 488	499	505-550 or 510-550
Alexa Fluor 488 (when imaged with Alexa Fluor 514)	488	495-525
Alexa Fluor 514	520	530-565 or 535-565
Alexa Fluor 546	557	565-610
GFP (EGFP, mEGFP, and mGFP5)	488	495-540 or 495-535
mScarlet-I	570	580-625
SP8		
Dye or fluorescent protein	**Exitation laser line (nm)**	**Detection range (nm)**
GFP	488	495-545

Table S4. Values of shape parameters for the FT pulse profile.

FT profile parameter	Value
tc	84
scalePar	14.265
peakWidth	9.5165
heightPar	5.4867

Table S5. Methods for representing mutants *in silico* by modifying parameter values.

Mutation	Biological description	Representation
lfy	Non-functional LFY transcripts are produced	lfybs = 0.0 xlfybs = 0.0 (4-node)
amiRLFY	LFY mRNA is depleted by artificial microRNAs	dLFY: 5×
pLFY-GLFY	LFY mRNA is not produced	bLFY = 0.0 ftbs = 0.0 (3-node and 4-node)
LFY overexpression	LFY mRNA is overexpressed	bLFY: 2×
tfl1	Non-functional TFL1 transcripts are produced	tfl1bs = 0.0
TFL1 degron	TFL1 protein is degraded	dTFL1: 5×
tfl1 heterozygote	The dosage of functional TFL1 mRNA is halved	tfl1bs: 0.5×
TFL1 overexpression	TFL1 mRNA is overexpressed	bTFL1: 2×
dVII *tfl1* or criVII	TFL1 mRNA production is reduced and LFY cannot induce TFL1 expression	bLFY: 0.5× lfybs = 0.0
mLFYBS *tfl1*	LFY cannot induce TFL1 expression	lfybs = 0.0
FT overexpression	FT production is increased	ftmod: 3×
Negative feedback loop removal	TFL1 mRNA production is increased and LFY cannot induce TFL1 expression	bTFL1: 2× lfybs = 0.0

Table S6. Criteria used to evaluate all models. Each criterion specifies an expected fold-change in the end-point value of the indicated model species given a mutated parameter set, relative to the wild type parameter values. Simulations of 3-node and 4-node models are performed using constant FT inputs.

Criterion #	Experimental data	Expectation	Fold-change threshold relative to WT
1	fig. S11	[LFY] is increased in a LFY overexpression mutant	≥ 1.0
2	fig. S11	[TFL1] is increased in a LFY overexpression mutant	≥ 1.2
3	Fig. 3, A and B	[LFY] is reduced in an amiRLFY mutant	$\leq \frac{2}{3}$
4	Fig. 3, A and B	[TFL1] is reduced in an amiRLFY mutant	$\leq \frac{2}{3}$
5	*lfy*: Fig. 2D, mLFYBS *tfl1*: Fig. 1, G to I	[TFL1] is reduced in a *lfy* mutant (or mLFYBS *tfl1* mutant)	$\leq \frac{2}{3}$
6	fig. S12	[LFY] is reduced in a TFL1 overexpression mutant	$\leq \frac{2}{3}$
7	fig. S12	[TFL1] is increased in a TFL1 overexpression mutant	≥ 1.0
8	Fig. 3, C and D	[LFY] is increased in a TFL1 degron mutant	≥ 2.0
9	Fig. 3, C and D	[TFL1] is reduced in a TFL1 degron mutant	$\leq \frac{2}{3}$
10	Fig. 1, G to I	[TFL1] is reduced in a dVII *tfl1* mutant	$\leq \frac{2}{3}$

Table S7. Additional criteria used to evaluate the 3-node model when FT is held constant. The first parameterization of the 3-node model is evaluated using the criteria #1 to #10 in table S6 and the following criteria. Simulations are performed using constant FT inputs.

Criterion #	Experimental data	Expectation	Fold-change threshold relative to WT
11	Fig. 4, A to D	[LFY] is increased in an FT overexpression mutant	≥ 1.5
12	Fig. 4, A to D	[TFL1] is increased in an FT overexpression mutant	≥ 1.5

Table S8. Additional criteria used to evaluate the 3-node model when FT is pulsed. The second parameterization of the 3-node model is evaluated using the criteria #1 to #10 in table S6 and the following criteria. Time 1 to 4 corresponds to 48, 72, 96, 120 units of time in the wild-type simulation with a pulsed FT input. Simulations in this table are performed using pulsed FT inputs.

Criterion #	Experimental data	Expectation	Fold-change threshold
13	Fig. 5, A and B	[LFY] increases from Time 1 to Time 2	≥ 1.5
14	Fig. 5, A and B	[TFL1] increases from Time 1 to Time 2	≥ 1.5
15	Fig. 5, A and B	[LFY] decreases from Time 2 to Time 3	$\leq \frac{1}{1.2}$
16	Fig. 5, A and B	[TFL1] increases from Time 2 to Time 3	≥ 1.5
17	Fig. 5, A and B	[TFL1] decreases from Time 3 to Time 4	$\leq \frac{2}{3}$
18	Fig. 5, A and B	[LFY] increases from Time 1 to Time 4	≥ 1.5
19	Fig. 5, A and B	[TFL1] increases from Time 1 to Time 4	≥ 1.5

Table S9. Additional criteria used to evaluate the 4-node model. The parameterization of the 4-node model is evaluated using the criteria #1 to #10 in table S6, the criteria #13 to #19 in table S8, and the following criteria. Simulations in this table are performed using constant FT inputs.

Criterion #	Experimental data	Expectation	Fold-change threshold relative to WT
20	fig. S23, A to C	[TFL1] is reduced in a strong LFY overexpression mutant (bLFY: 3×)	$\leq \frac{2}{3}$

Table S10. Permitted parameter ranges for the 2-node (LFY and TFL1 only) model.

ID	Lower bound	Upper bound	Parameter description
bLFY	0.0005	20	Basal LFY production rate
bTFL1	0.0005	20	Basal TFL1 production rate
lfybs	0.005	200	Maximum TFL1 production rate as f(LFY)
tfl1bs	0.005	200	Maximum LFY repression rate as f(TFL1)
kLFY	0.015	600	LFY-to-pTFL1 half occupancy concentration
kTFL1	0.02	800	TFL1-to-pLFY half occupancy concentration
nLFY	0.4	10	Hill coefficient for LFY binding to pTFL1
nTFL1	0.4	10	Hill coefficient for TFL1 binding to pLFY
dLFY	0.01	1	LFY degradation rate
dTFL1	0.01	1	TFL1 degradation rate

Table S11. Permitted ranges for parameters introduced in the 3-node (LFY, TFL1, and FT) model. Parameters shared with the 2-node model are omitted for the sake of brevity.

ID	Lower bound	Upper bound	Parameter description
pExp	0.0005	20	Competition coefficient for FT/LFY binding to pLFY
ftbs	0.005	200	Maximum LFY production rate as f(FT)
kFT	0.02	800	FT-to-pLFY half occupancy concentration
nFT	0.4	10	Hill coefficient for FT binding to pLFY
FTmod	0.1	10	FT abundance modifier

Table S12. Permitted ranges for parameters introduced in the 4-node (LFY, TFL1, FT, and X) model. Parameters shared with the 2-node or 3-node models are omitted for the sake of brevity.

ID	Lower bound	Upper bound	Parameter description
bX	0.0009266	37.06	Basal X production rate
xlfybs	0.006028	241.1	Maximum X production rate as f(LFY)
tfl1xbs	0.006028	241.1	Maximum TFL1 repression rate as f(X)
kXLFY	0.01839	735.4	LFY-to-pX half occupancy concentration
nXLFY	0.2439	6.098	Hill coefficient for LFY binding to pX
kTFL1X	0.01839	735.4	X-to-pTFL1 half-occupancy concentration
nTFL1X	0.2439	6.098	Hill coefficient for X binding to pTFL1
dX	0.01979	1.979	X degradation rate

References and Notes

1. Y. Zhu, D. Wagner, Plant Inflorescence Architecture: The Formation, Activity, and Fate of Axillary Meristems. *Cold Spring Harb. Perspect. Biol.* **12**, a034652 (2020). doi:10.1101/cshperspect.a034652 Medline

2. Y. Eshed, Z. B. Lippman, Revolutions in agriculture chart a course for targeted breeding of old and new crops. *Science* **366**, eaax0025 (2019). doi:10.1126/science.aax0025 Medline

3. R. Claßen-Bockhoff, K. Bull-Hereñu, Towards an ontogenetic understanding of inflorescence diversity. *Ann. Bot. (Lond.)* **112**, 1523–1542 (2013). doi:10.1093/aob/mct009 Medline

4. R. Benlloch, A. Berbel, A. Serrano-Mislata, F. Madueño, Floral initiation and inflorescence architecture: A comparative view. *Ann. Bot. (Lond.)* **100**, 659–676 (2007). doi:10.1093/aob/mcm146 Medline

5. O. J. Ratcliffe, I. Amaya, C. A. Vincent, S. Rothstein, R. Carpenter, E. S. Coen, D. J. Bradley, A common mechanism controls the life cycle and architecture of plants. *Development* **125**, 1609–1615 (1998). doi:10.1242/dev.125.9.1609 Medline

6. F. D. Hempel, P. C. Zambryski, L. J. Feldman, Photoinduction of flower identity in vegetatively biased primordia. *Plant Cell* **10**, 1663–1676 (1998). doi:10.1105/tpc.10.10.1663 Medline

7. Y. Zhu, S. Klasfeld, C. W. Jeong, R. Jin, K. Goto, N. Yamaguchi, D. Wagner, TERMINAL FLOWER 1-FD complex target genes and competition with FLOWERING LOCUS T. *Nat. Commun.* **11**, 5118 (2020). doi:10.1038/s41467-020-18782-1 Medline

8. F. D. Hempel, D. Weigel, M. A. Mandel, G. Ditta, P. C. Zambryski, L. J. Feldman, M. F. Yanofsky, Floral determination and expression of floral regulatory genes in Arabidopsis. *Development* **124**, 3845–3853 (1997). doi:10.1242/dev.124.19.3845 Medline

9. S. Balasubramanian, S. Sureshkumar, J. Lempe, D. Weigel, Potent induction of Arabidopsis thaliana flowering by elevated growth temperature. *PLOS Genet.* **2**, e106 (2006). doi:10.1371/journal.pgen.0020106 Medline

10. C. Ibañez, Y. Poeschl, T. Peterson, J. Bellstädt, K. Denk, A. Gogol-Döring, M. Quint, C. Delker, Ambient temperature and genotype differentially affect developmental and phenotypic plasticity in Arabidopsis thaliana. *BMC Plant Biol.* **17**, 114 (2017). doi:10.1186/s12870-017-1068-5 Medline

11. X. Ma, N. L. Sukiran, H. Ma, Z. Su, Moderate drought causes dramatic floral transcriptomic reprogramming to ensure successful reproductive development in Arabidopsis. *BMC Plant Biol.* **14**, 164 (2014). doi:10.1186/1471-2229-14-164 Medline

12. L. Corbesier, C. Vincent, S. Jang, F. Fornara, Q. Fan, I. Searle, A. Giakountis, S. Farrona, L. Gissot, C. Turnbull, G. Coupland, FT protein movement contributes to long-distance signaling in floral induction of Arabidopsis. *Science* **316**, 1030–1033 (2007). doi:10.1126/science.1141752 Medline

13. P. Prusinkiewicz, Y. Erasmus, B. Lane, L. D. Harder, E. Coen, Evolution and development of inflorescence architectures. *Science* **316**, 1452–1456 (2007). doi:10.1126/science.1140429 Medline

14. R. Jin, S. Klasfeld, Y. Zhu, M. Fernandez Garcia, J. Xiao, S.-K. Han, A. Konkol, D. Wagner, LEAFY is a pioneer transcription factor and licenses cell reprogramming to floral fate. *Nat. Commun.* **12**, 626 (2021). doi:10.1038/s41467-020-20883-w Medline

15. S. Shannon, D. R. Meeks-Wagner, A Mutation in the Arabidopsis TFL1 Gene Affects Inflorescence Meristem Development. *Plant Cell* **3**, 877–892 (1991). doi:10.2307/3869152 Medline

16. D. Bradley, O. Ratcliffe, C. Vincent, R. Carpenter, E. Coen, Inflorescence commitment and architecture in Arabidopsis. *Science* **275**, 80–83 (1997). doi:10.1126/science.275.5296.80 Medline

17. L. Conti, D. Bradley, TERMINAL FLOWER1 is a mobile signal controlling Arabidopsis architecture. *Plant Cell* **19**, 767–778 (2007). doi:10.1105/tpc.106.049767 Medline

18. M. Cerise, V. da Silveira Falavigna, G. Rodríguez-Maroto, A. Signol, E. Severing, H. Gao, A. van Driel, C. Vincent, S. Wilkens, F. R. Iacobini, P. Formosa-Jordan, A. Pajoro, G. Coupland, Two modes of gene regulation by TFL1 mediate its dual function in flowering time and shoot determinacy of Arabidopsis. *Development* **150**, dev202089 (2023). doi:10.1242/dev.202089 Medline

19. D. Goretti, M. Silvestre, S. Collani, T. Langenecker, C. Méndez, F. Madueño, M. Schmid, TERMINAL FLOWER1 Functions as a Mobile Transcriptional Cofactor in the Shoot Apical Meristem. *Plant Physiol.* **182**, 2081–2095 (2020). doi:10.1104/pp.19.00867 Medline

20. K. Kaufmann, F. Wellmer, J. M. Muiño, T. Ferrier, S. E. Wuest, V. Kumar, A. Serrano-Mislata, F. Madueño, P. Krajewski, E. M. Meyerowitz, G. C. Angenent, J. L. Riechmann, Orchestration of floral initiation by APETALA1. *Science* **328**, 85–89 (2010). doi:10.1126/science.1185244 Medline

21. A. Serrano-Mislata, P. Fernández-Nohales, M. J. Doménech, Y. Hanzawa, D. Bradley, F. Madueño, Separate elements of the TERMINAL FLOWER 1 cis-regulatory region integrate pathways to control flowering time and shoot meristem identity. *Development* **143**, 3315–3327 (2016). doi:10.1242/dev.135269 Medline

22. A. Serrano-Mislata, K. Goslin, B. Zheng, L. Rae, F. Wellmer, E. Graciet, F. Madueño, Regulatory interplay between LEAFY, APETALA1/CAULIFLOWER and TERMINAL FLOWER1: New insights into an old relationship. *Plant Signal. Behav.* **12**, e1370164 (2017). doi:10.1080/15592324.2017.1370164 Medline

23. F. Hammal, P. de Langen, A. Bergon, F. Lopez, B. Ballester, ReMap 2022: A database of Human, Mouse, Drosophila and Arabidopsis regulatory regions from an integrative analysis of DNA-binding sequencing experiments. *Nucleic Acids Res.* **50** (D1), D316–D325 (2022). doi:10.1093/nar/gkab996 Medline

24. T. Bieluszewski, M. Szymanska-Lejman, W. Dziegielewski, L. Zhu, P. A. Ziolkowski, Efficient Generation of CRISPR/Cas9-Based Mutants Supported by Fluorescent Seed Selection in Different Arabidopsis Accessions. *Methods Mol. Biol.* **2484**, 161–182 (2022). doi:10.1007/978-1-0716-2253-7_13 Medline

25. D. Weigel, O. Nilsson, A developmental switch sufficient for flower initiation in diverse plants. *Nature* **377**, 495–500 (1995). doi:10.1038/377495a0 Medline

26. E. A. Schultz, G. W. Haughn, LEAFY, a Homeotic Gene That Regulates Inflorescence Development in Arabidopsis. *Plant Cell* **3**, 771–781 (1991). doi:10.2307/3869271 Medline

27. E. G. Minguet, S. Segard, C. Charavay, F. Parcy, MORPHEUS, a Webtool for Transcription Factor Binding Analysis Using Position Weight Matrices with Dependency. *PLOS ONE* **10**, e0135586 (2015). doi:10.1371/journal.pone.0135586 Medline

28. E. Moyroud, E. G. Minguet, F. Ott, L. Yant, D. Posé, M. Monniaux, S. Blanchet, O. Bastien, E. Thévenon, D. Weigel, M. Schmid, F. Parcy, Prediction of regulatory interactions from genome sequences using a biophysical model for the Arabidopsis LEAFY transcription factor. *Plant Cell* **23**, 1293–1306 (2011). doi:10.1105/tpc.111.083329 Medline

29. D. Wagner, R. W. Sablowski, E. M. Meyerowitz, Transcriptional activation of APETALA1 by LEAFY. *Science* **285**, 582–584 (1999). doi:10.1126/science.285.5427.582 Medline

30. M. A. Blázquez, L. N. Soowal, I. Lee, D. Weigel, LEAFY expression and flower initiation in Arabidopsis. *Development* **124**, 3835–3844 (1997). doi:10.1242/dev.124.19.3835 Medline

31. X. Wu, J. R. Dinneny, K. M. Crawford, Y. Rhee, V. Citovsky, P. C. Zambryski, D. Weigel, Modes of intercellular transcription factor movement in the Arabidopsis apex. *Development* **130**, 3735–3745 (2003). doi:10.1242/dev.00577 Medline

32. A. Sessions, M. F. Yanofsky, D. Weigel, Cell-cell signaling and movement by the floral transcription factors LEAFY and APETALA1. *Science* **289**, 779–782 (2000). doi:10.1126/science.289.5480.779 Medline

33. F. Parcy, O. Nilsson, M. A. Busch, I. Lee, D. Weigel, A genetic framework for floral patterning. *Nature* **395**, 561–566 (1998). doi:10.1038/26903 Medline

34. D. S. Glass, X. Jin, I. H. Riedel-Kruse, Nonlinear delay differential equations and their application to modeling biological network motifs. *Nat. Commun.* **12**, 1788 (2021). doi:10.1038/s41467-021-21700-8 Medline

35. S. Shannon, D. R. Meeks-Wagner, Genetic Interactions That Regulate Inflorescence Development in Arabidopsis. *Plant Cell* **5**, 639–655 (1993). doi:10.2307/3869807 Medline

36. Y. H. Song, A. Kubota, M. S. Kwon, M. F. Covington, N. Lee, E. R. Taagen, D. Laboy Cintrón, D. Y. Hwang, R. Akiyama, S. K. Hodge, H. Huang, N. H. Nguyen, D. A. Nusinow, A. J. Millar, K. K. Shimizu, T. Imaizumi, Molecular basis of flowering under natural long-day conditions in Arabidopsis. *Nat. Plants* **4**, 824–835 (2018). doi:10.1038/s41477-018-0253-3 Medline

37. S. Y. Kim, X. Yu, S. D. Michaels, Regulation of CONSTANS and FLOWERING LOCUS T expression in response to changing light quality. *Plant Physiol.* **148**, 269–279 (2008). doi:10.1104/pp.108.122606 Medline

38. S.-J. Kim, S. M. Hong, S. J. Yoo, S. Moon, H. S. Jung, J. H. Ahn, Post-Translational Regulation of FLOWERING LOCUS T Protein in Arabidopsis. *Mol. Plant* **9**, 308–311 (2016). doi:10.1016/j.molp.2015.11.001 Medline

39. M. A. Félix, M. Barkoulas, Pervasive robustness in biological systems. *Nat. Rev. Genet.* **16**, 483–496 (2015). doi:10.1038/nrg3949 Medline

40. S. B. Gelvin, Integration of Agrobacterium T-DNA into the Plant Genome. *Annu. Rev. Genet.* **51**, 195–217 (2017). doi:10.1146/annurev-genet-120215-035320 Medline

41. A. R. Plackett, S. J. Conway, K. D. Hewett Hazelton, E. H. Rabbinowitsch, J. A. Langdale, V. S. Di Stilio, *LEAFY* maintains apical stem cell activity during shoot development in the fern *Ceratopteris richardii*. *eLife* **7**, e39625 (2018). doi:10.7554/eLife.39625 Medline

42. C. Sayou, M. Monniaux, M. H. Nanao, E. Moyroud, S. F. Brockington, E. Thévenon, H. Chahtane, N. Warthmann, M. Melkonian, Y. Zhang, G. K.-S. Wong, D. Weigel, F. Parcy, R. Dumas, A promiscuous intermediate underlies the evolution of LEAFY DNA binding specificity. *Science* **343**, 645–648 (2014). doi:10.1126/science.1248229 Medline

43. N. N. Rao, K. Prasad, P. R. Kumar, U. Vijayraghavan, Distinct regulatory role for RFL, the rice LFY homolog, in determining flowering time and plant architecture. *Proc. Natl. Acad. Sci. U.S.A.* **105**, 3646–3651 (2008). doi:10.1073/pnas.0709059105 Medline

44. K. Ikeda-Kawakatsu, M. Maekawa, T. Izawa, J. Itoh, Y. Nagato, ABERRANT PANICLE ORGANIZATION 2/RFL, the rice ortholog of Arabidopsis LEAFY, suppresses the transition from inflorescence meristem to floral meristem through interaction with APO1. *Plant J.* **69**, 168–180 (2012). doi:10.1111/j.1365-313X.2011.04781.x Medline

45. D. Bradley, R. Carpenter, L. Copsey, C. Vincent, S. Rothstein, E. Coen, Control of inflorescence architecture in Antirrhinum. *Nature* **379**, 791–797 (1996). doi:10.1038/379791a0 Medline

46. R. Carpenter, L. Copsey, C. Vincent, S. Doyle, R. Magrath, E. Coen, Control of flower development and phyllotaxy by meristem identity genes in antirrhinum. *Plant Cell* **7**, 2001–2011 (1995). Medline

47. F. Parcy, K. Bomblies, D. Weigel, Interaction of LEAFY, AGAMOUS and TERMINAL FLOWER1 in maintaining floral meristem identity in Arabidopsis. *Development* **129**, 2519–2527 (2002). doi:10.1242/dev.129.10.2519 Medline

48. K. Goslin, B. Zheng, A. Serrano-Mislata, L. Rae, P. T. Ryan, K. Kwaśniewska, B. Thomson, D. S. Ó'Maoiléidigh, F. Madueño, F. Wellmer, E. Graciet, Transcription Factor Interplay between LEAFY and APETALA1/CAULIFLOWER during Floral Initiation. *Plant Physiol.* **174**, 1097–1109 (2017). doi:10.1104/pp.17.00098 Medline

49. G. Wu, G. Rossidivito, T. Hu, Y. Berlyand, R. S. Poethig, Traffic lines: New tools for genetic analysis in Arabidopsis thaliana. *Genetics* **200**, 35–45 (2015). doi:10.1534/genetics.114.173435 Medline

50. R. S. Poethig, W. L. Cullina, E. Doody, T. Floyd, J. P. Fouracre, T. Hu, M. Xu, J. Zhao, Short-interval traffic lines: Versatile tools for genetic analysis in Arabidopsis thaliana. *G3* **12**, jkac202 (2022). doi:10.1093/g3journal/jkac202 Medline

51. C. Mayor, M. Brudno, J. R. Schwartz, A. Poliakov, E. M. Rubin, K. A. Frazer, L. S. Pachter, I. Dubchak, VISTA : Visualizing global DNA sequence alignments of arbitrary length. *Bioinformatics* **16**, 1046–1047 (2000). doi:10.1093/bioinformatics/16.11.1046 Medline

52. K. A. Frazer, L. Pachter, A. Poliakov, E. M. Rubin, I. Dubchak, VISTA: Computational tools for comparative genomics. *Nucleic Acids Res.* **32**, W273–W279 (2004). doi:10.1093/nar/gkh458 Medline

53. M. Brudno, S. Malde, A. Poliakov, C. B. Do, O. Couronne, I. Dubchak, S. Batzoglou, Glocal alignment: Finding rearrangements during alignment. *Bioinformatics* **19** (Suppl 1), i54–i62 (2003). doi:10.1093/bioinformatics/btg1005 Medline

54. J. T. Robinson, H. Thorvaldsdóttir, W. Winckler, M. Guttman, E. S. Lander, G. Getz, J. P. Mesirov, Integrative genomics viewer. *Nat. Biotechnol.* **29**, 24–26 (2011). doi:10.1038/nbt.1754 Medline

55. S. Hanano, K. Goto, Arabidopsis TERMINAL FLOWER1 is involved in the regulation of flowering time and inflorescence development through transcriptional repression. *Plant Cell* **23**, 3172–3184 (2011). doi:10.1105/tpc.111.088641 Medline

56. A.-K. Schürholz, V. López-Salmerón, Z. Li, J. Forner, C. Wenzl, C. Gaillochet, S. Augustin, A. V. Barro, M. Fuchs, M. Gebert, J. U. Lohmann, T. Greb, S. Wolf, A Comprehensive Toolkit for Inducible, Cell Type-Specific Gene Expression in Arabidopsis. *Plant Physiol.* **178**, 40–53 (2018). doi:10.1104/pp.18.00463 Medline

57. R. Schwab, S. Ossowski, M. Riester, N. Warthmann, D. Weigel, Highly specific gene silencing by artificial microRNAs in Arabidopsis. *Plant Cell* **18**, 1121–1133 (2006). doi:10.1105/tpc.105.039834 Medline

58. D. R. Gallie, D. E. Sleat, J. W. Watts, P. C. Turner, T. M. Wilson, Mutational analysis of the tobacco mosaic virus 5′-leader for altered ability to enhance translation. *Nucleic Acids Res.* **16**, 883–893 (1988). doi:10.1093/nar/16.3.883 Medline

59. P. C. Fridy, Y. Li, S. Keegan, M. K. Thompson, I. Nudelman, J. F. Scheid, M. Oeffinger, M. C. Nussenzweig, D. Fenyö, B. T. Chait, M. P. Rout, A robust pipeline for rapid production of versatile nanobody repertoires. *Nat. Methods* **11**, 1253–1260 (2014). doi:10.1038/nmeth.3170 Medline

60. E. Sorge, D. Demidov, I. Lermontova, A. Houben, U. Conrad, Engineered degradation of EYFP-tagged CENH3 via the 26S proteasome pathway in plants. *PLOS ONE* **16**, e0247015 (2021). doi:10.1371/journal.pone.0247015 Medline

61. A. Y. Husbands, A. Feller, V. Aggarwal, C. E. Dresden, A. S. Holub, T. Ha, M. C. P. Timmermans, The START domain potentiates HD-ZIPIII transcriptional activity. *Plant Cell* **35**, 2332–2348 (2023). doi:10.1093/plcell/koad058 Medline

62. M. Michniewicz, E. M. Frick, L. C. Strader, Gateway-compatible tissue-specific vectors for plant transformation. *BMC Res. Notes* **8**, 63 (2015). doi:10.1186/s13104-015-1010-6 Medline

63. J. P. Concordet, M. Haeussler, CRISPOR: Intuitive guide selection for CRISPR/Cas9 genome editing experiments and screens. *Nucleic Acids Res.* **46** (W1), W242–W245 (2018). doi:10.1093/nar/gky354 Medline

64. T. Huang, B. Guillotin, R. Rahni, K. D. Birnbaum, D. Wagner, A rapid and sensitive, multiplex, whole mount RNA fluorescence in situ hybridization and immunohistochemistry protocol. *Plant Methods* **19**, 131 (2023). doi:10.1186/s13007-023-01108-9 Medline

65. D. Kurihara, Y. Mizuta, Y. Sato, T. Higashiyama, ClearSee: A rapid optical clearing reagent for whole-plant fluorescence imaging. *Development* **142**, 4168–4179 (2015). doi:10.1242/dev.127613 Medline

66. T. Pasternak, O. Tietz, K. Rapp, M. Begheldo, R. Nitschke, B. Ruperti, K. Palme, Protocol: An improved and universal procedure for whole-mount immunolocalization in plants. *Plant Methods* **11**, 50 (2015). doi:10.1186/s13007-015-0094-2 Medline

67. O. Hamant, P. Das, A. Burian, *Plant Cell Morphogenesis: Methods and Protocols*, V. Žárský, F. Cvrčková, Eds. (Humana Press, 2014), pp. 111–119.

68. J. Schindelin, I. Arganda-Carreras, E. Frise, V. Kaynig, M. Longair, T. Pietzsch, S. Preibisch, C. Rueden, S. Saalfeld, B. Schmid, J.-Y. Tinevez, D. J. White, V. Hartenstein, K. Eliceiri, P. Tomancak, A. Cardona, Fiji: An open-source platform for biological-image analysis. *Nat. Methods* **9**, 676–682 (2012). doi:10.1038/nmeth.2019 Medline

69. D. R. Smyth, J. L. Bowman, E. M. Meyerowitz, Early flower development in Arabidopsis. *Plant Cell* **2**, 755–767 (1990). Medline

70. N. Yamaguchi, C. M. Winter, M.-F. Wu, C. S. Kwon, D. A. William, D. Wagner, PROTOCOLS: Chromatin Immunoprecipitation from Arabidopsis Tissues. *Arabidopsis Book* **12**, e0170 (2014). doi:10.1199/tab.0170 Medline

71. K. J. Livak, T. D. Schmittgen, Analysis of relative gene expression data using real-time quantitative PCR and the 2(-Delta Delta C(T)) Method. *Methods* **25**, 402–408 (2001). doi:10.1006/meth.2001.1262 Medline

72. C. Hodgens, T. Huang, LFY-TFL1 negative feedback loop model, Zenodo (2025); https://doi.org/10.5281/zenodo.14343022.

73. M. Endo, M. Yoshida, Y. Sasaki, K. Negishi, K. Horikawa, Y. Daimon, K.-I. Kurotani, M. Notaguchi, M. Abe, T. Araki, Re-Evaluation of Florigen Transport Kinetics with Separation of Functions by Mutations That Uncouple Flowering Initiation and Long-Distance Transport. *Plant Cell Physiol.* **59**, 1621–1629 (2018). doi:10.1093/pcp/pcy063 Medline

74. L. F. Shampine, S. Thompson, J. A. Kierzenka, G. D. Byrne, Non-negative solutions of ODEs. *Appl. Math. Comput.* **170**, 556–569 (2005). doi:10.1016/j.amc.2004.12.011

75. K. Cranmer, J. Brehmer, G. Louppe, The frontier of simulation-based inference. *Proc. Natl. Acad. Sci. U.S.A.* **117**, 30055–30062 (2020). doi:10.1073/pnas.1912789117 Medline

76. M. A. Beaumont, W. Zhang, D. J. Balding, Approximate Bayesian computation in population genetics. *Genetics* **162**, 2025–2035 (2002). doi:10.1093/genetics/162.4.2025 Medline

77. C. Hodgens, D. T. Flaherty, A.-M. Pullen, I. Khan, N. J. English, L. Gillan, M. Rojas-Pierce, B. S. Akpa, Model-based inference of a dual role for HOPS in regulating guard cell vacuole fusion. *In Silico Plants* **6**, diae015 (2024). doi:10.1093/insilicoplants/diae015 Medline

78. X. Y. Zhang, M. N. Trame, L. J. Lesko, S. Schmidt, Sobol Sensitivity Analysis: A Tool to Guide the Development and Evaluation of Systems Pharmacology Models. *CPT Pharmacometrics Syst. Pharmacol.* **4**, 69–79 (2015). doi:10.1002/psp4.6 Medline

79. M. Shibata, C. Breuer, A. Kawamura, N. M. Clark, B. Rymen, L. Braidwood, K. Morohashi, W. Busch, P. N. Benfey, R. Sozzani, K. Sugimoto, GTL1 and DF1 regulate root hair growth through transcriptional repression of *ROOT HAIR DEFECTIVE 6-LIKE 4* in *Arabidopsis*. *Development* **145**, dev159707 (2018). doi:10.1242/dev.159707 Medline

80. F. Khorashadi Zadeh, J. Nossent, F. Sarrazin, F. Pianosi, A. van Griensven, T. Wagener, W. Bauwens, Comparison of variance-based and moment-independent global sensitivity analysis approaches by application to the SWAT model. *Environ. Model. Softw.* **91**, 210–222 (2017). doi:10.1016/j.envsoft.2017.02.001

81. U. Alon, *An introduction to systems biology: Design principles of biological circuits* (CRC Press, 2019).

82. J. Bezanson, A. Edelman, S. Karpinski, V. B. Shah, Julia: A Fresh Approach to Numerical Computing. *SIAM Rev.* **59**, 65–98 (2017). doi:10.1137/141000671

83. C. Rackauckas, Q. Nie, DifferentialEquations.jl – A Performant and Feature-Rich Ecosystem for Solving Differential Equations in Julia. *J. Open Res. Softw.* **5**, 15 (2017). doi:10.5334/jors.151

84. S. Christ, D. Schwabeneder, C. Rackauckas, M. K. Borregaard, T. Breloff, Plots.jl – A User Extendable Plotting API for the Julia Programming Language. *J. Open Res. Softw.* **11**, 5 (2023). doi:10.5334/jors.431

85. E. Tankhilevich, J. Ish-Horowicz, T. Hameed, E. Roesch, I. Kleijn, M. P. H. Stumpf, F. He, GpABC: A Julia package for approximate Bayesian computation with Gaussian process emulation. *Bioinformatics* **36**, 3286–3287 (2020). doi:10.1093/bioinformatics/btaa078 Medline

86. V. K. Dixit, C. Rackauckas, GlobalSensitivity.jl: Performant and Parallel Global Sensitivity Analysis with Julia. *J. Open Source Softw.* **7**, 4561 (2022). doi:10.21105/joss.04561

87. Y. Ma, V. Dixit, M. J. Innes, X. Guo, C. Rackauckas, "A Comparison of Automatic Differentiation and Continuous Sensitivity Analysis for Derivatives of Differential Equation Solutions," 2021 IEEE High Performance Extreme Computing Conference, Waltham, MA, 20 to 24 September 2021 (IEEE, 2021).

88. R Core Team, R: A Language and Environment for Statistical Computing. (2023).

89. H. Wickham, *ggplot2: Elegant Graphics for Data Analysis* (Springer, 2016).

90. A. Kassambara, ggpubr: 'ggplot2' Based Publication Ready Plots (2025).

91. A. Pajoro, P. Madrigal, J. M. Muiño, J. T. Matus, J. Jin, M. A. Mecchia, J. M. Debernardi, J. F. Palatnik, S. Balazadeh, M. Arif, D. S. Ó'Maoiléidigh, F. Wellmer, P. Krajewski, J.-L. Riechmann, G. C. Angenent, K. Kaufmann, Dynamics of chromatin accessibility and gene regulation by MADS-domain transcription factors in flower development. *Genome Biol.* **15**, R41 (2014). doi:10.1186/gb-2014-15-3-r41 Medline